Ministry of Higher Education and Scientific Research

Hassiba Benbouali University of Chlef

Faculty of Technology

Department of Mechanical Engineering

THESIS

Submitted in fulfillment of the requirements for the degree of:

DOCTORATE (SCIENCE)

Field: Mechanical Engineering

Specialty: Mechanical Construction

By

ABD EL HAMID GHOUAOULA

Title:

DEVELOPMENT OF A LIFETIME MODEL OF COMPOSITE STRUCTURES IN STATIC AND FATIGUE

Defended on: 14-01-2026 in front of the committee members:

Mr BELALIA Azeddine	SeniorLucturer	Hassiba Benbouali University of Chlef	President
Mr HOCINE Abdelkader	Professor	Hassiba Benbouali University of Chlef	Supervisor
Mr CHAPELLE David	Professor	DMA, FEMTO-ST Institute, Marie et Louis PASTEUR University	Co-Supervisor
Mr BEZAZI Abderrezak	Professor	Mai 08 1945 Guelma University	Examiner
Mr AID Abdelkrim	Professor	Mustapha Stambouli Mascara University	Examiner
Mr MEDJDOUB Sidi Mohamed	Senior Lucturer	Djillali Liabes Sidi Bel Abbes University	Examiner
Mr BAALI Ibrahim	Dr	Maghreb Pipe Industry Msila	Invited
Mr MAIZIA Abdelhakim	Dr	Hassiba Benbouali University of Chlef	Invited

ACKNOWLEDGEMENT

First of all, I thank God Almighty for the courage and patience that gave me to complete this work.

I would like to express my most profound gratitude to my supervisor **Pr. HOCINE Abdelkader** for his constant supervision, guidance, support, trust, encouragement, advices and for helpful discussions and useful comments. His leadership, motivation, insights and passion for science and research were the driving force behind the success of this doctorate thesis. Although having a huge amount of responsibilities, He was always approachable kind and generous. His rich knowledge and experience offered clear guidance throughout my doctorate period.

I would like to extend my appreciation to **Pr. CHAPELLE David** as my co-supervisor from: University of Marie et Louis PASTEUR – Besancon France, for his valuable support and advice. His continuous assistance was a great value in overcoming the obstacles that I encountered.

I would like to extend my appreciation to **Pr. BOUBAKER Mohamed Lamine** as my co-supervisor from University of Marie et Louis PASTEUR – Besancon France for his valuable support and advice.

I would also like to extend my sincere appreciation to the president examination committee Dr **BELALIA Azedin** and the members Pr **BEZAZI Abderrezak**, Pr **Aid Abdelkrim** Dr. **Medjdoub Sidi Mohamed** and Dr **BAALI Ibrahim**, Dr **MAIZIA Abdelhakim** for given me the honor and agreed to review this research and evaluate to contents of this doctoral project.

I would also like to thank all the teachers and staff of the faculty of technology and department of mechanical engineering at Hassiba Benbouali University of Chlef.

To my earliest teachers sand all the professors who inspired me a desire for lifelong learning.

Finally, my huge thanks and appreciations to everyone who has helped, supported, and guided me through this period of my academic life.

Abd el hamid

DEDICATION

I dedicate this completion:

To **my dear parents** to whom all my successes and achievements in all areas are due,

To my little family: **My wife** who took care of me during this period and **my children**,.

To **my brothers** and **sisters** with whom we shared a childhood full of innocence, love and joy and through to all **my nieces** and **nephews**,

To my colleagues and friends, who helped make this work a reality with their support, assistance, and motivation.

الملخص

الهدف من هذا المشروع هو تطوير نموذج تحليلي يتنبأ بعمر الهياكل الأنبوبية متعددة الطبقات. هذه الهياكل مصنوعة من ألياف زجاجية طويلة ومصفوفة إيبوكسي. تحتوي هذه الأنابيب على ست طبقات بزاوية اتجاه 55 درجة. يحاكي النموذج المطور الاستجابة الميكانيكية للهيكل المركب الأسطواني تحت أنواع مختلفة من التحميل، مثل الضغط الداخلي الخالص، والضغط الداخلي مع تأثيرات الخلفية، والتوتر، والإجهاد الدوري. تم إجراء اختبارات الشد والجر الدوري على الأنابيب المركبة. تسمح لنا اختبارات الشد بتقدير الإجهاد النهائي حتى الفشل. تسمح لنا اختبارات التفاعل الدوري بتقدير الإمكانات المتبقية. يسمح لنا النموذج المطور بتقدير عدد دورات فشل الأنبوب المركب. تسمح لنا اختبارات الشد الدورية بتحديد الإمكانات المتبقية للأنابيب المركبة. تُظهر النتائج أنه عند تعريض الأنابيب المركبة للتحميل الدوري، فإن عدد الدورات يؤدي إلى تغيير كبير في شكل منحنى إجهاد الشد والانفعال وانخفاض في معامل المرونة. بالإضافة إلى ذلك، يتم إجراء اختبارات التحميل الدوري عند سعات إجهاد متعددة (40%، و60%، و80% من قوة الشد القصوى) لتقييم عمر إجهاد المادة وتطور التلف عند مستويات تحميل مختلفة. تقيس هذه الاختبارات العلاقة بين سعة الإجهاد وعدد الدورات حتى الفشل.

الكلمات المفتاحية: الهيكل الأنبوبي، مركب متعدد الطبقات، مرونة اللزوجة، التلف، تحميل الضغط، العمر.

Abstract

The objective of this project is to develop an analytical model that predicts the lifetime of multilayer tubular structures. These structures are made with long glass fibers and an epoxy matrix. These tubes contain six layers with an orientation angle of 55°. The developed model simulates the mechanical response of a cylindrical composite structure under different types of loading, such as pure internal pressure, internal pressure with background effects, tension, and cyclic fatigue. Tensile and cyclic traction tests were performed on composite tubes. Tensile tests allow us to estimate ultimate stress to failure. Cyclic reaction tests allow us to estimate the remaining potential. The developed model allows us to estimate the number of cycles to failure of the composite tube. Cyclic tensile tests allow us to determine the remaining potential of composite tubes. The results show that when composite tubes are exposed to cyclic loading, the number of cycles induces a significant change in the shape of the tensile stress-strain curve and a decrease in the elastic modulus. Additionally, cyclic loading tests are conducted at multiple stress amplitudes (40%, 60%, and 80% of the ultimate tensile strength) to evaluate the material's fatigue life and damage progression at different load levels. These tests quantify the relationship between stress amplitude and the number of cycles to failure.

***Keywords*:** Tubular structure, Multilayer composite, Viscoelastic, Damage, Pressure loading , Lifetime.

TABLE OF CONTENTS

CHAPTER II: MATERIALS AND EXPERIMENTAL PROCEDURE

CHAPTER III: ANALYTICAL MODEL AND MATHEMATICAL FORMULATION

List of Figures

LIST OF TABLES

LIST OF SYMBOLS

Symbol latries

C^c : The stiffness matrix of the composite.

D_I : Parameter of damage.

E_x :Young's modulus

E_y :Young's modulus

E_z :Young's modulus

G_{xy} :Shearing module

G_{xz} :Shearing module

G_{yz} :Shearing module

H :The correction matrix

R^d : Hardening function.

$R_{int}^{(k)}$:Internal radius of the layer

$R_{ext}^{(k)}$:Outer radius of the layer

S^c :The stiffness matrix of the composite

Ur :radial displacement

X :longitudinal direction

Y :Driving force

Y_c :The damage threshold

e_k :Thickness of the layer

f^d :Charging function

r : Radius

v_{xy} : Poisson coefficient

v_{xz} : Poisson coefficient

v_{yz} : Poisson coefficient

Greek symbols:

θ :circumferential direction

$\boldsymbol{\alpha}$:directing coefficient

$\boldsymbol{\varphi}$:Winding angle

$\boldsymbol{\acute{\varepsilon}}$:Lagrange multiplier

$\boldsymbol{\psi}$:Density of free energy

$\boldsymbol{\acute{\sigma}}$: Vector strain in the reference (*r, z, è*).

$\boldsymbol{\dot{\lambda}^{d}}$:Torsion per unit of length

$\boldsymbol{\gamma_{0}}$:axial strain

$\boldsymbol{\varepsilon_{0}}$:elastic deformation

$\boldsymbol{\varepsilon^{e}}$:viscoelastic deformation

$\boldsymbol{\varepsilon^{ve}}$:relaxation time

$\boldsymbol{\tau_{i}}$:circumferential direction

$\boldsymbol{\mu_{i}}$:directing coefficient

Indices

r :radial direction

z :axial direction

θ :Circumferential direction

x :Longitudinal and transverse direction of the fiber

Y :Longitudinal and transverse direction of the fiber

Introduction

Introduction

The hydrogen sector includes different key stages: production, distribution, storage and exploitation [01]. Where the three last stages constitute the same field of research and present the obstacles. Pipelines, ships, trucks and railways or planes are transportation and distribution solutions [02]. It can be transmitted in the form of liquid, gas, and metal hydrides through the ocean, road, and pipelines [03].

The current transportation and distribution system for delivering conventional fuels to consumers cannot be easily transformed for use with hydrogen. The present options for transporting hydrogen include compressed gas (200 bars) in steel tube cylinders, liquid hydrogen tanks and a few examples of local networks of hydrogen pipelines [04].

The rapid growth of composite materials expands their feather almost to all the engineering applications. This is due to their unique advantage of lower weight to higher specific strength [5,6].

In recent years, composite pipes have emerged as a strong alternative to conventional steel pipes in the oil and gas sector. These pipes provide a lightweight, flexible, corrosion-resistant, and easily transportable option for moving liquids and gases. Globally, thousands of kilometers of composite piping systems have already been deployed, primarily for hydrocarbon and water transportation. To expand their use into hydrogen applications—particularly for storage and distribution—research initiatives started approximately a decade ago are focusing on making composite pipes a viable competitor to steel in terms of both cost efficiency and dependability

In hydrogen transport and storage applications, research has prioritized evaluating the unique characteristics of composite materials, such as superior shock absorption, high mechanical performance, and long-term durability. More recently, fatigue resistance has emerged as a critical design factor to meet the demands of hydrogen infrastructure.

Today, composite materials are increasingly employed in high-stress applications, particularly within the hydrogen sector. To select the most appropriate material and enhance both quasi-static and fatigue performance, it is essential to analyze three key aspects: first, the response of composites to internal pressure and tensile loads; second, the mechanisms behind fatigue-induced degradation; and finally, their behavior under combined loading conditions.

This thesis focuses on an analysis of research into the assessment and prediction of fatigue life of damaged tubular composite structures under internal and axial pressure.

High-pressure hydrogen transport—whether through pipelines or composite tanks—offers a promising solution to meet the growing demand for clean and sustainable energy [07]. However, this technology faces significant challenges related to the durability and reliability of the materials used. The extreme operating conditions—characterized by high pressures and repeated loading/unloading cycles—subject the structures to complex mechanical stresses that can become critical over time [08]. Structural components in hydrogen systems must maintain integrity under diverse operational loads, which may include combined bending moments, internal/external pressure differentials, elevated temperature conditions, as well as complex axial and torsional stress states - with specific loading profiles being application-dependent. [9].

Among these stress factors, axial loading plays a predominant role in material degradation. Three primary failure mechanisms can be identified: (1) pure tension, caused by internal pressure and residual stresses from manufacturing processes [10]; (2) axial fatigue, resulting from repeated pressure cycles during hydrogen transport, which may induce crack initiation and propagation [11] ; and to accurately assess the structural performance of hydrogen transport infrastructure, it is essential to evaluate the combined effects of tension and fatigue loading (3), as these conditions reflect real-world operational stresses. However, characterizing material behavior under such multiaxial loading scenarios presents a significant research challenge, primarily because existing studies often examine these loads in isolation rather than their interactive effects [12].

A systematic investigation of these mechanisms—whether acting independently or concurrently—is critical, as they can lead to progressive degradation of pipelines and storage tanks. This degradation not only compromises structural integrity but also raises safety concerns and efficiency limitations in hydrogen transport systems. A comprehensive experimental and computational approach is needed to better understand these interactions and develop robust design criteria to estimate the burst pressure in static and fatigue loading.
In this context, Prabhakar et al. [05] developed burst pressure studies of composite pipes, where a ±55° winding angle in E-glass/epoxy materials demonstrates optimal performance by minimizing failure modes (matrix cracking, whitening, leakage, and fracture). The underlying failure mechanism appears fundamentally governed by the ratio between the longitudinal σ_{zz} and circumferential $\sigma_{\theta\theta}$ stresses [13]. This stress-state ratio variation, provide a critical

guidance for failure-prediction modeling and design optimization of composite pressure pipes and vessels.

The investigation of fatigue behavior in composite pipes under internal pressure loading constitutes an essential research focus, particularly for hydrogen transport applications [14]. Experimental work by Tarakcioglu et al. [15] and Meijer et al. [16] has systematically characterized this phenomenon through pressure cycling tests across multiple load levels (30-70% of ultimate strength). Their findings demonstrate the complex interplay of material factors governing fatigue resistance, as later analyzed by Feki et al. [17], who identified four key determinants: (i) fiber and matrix material properties, (ii) laminate stacking sequence, (iii) fiber-matrix interfacial integrity, and (iv) manufacturing-induced residual stresses.

These fatigue studies correlate with burst pressure research showing optimal performance at ±55° winding angles in glass/epoxy systems (as evidenced in 90% of reviewed studies), suggesting similar parametric dependencies may govern both static and cyclic failure modes. However, as noted in recent analyses (15,16,17), critical knowledge gaps remain regarding damage progression under combined static-fatigue loading conditions characteristic of hydrogen service environments. This underscores the need for integrated experimental-computational approaches to develop comprehensive life prediction models for industrial applications.

To characterize the synergistic degradation effects in marine environments, Deniz et al. [18] performed a systematic experimental investigation on glass-epoxy composite pipes subjected to combined environmental and mechanical loading conditions. Their study specifically examined:

1. Seawater aging effects on material properties through controlled immersion testing
2. Low-velocity impact damage characterization using standardized impact protocols
3. Cyclic pressure fatigue performance (post-impact and seawater exposure) through accelerated life testing

The paper developed by Nghiep et al. [19] focuses on developing a predictive modeling tool for hydrogen (H2) storage composite pressure vessels, integrating micromechanics of matrix cracking with continuum damage mechanics (CDM) and 3D finite element (FE) modeling to analyze damage evolution and structural response.

Despite these advances, critical knowledge gaps remain regarding degradation mechanisms in composite materials under complex axial-tensile and fatigue loading conditions highly relevant to hydrogen transport systems.

This study aims to address these gaps by systematically investigating the mechanical behaviour of materials under axial loads representative of real-world hydrogen transport conditions. Using an experimental approach, we aim to quantify the effects of pure tension, axial fatigue and combined loading on the strength and durability of multilayer composite tubes. The results will enable the establishment of more robust design criteria and the development of strategies to improve the reliability of high pressure hydrogen transport systems.

By advancing the understanding of degradation mechanisms under axial loading, this research will contribute to efforts to support the safe and efficient deployment of hydrogen as a key energy carrier in the global energy transition.

This thesis aims to investigate the influence of static and fatigue loading on multilayered tubular composite structures, with a focus on characterizing the initiation and progression of damage mechanisms leading to failure. To achieve this, an experimental study was conducted on composite tubular specimens subjected to three loading regimes: (1) monotonic tensile loading to failure, (2) cyclic fatigue loading to failure, and (3) a sequential combination of cyclic fatigue followed by tensile loading to failure. The experimental data serves as the foundation for developing an analytical lifespan prediction model, implemented in MATLAB, which integrates constitutive laws capturing the visco-elasto-plastic response and progressive damage behavior of the composite material.

Within this framework and to achieve these objectives, the present thesis is structured into four complementary chapters, organized as follows:

This literature review chapter provides the critical foundation for the thesis "Development of a Lifetime Model of Composite Structures in Static and Fatigue" by examining the dual challenge of hydrogen transport effects and pressure-induced axial loading in composite tubes. The analysis first contextualises hydrogen service conditions where internal pressure produces dominant axial stresses that interact synergistically with hydrogen embrittlement mechanisms. Through a systematic assessment of stress state anisotropy in pressurised hydrogen containment systems, the review demonstrates how existing studies fail to adequately characterise the triaxial damage progression (matrix plastication → hydrogen-assisted interfacial cracking → fibre overload) unique to these service conditions. The critique

then identifies fundamental limitations of current modelling approaches, in particular their inability to couple hydrogen diffusion kinetics with mechanical damage accumulation under transport relevant loading spectra. By quantifying these knowledge gaps, particularly in the prediction of lifetime under cyclic pressure cycling in hydrogen environments, the analysis convincingly justifies the novel multi-physics damage model developed in this thesis. The chapter concludes by highlighting how this advancement addresses critical needs in hydrogen infrastructure design codes, where conventional approaches dangerously overestimate safe service life.

Building on Chapter 1's critical review of hydrogen transport pipe failure models, the second chapter provides the experimental validation required to develop the proposed lifetime prediction framework. This chapter systematically characterizes the mechanical behavior of filament-wound Glass/Epoxy pipes under three critical loading regimes: (1) static tensile loading to establish baseline strength (σ_{UTS}) and stiffness, (2) cyclic fatigue loading (40–60% and 80%) to quantify S-N relationships and damage progression rates, and (3) combined cyclic-static loading to assess residual strength degradation.

The third chapter develops an analytical model to predict the mechanical behavior of composite pipes under static and fatigue loading, building directly on Chapter 2's experimental results. The three-stage model first simulates static loading using elastic-plastic theory calibrated to the measured ultimate stress, then calculates progressive damage accumulation during cyclic loading based on the obtained S-N curves (40-80% UTS), and finally evaluates residual strength after combined loading sequences. Implemented in MATLAB, the model successfully reproduces the experimental failure progression (matrix cracking → delamination → fiber rupture) and predicts lifetimes of the multilayered composite pipe.

The last and the forth chapter is dedicated to present the main results of the model developed and compared to some experimental results obtained and present through chapter 2.

Finally we close this thesis by main conclusion and perspectives for the forthcoming studies.

Reference

1. Imen Feki, Mohammadali Shirinbayan, Samia Nouira, RobertTie Bi, JeanBaptiste Mae so, Cedric Thomas, Joseph Fitoussi. Composites in high-pressure hydrogen storage: A review of multiscale characterization and mechanical behavior Composites Part C: Open Access - Volume 16, March 2025, 100555. https://doi.org/10.1016/j.jcomc.2024.100555.
2. Shin-ichi Orimo, Yuko Nakamori, Jennifer R. Eliseo, Andreas Züttel, Craig M. Jensen .Complex Hydrides for Hydrogen Storage. Chemical reviews 107 (10), 4111-4132. https://pubs.acs.org/doi/10.1021/cr0501846
3. Elham Abohamzeh, Fatemeh Salehi, Mohsen Sheikholeslami, Rouzbeh Abbassi, Faisal Khan. Review of hydrogen safety during storage, transmission, and applications processes. Journal of Loss Prevention in the Process Industries - Volume 72, September 2021, 104569. https://doi.org/10.1016/j.jlp.2021.104569
4. James G. Speight, Laramie, WY. Heavy Oil Recovery and Upgrading. **Book** 2019 Pages 807-821 ISBN 978-0-12-813025-4 https://doi.org/10.1016/C2016-0-04682-X
5. M. ManojPrabhakar, N. Rajini, Nadir Ayrilmis, K. Mayandi, Suchart Siengchin, K. Sen thilkumar, S. Karthikeyan, Sikiru O. Ismail. An overview of burst, buckling, durability and corrosion analysis of lightweight FRP composite pipes and their applicability. Composite Structures Volume 230, 15 December 2019, 111419. https://doi.org/10.1016/j.compstruct.2019.111419
6. Ammar Maziz, Mostapha Tarfaoui, Lokman Gemi, Said Rechak, Mourad Nachtane. A progressive damage model for pressurized filament-wound hybrid composite pipe under low-velocity impact. Composite Structures - Volume 276, 15 November 2021, 114520. https://doi.org/10.1016/j.compstruct.2021.114520
7. Robert Hren, Annamaria Vujanović, Yee VanFan, JiříJaromír Klemeš, Damjan Krajnc, Lidija Čuček.Hydrogen production, storage and transport for renewable energy and chemicals: An environmental footprint assessment. Renewable and Sustainable Energy Reviews Volume 173, March 2023, 113113. https://doi.org/10.1016/j.rser.2022.113113
8. Allih John Eko, Jayantha Epaarachchi, Janitha Jewewantha, Xuesen Zeng. A review of type IV composite overwrapped pressure vessels. International Journal of Hydrogen Energy . Volume 109, 14 March 2025, Pages 551-573. https://doi.org/10.1016/j.ijhydene.2025.02.108

9. Ateeb Ahmad Khan, Indra Vir Singh, Bhanu Kumar Mishra, Ramadas Chennamsetti. A novel experimental method to evaluate the fatigue behaviour and damage evolution of bi-directional composites under variable amplitude loading. International Journal of Fatigue - Available online 7 April 2025, 108979. https://doi.org/10.1016/j.ijfatigue.2025.108979
10. Hamzat, A.K., Murad, M.S., Adediran, I.A. et al. Fiber-reinforced composites for aerospace, energy, and marine applications: an insight into failure mechanisms under chemical, thermal, oxidative, and mechanical load conditions. Adv Compos Hybrid Mater 8, 152 (2025). https://doi.org/10.1007/s42114-024-01192-y
11. Nerea deMiguel, Beatriz Acosta, P. Moretto, Laurent Briottet, Paolo Bortot, Elisabetta Mecozzi. Hydrogen enhanced fatigue in full scale metallic vessel tests – Results from the MATHRYCE project. International Journal of Hydrogen Energy- Volume 42, Issue 19, 11 May 2017, Pages 13777-13788 - https://doi.org/10.1016/j.ijhydene.2017.01.144.
12. T. Wang, O. Menshykov, M. Menshykova. Composite pipes failure under combined axisymmetric and asymmetric loading: Semi-analytical solution and stress superposition. Composite Structures - Volume 363, 1 July 2025, 119109. https://doi.org/10.1016/j.compstruct.2025.119109.
13. E.N. Buarque, J.R.M. d'Almeida. The effect of cylindrical defects on the tensile strength of glass fiber/vinyl-ester matrix reinforced composite pipes. Composite Structures 79 (2007) 270–279. doi:10.1016/j.compstruct.2006.01.011
14. Mehmet Emin Deniz, Mustafa Ozen, Okan Ozdemir, Ramazan Karakuzu, Bulent Murat Icten. Environmental effect on fatigue life of glass–epoxy composite pipes subjected to impact loading. Composites Part B: Engineering Volume 44, Issue 1, January 2013, Pages 304-312. https://doi.org/10.1016/j.compositesb.2012.05.001]
15. N. Tarakcioglu *et al.* Strength of filament wound GRP pipes with surface crack. Compos Part B – Eng (2001)
16. G. Meijer et al. A failure envelope for ±60° filament wound glass fibre reinforced epoxy tubulars Compos Part A – Appl Sci Technol (2008).
17. Imen Feki, Mohammadali Shirinbayan,Samia Nouira, Robert Tie Bi, Jean-Baptiste Maeso, Cedric Thomas, Joseph Fitoussi. Multi-scale fatigue damage analysis in filament-wound carbon fiber reinforced epoxy composites for hydrogen storage tanks. Composites Part C: Open Access 15 (2024) 100537. https://doi.org/10.1016/j.jcomc.2024.100537.

18. Mehmet Emin Deniz, Mustafa Ozen, Okan Ozdemir, Ramazan Karakuzu, Bulent Murat Icten. Environmental effect on fatigue life of glass–epoxy composite pipes subjected to impact loading. Composites Part B: Engineering Volume 44, Issue 1, January 2013, Pages 304-312. https://doi.org/10.1016/j.compositesb.2012.05.001
19. Nghiep Nguyen, Ba & Roh, Hee Seok & Merkel, Daniel & Simmons, Kevin. A predictive modeling tool for damage analysis and design of hydrogen storage composite pressure vessels,.International Journal of Hydrogen Energy 46(39):20573-20585(2021). DOI:10.1016/j.ijhydene.2021.03.139

CHAPTER I:

A REVIEW ANALYSIS

I-1.Introduction

Hydrogen has become an important element in the deep decarbonisation of the global energy system as a replacement for fossil fuels in all sectors, including industry, power generation, transport and heating. The development of the hydrogen chain has become increasingly necessary by establishing optimal production, efficient and adapted hydrogen storage, transport and distribution infrastructure.

The process of storing and transporting hydrogen is associated with risks [1]. These risks are due to its low volumetric energy density. Another limitation is the small size of the molecules, which can cause traditional steel structures to become brittle. Brittleness can lead to degradation and cause cracks or leaks. To minimise these disadvantages of hydrogen, the research of composites pipes is more than necessary [2].

Over the past decade, composite pipe has challenged traditional steel pipe in the oil and gas industry. It offers a lightweight, ductile, coilable and corrosion-free solution for transporting liquids and gases. Thousands of kilometres of composite pipe have been installed around the world. This is mainly for the transport of hydrocarbons and water. In order to extend the application of composite tubes to the hydrogen chain, mainly for transport and storage, research projects launched about ten years ago are working on competing with traditional steel solutions on two main aspects: cost and reliability.

Particularly in the field of hydrogen transport and storage, research has focused on determining the specific properties of composite materials (optimal shock absorption, high mechanical properties, good long-term strength, etc.). Recently, however, a design criterion that has become essential for the requirements of the hydrogen industry are the static and the fatigue design of transport and storage structures.

Composite materials are now used in highly stressed structures, mainly in the hydrogen field. In order to use the most suitable material for the intended application, while improving fatigue resistance, it is necessary to understand first the quasi-static behavior and the fatigue degradation mechanisms.

In composite pipelines used for hydrogen transport, axial tensile loading—generated by internal pressure, thermal expansion, or external mechanical forces—plays a critical role in influencing hydrogen diffusion and material integrity. Unlike isotropic metals, fiber-reinforced composites exhibit anisotropic behavior, meaning hydrogen transport and mechanical responses vary with direction (e.g., along fibers vs. through the matrix).

Axial tension in composite pipelines promotes hydrogen transport by creating microcracks and interfacial defects that act as diffusion pathways. Stress gradients drive hydrogen toward high-stress zones (e.g., crack tips), accelerating embrittlement. The anisotropic structure causes directional diffusion—slower along fibers but faster through damaged matrix regions. These interactions critically reduce pipeline integrity under hydrogen exposure.

Axial fatigue loading in composite pipelines arises primarily from operational pressure fluctuations**,** thermal cycling, and mechanical vibrations inherent to hydrogen transport systems. During service, pipelines experience repeated internal pressure variations as hydrogen is injected, withdrawn, or regulated, generating cyclic hoop and axial stresses. Temperature swings—from cryogenic hydrogen storage or environmental changes—induce thermal expansion/contraction stresses, particularly at constrained sections like joints or supports. Additionally, external dynamic loads, such as ground movement**,** pump-induced vibrations**,** or vortex-induced vibrations (VIV) in offshore pipelines, contribute to fatigue-inducing axial stress cycles. Unlike static loads, these time-varying stresses progressively damage the composite microstructure, creating a synergistic effect with hydrogen exposure that accelerates material degradation. The combination of mechanical fatigue and hydrogen diffusion is especially critical in Type IV composite tanks (polymer-lined carbon fiber vessels), where cyclic stresses can exacerbate microcracking in the matrix and liner, facilitating hydrogen permeation and embrittlement. Understanding these loading sources is essential for designing fatigue-resistant pipelines and predicting their lifespan in hydrogen service.

Axial tensile loading and axial fatigue loading are interconnected phenomena critical to the structural integrity of hydrogen transport pipelines, especially in demanding environments like offshore applications. Static axial tensile loads (e.g., from internal pressure or thermal expansion) create stress concentrations that initiate microcracks and accelerate hydrogen diffusion. However**,** cyclic axial fatigue loading (from pressure fluctuations, waves, or vibrations) progressively worsens this damage by extending cracks with each cycle, enhancing hydrogen trapping at crack tips, promoting embrittlement and finally accelerating failure at stresses below the material's static strength (hydrogen-assisted fatigue).

The mechanical behavior of composite tubes under combined tensile and fatigue loading presents critical challenges due to coupled damage mechanisms, defect-sensitive failure initiation, and inadequate load-sequence modeling. While tensile overloading is known to

accelerate subsequent fatigue damage, current approaches treat these loading regimes independently, and manufacturing flaws further complicate predictions by inducing premature failure. This review will systematically address these gaps by (1) synthesizing damage theories and principal models for composite pipe structures, (2) evaluating key fatigue parameters governing damage kinetics, and (3) assessing lifetime prediction models for realistic loading conditions. By quantifying tensile damage's role in fatigue life reduction and developing validated models, this work will enable more reliable life prediction and safer composite tube applications in pressure systems and structural components.

This chapter review focuses on an analysis of research into the assessment and prediction of fatigue life of damaged tubular composite structures.

I.2. Composite damage mechanism

Damage prediction is a key factor in the design of composite tubular structures. As shown in Figure 1, porosities, delaminations, cracks, fractures, and fibre/matrix separation are some of the most common types of damage that can occur during the life of a composite as a result of load levels or manufacturing. The accumulation of damage in composites is a consequence of the development of micro-defects, initially in the matrix, leading to fibre damage and eventual failure of the material due to delamination between the layers on one side and the resin fibres on the other (see Fig. I.1). These phenomena are modeled by Continuum Damage Mechanics (CDM) model, which has been successfully applied to model failure in composite structures.

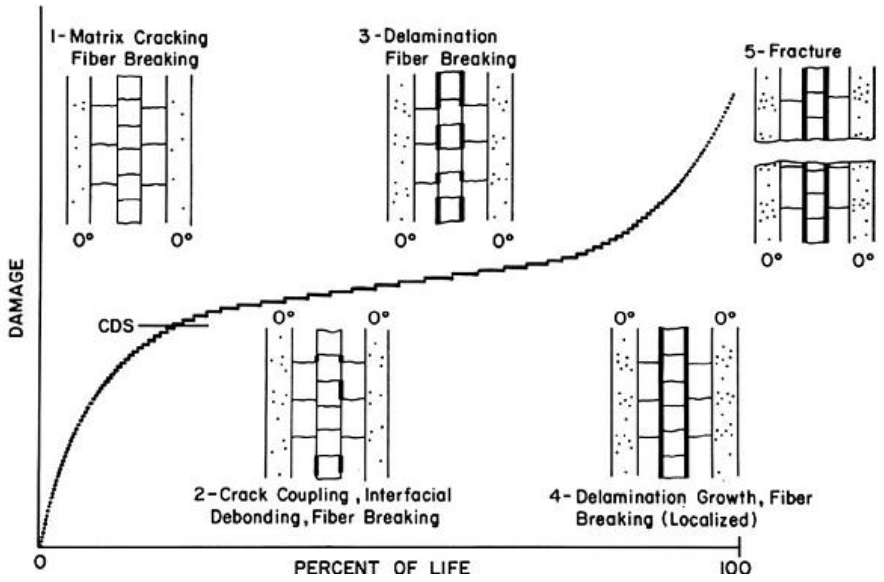

Fig. I.1.Damage accumulation during a composite material's lifetime [3].

I.2.1. Damage mechanisms

Damage mechanisms in long fiber laminate composites are now clearly identified. Different factors can influence the appearance and development of these degradations: the stacking sequence, the nature of the matrix, the manufacturing process, subjected to external stresses, the composite materials are the site of degradations at the level of the fibers (fiber breaks), the matrix (micro-voids, intra-laminar cracks) or at the level of the fiber / matrix interfaces (fiber / matrix de-cohesion) or inter-fold interfaces (delamination). **Fig. I.2** shows schematically the different mechanisms of damage. In what follows we propose to detail the characteristics of the different mechanisms.

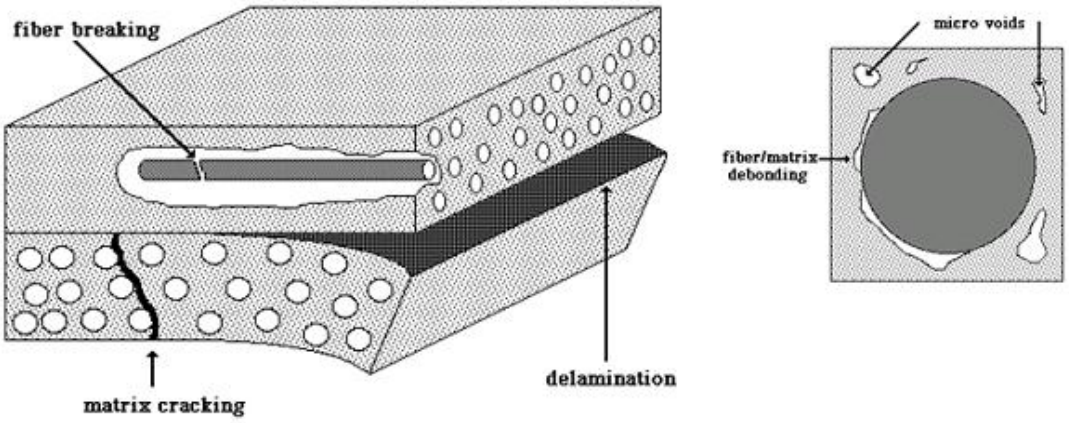

Fig. I.2. The different mechanisms of damage [4].

I.2.2. Matrix fiber decohesion and micro voids

At the microscopic level, decohesions appear at the interfaces between the different constituents (fibers and matrix). This is the first type of damage that occurs in composite materials. The zones of decohesion are privileged places for the initiation of the intra-laminar cracking (Fig. I.3). These degradations are initiated by micro-defects within each fold. Moreover, because of the manufacturing processes, the distribution of the fibers in the matrix is often random.

The work of Violleau, **[5]** shows that the distribution of fibers can be at the origin of stress concentration zones where decohesions can be initiated (Fig 1.4) also the manufacturing process may lead to the appearance of heat-induced stresses also responsible for decohesions. Adhesion problems between the fibers and the matrix as well as micro-voids that can coalesce to form a crack at the mesoscopic scale. The influence of decohesion fiber matrix yet difficult to evaluated.

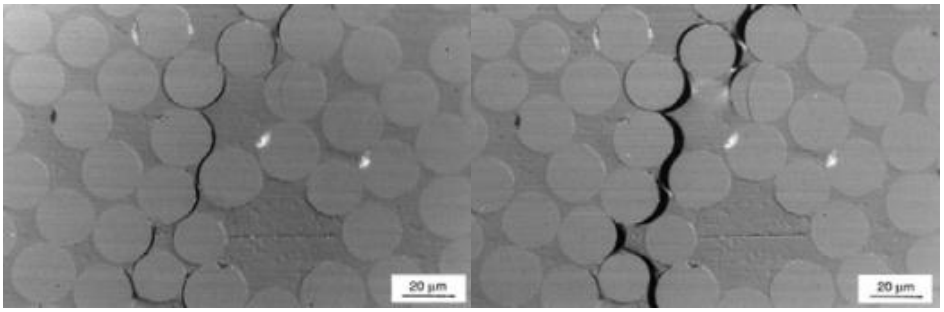

Fig. I.3.Fiber- Matrix Decohesion (a) and Coalescence in a crack (b) [6].

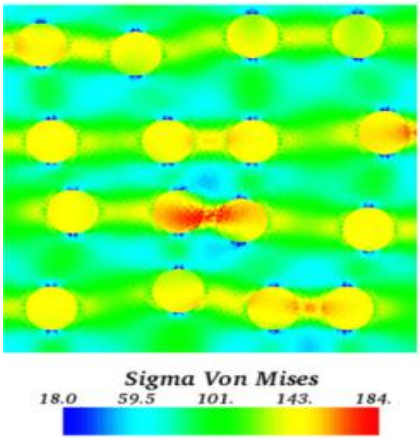

Fig. I.4.stress concentration in a composite fiber / matrix [6].

I.2.3. Intralaminar cracking

It appears first in the most disoriented folds with respect to the direction of loading (Fig. I.5) (it is recalled that one is placed in the case of a plate in uni-axial traction).

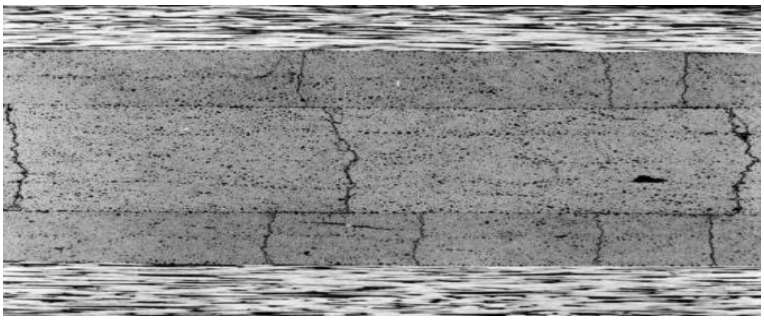

Fig. I.5.Network of transverse cracks [7].

I.2.4. Delamination

In the case of a laminated composite, an interlayer detachment mechanism called delamination. The different orientations of the folds forming the laminate lead to anisotropy differences relative to the reference frame which are causing interlaminar stresses. These

constraints drived the appearance and the propagation of delamination. A flat plate structure has free edges which may be at the origin of singularities at the interlaminar stresses close to the free edges.

This phenomenon, more commonly known as "edge effect", can accelerate the development of delamination. First studied analytically [8], [9], the singularities of free-edge constraints have long been the subject of numerous numerical investigations based on different techniques. Among the main ones we find. The finite difference method [10], the finite element method [11], multiparticulate models [12] or cohesive zone models [13].

I.2.5. Fiber breakage

In a stratified composite loading in tension, the fibers are solicited differently depending on the orientation of the fold in which they are located. Fiber breakage occurs abruptly in the folds, this phenomenon occurs mostly in the folds oriented in the direction of the solicitation. Camanho, P et all [14] find that the presence of cracks is at the origin of stress concentration zones favoring fiber breaks.

As show in the Fig.6, the occurrence of fiber breaks generally leads to completed failure of the laminate.The power of computers today allows to study this phenomenon within real structures (tank type) by the finite element method using a process multi-scale [15].

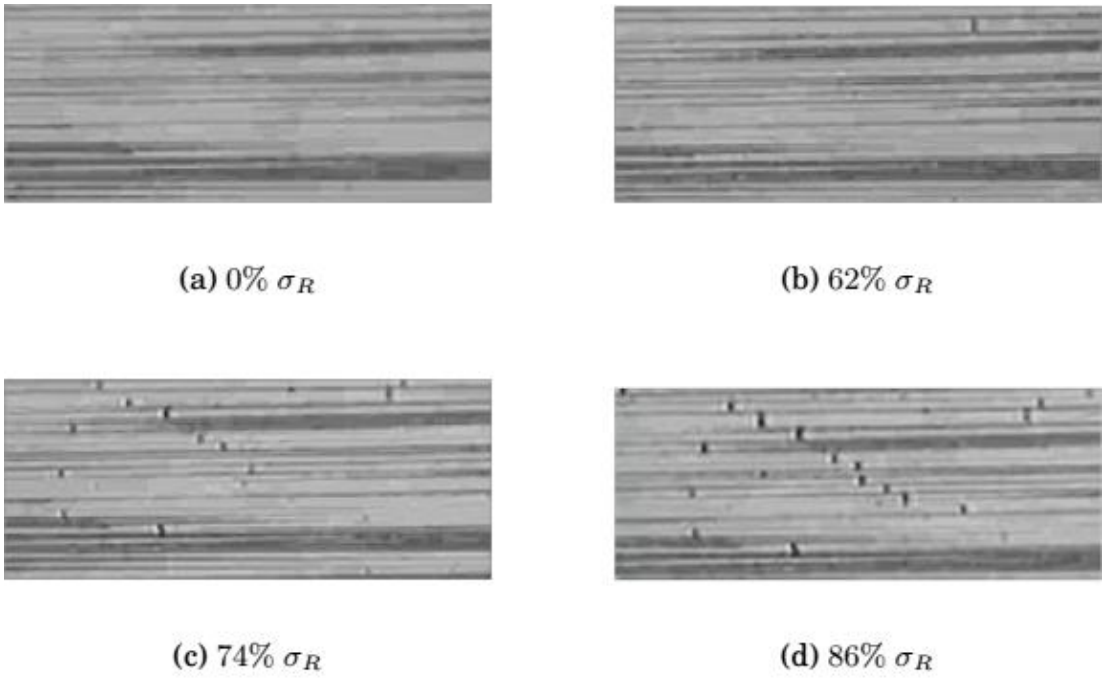

Fig. I.6. Illustration of breakage damage of fibers in composite laminate [16].

I.3. Damage modelling approaches types

The first studies consisted of applying decades of knowledge on metals to composites .These empirical methods (Wöhler curve) use a fracture criterion to understand the behaviour of any stack, but are disconnected from the physics of degradation. In particular, they do not reflect their progressive aspect.

J. DEGRIECK et al [17] have classified the main models proposed in recent decades into *three broad categories:*

- **Lifetime models'** do not really take into account the degradation mechanism (such as transverse cracks in the matrix, fibre breakage, etc.), but use the S-N failure curve (or Goodman diagram) and introduce certain fatigue failure criteria, these approaches require considerable experimental work.

- Phenomenological' models relate to residual stiffness and strength. These models propose an evolutionary law for the degradation of properties on the macroscopic scale of laminates.

-Finally, '**progressive damage models'** introduce one or more damage variables to describe the degradation of composite laminates damage variables to describe the degradation of composite laminate

1-The mechanical approach to fracture.

2-Thermodynamic formalisms with internal variables associated with cracks: (vector variables, scalar variables, etc)**.**

H. NOURI et al [19] proposed another classification, where five types of approach have been adopted:

a**) Empirical approaches**: These models are based on experimental results obtained for specific stresses and models. Empirical theories can be used to obtain (S-N) curves. However, these theories should be used with caution in certain test configurations where the stress field is complex .

b) - **Approaches based on residual resistance:** These fall into two categories:

Probabilistic models and Phenomenological models. These models have been developed for the uniaxial case and do not take into account the behaviour of composites under complex loading.

c)- Approaches based on fatigue failure criteria: These are derived from a quadratic criterion usually used for static loading. criterion usually used for static loading. The fitting parameters of these models are highly dependent on the stress level applied.

d)- **Micromechanical approaches:** These approaches are based on observations of damage mechanisms and local measurements at the microstructure scale. The overall behaviour of the damaged material is obtained by homogenisation techniques on the VER. The major disadvantage of these approaches is that they are too local. It is difficult to obtain a macroscopic variable and an evolution law that can be easily used in calculation codes on the scale of a structure.

e)- **Macroscopic approaches:** These approaches are based on the thermodynamics of irreversible processes. They use internal state variables defined on a VER, which constitutes the modelling scale. The behaviour of the damaged material is obtained by energy equivalence with an equivalent homogeneous material. Furthermore, these approaches remain global and do not distinguish between the different damage processes and their interaction.

I.4. Principal models of composite damage

Research into the modelling of damage in initially anisotropic materials is fairly well developed. The main difficulty lies in modelling the interaction and coupling effects between primary anisotropy and damage-induced anisotropy. In the context of anisotropic materials, existing damage models are built within a macroscopic framework. They are essentially based on the choice of internal variables characterising the damage, and use the classic formalism of the thermodynamics of irreversible processes. Numerous phenomenological models have been introduced in recent years to study fatigue in composite materials. Kachanov [18] was the first to introduce the notion of an internal damage variable to translate the loss of stiffness in isotropic materials. This idea was then extended to anisotropic materials by Cordebois and Sidoroff **[19].** The state of damage is defined by a finite number of internal $\boldsymbol{d_\alpha}$ *(d= dα , α=1,…n)*. According to Marigo [20], once the state of damage has been defined, the macroscopic elastic behaviour of the damaged material can be calculated as a function of its stiffness $C_{ijkl} = C_{ijkl}(d_a)$.In the following paragraph, we present some macroscopic modelling of damage in composites.

I.4.1. Miner's linear law [21]

The Palmgren-Miner law, the first and most widely used, relates damage to the cumulative life fractions at each stress level. The assumptions of this law are as follows:

- The loading is sinusoidal.

- The work absorbed by the material leads to fatigue failure.

- The propagation of a macroscopic crack is the indicator of the total damage to the material.

- The experimental behaviour of the material is represented by the endurance diagram and the modified Goodman line.

$$d = \sum \left(\frac{n_i}{N_{fi}} \right) \quad \text{(I.1)}$$

with :

d: cumulative damage

N_i : Number of cycles at stress level $\boldsymbol{\sigma_i}$

N_f : number of cycles to failure (service life) at stress level $\boldsymbol{\sigma_i}$

Failure occurs when d = 1 (critical damage)

The main shortcomings of the model are: the linearity of the accumulation, and its independence from the loading history. Nevertheless, this model is still the most widely used because of its simplicity.

I.4.2. Chang's model [22]

The model proposed by Chang is a one-dimensional model of a unidirectional composite loaded in cyclic tension. It uses a thermodynamic approach coupled

to damage kinetics, using a scalar variable d:

$$d = 1 - \frac{E}{E_0} \quad \text{(I.2)}$$

With E and E_0 the Young's modulus of the damaged material and that of the virgin material.The free energy is taken as the thermodynamic potential, which in the case of a damaged material is written:

$$Wl = \frac{1}{2}(1 - d)E\varepsilon^2 + \in \left(\bar{d}\right) \quad \text{(I.3)}$$

Where

$\bar{d}$: is a cumulative variable.

In the case of a periodic tensile test and d varies very little during each cycle, the evolution law is written as follows:

$$\frac{\partial d}{\partial N} = A \frac{\Delta \varepsilon^b}{(1-d)^{-1}} \tag{I.4}$$

Where A and b are material parameters. They are influenced by the ratio R, the frequency $\boldsymbol{f}$ and the level of loading imposed. Equation (I,4) shows that at constant strain damage evolves linearly.

I.4.3. Chaboche's continuous non-linear law [23]

The law modelling fatigue damage, known as the NLCD (Non-Linear Continuous fatigue Damage model) makes it possible to determine the damage accumulated during each cycle according to the expression:

$$\frac{\delta d}{\delta N} = f_F(\sigma_M, \bar{\sigma}, d, T) \tag{I.5}$$

Where $\boldsymbol{\sigma_M}$ is the maximum stress seen during the cycle $\bar{\boldsymbol{\sigma}}$ is the average stress ,$\boldsymbol{T}$ is the temperature and d is the damage variable, $\boldsymbol{f_F}$ is a function of the variable $\boldsymbol{d}$, a property that allows in conjunction with the introduction of a loading-dependent exponent $\boldsymbol{\alpha}$ to obtain a non-linear evolution of the damage under cyclic loading. The specific form chosen for the law (14) is as follows:

$$\frac{\delta d}{\delta N} = d^{\alpha(\sigma_M, \bar{\sigma})} \left[\frac{\sigma_M - \bar{\sigma}}{M(\bar{\sigma})}\right]^{\beta} \tag{I.6}$$

The integration of this equation for the maximum stress isσ_M

A constant average stress $\bar{\sigma}$, between $\boldsymbol{d = 0}$ and $\boldsymbol{d_c}$ = 1 gives the number of cycles to $\boldsymbol{N_{RF}}$ fatigue failure:

$$d = \left(\frac{N}{N_{RF}}\right)^{\frac{1}{1-\alpha}} \tag{I.7}$$

$$N_{RF} = \frac{1}{1-\alpha}\left[\frac{\sigma_M - \bar{\sigma}}{M(\bar{\sigma})}\right]^{\beta} \tag{I.8}$$

The function $\boldsymbol{M}$ is chosen to describe the linear relationship between the mean stress and the fatigue limit. We can write:

$$M(\overline{\sigma}) = M_0(1 - b\bar{\sigma}) \tag{I.9}$$

Or b and M_0, just as α and β are material-dependent parameters.

Model identification is easier if the α function is written as follows:

$$\alpha = 1 - \alpha < \frac{\sigma_M - \sigma_{l(\bar{\sigma})}}{\sigma_u - \sigma_M} \quad (I.20)$$

$$\sigma_{l(\bar{\sigma})} = \bar{\sigma} + \sigma_{l0}(1 - b\bar{\sigma}) \quad (I.21)$$

is the maximum fatigue Where σ_{l0} is the fatigue limit when $\bar{\sigma} = 0$ (alternating fatigue) $\sigma_{l(\bar{\sigma})}$ limit at non-zero mean stress $(\bar{\sigma} \neq 0)$.The positive part in the expression of α causes it to take the value 1 when the maximum stress is less than the fatigue limit $\sigma_{l(\bar{\sigma})}$.We can then calculate the number of cycles to failure in pure N_{RF} fatigue :

$$N_{RF} = \frac{\sigma_u - \sigma_M}{\alpha < \sigma_M - \sigma_l(\bar{\sigma}) >} \left(\frac{\sigma_M - \bar{\sigma}}{M(\bar{\sigma})}\right)^{-\beta} \quad (I.22)$$

The ultimate tensile stress σ_u plays no role in fatigue at a high number of cycles, but is used as a normalisation parameter, capable of representing the asymptotic shape of fatigue life curves during regimes with a very low number of cycles.

Relation (21) also translates the limiting cases, when $N_{RF} = 0$ for $\sigma_M = \sigma_u$ and when $N_{FR} = \infty$ for $\sigma_M = \sigma_l(\bar{\sigma})$.It correctly describes the fatigue life curves for numbers of cycles ranging from 10 to 107. The cumulative effects can only be described by specifying the ultimate tensile stress and the fatigue limit. This formulation allows test results for a wide range of materials to be described quantitatively.

However, evaluating d through the remaining service life is not sufficient to fix its value completely at each moment. A second type of evaluation is therefore used, based on the concept of effective stress, the measured evolution of which is extremely non-linear. To combine this evaluation with that corresponding to the remaining service life, we change the variable by replacing d by $1 - (1 - d)^{\beta+1})$. The differential law can then be written as follows:

$$\frac{\delta d}{\delta N} = \left[1 - (1 - d)^{\beta+1}\right]^{\alpha(\sigma_M, \bar{\sigma})} \left[\frac{\sigma_M - \bar{\sigma}}{M(\bar{\sigma})(1-d)}\right]^{\beta} \quad (I.23)$$

The number of cycles to failure becomes :

$$N_{RF} = \frac{1}{(1-\beta)[1-\alpha(\sigma_M, \bar{\sigma})]} \left(\frac{\sigma_M - \bar{\sigma}}{M(\bar{\sigma})}\right)^{-\beta} \quad (I.24)$$

I.4.4. Lin Ye model [24]

This model is based on the variation of the fatigue crack propagation with respect to the number of cycles ∂a /∂N. This variation is written according to the Paris formula:

$$\frac{\partial a}{\partial N} = C(\Delta K)^n = C_1(S_a^2 a)^m \quad (I.25)$$

Where C_1, C, m and n as well as S_a are material constants. By analogy, the author proposes a fatigue law for composites: if the applied cyclic stress is :

$$\frac{\partial a}{\partial N} = C\left(\frac{\sigma_{max}^2}{d}\right)^n \quad (I.26)$$

Where C and n are material constants, $\frac{\sigma_{max}^2}{d}$ is the rate of damage development and $\sigma_{max}$is the maximum stress. Integrating equation (I.26), with initial conditions d = 0 when N = 0, gives the following expression :

$$d = ((n+1)C.N.\sigma_{max}^{\frac{2n}{n+1}} \quad (I.27)$$

The number of cycles corresponding to critical damage:

$$N_1 = \frac{d_c^{n+1}}{(n+1)C\sigma_{max}^2} \quad (I.28)$$

Where $\mathbf{d_c}$: critical damage.

The damage degradation model is written as follows:

$$\frac{dE}{dN} = -E_0.C\left(\frac{\sigma_{max}^2}{1-\frac{E}{E_0}}\right) \quad (I.29)$$

$$\frac{E}{E_0} = 1 - [N.C(n+1)]^{\frac{1}{1+n}}.\sigma_{max}^{\frac{2n}{n+1}} \quad (I.30)$$

This model can be used to predict the fatigue life of composite materials in the uniaxial case, and has been formulated in terms of stress.

I.4.5. Ladevèze and Dantec model [25]

The model is based on damage mechanics and uses internal variables to describe the progressive reduction in layer stiffness.The evolution of these damage variables depends on monotonic and cyclic static loading. For unidirectional layers, damage is defined at the mesoscopic scale by two scalars representing the degradation of the transverse modulus of elasticity E_2 and the planar shear modulus G_{12}.

On compression transverse to the fibres, the cracks close and the modulus of rigidity returns to its initial value. This model also does not consider damage in the direction of the fibres. The author therefore defines two scalar damage variables, ***d*** and ***d'***, to express the loss of layer stiffness:

$$\begin{cases} E_2 = E_2^0(1-d') \ \ withe\ d' \in [0,1] for\ \sigma_2 \geq 0 \\ \ \ G_{12} = G_{12}^0 \ \ withe \ \ d \in [0,1] \\ E_2 = E_2^0 \ for\ \sigma_2 < 0 \end{cases} \quad (I.31)$$

These two variable damage scalars are assumed to be constant throughout the thickness of the ply. They are associated with cracks parallel to the fibre direction. The plane strain energy is written as :

$$E_D = \frac{1}{2}\left[\frac{\sigma_1^2}{E_1^0} - \frac{2\nu_{12}}{E_1^0} + \frac{<\sigma_2>_+^2}{E_2^0(1-d)} + \frac{<\sigma_2>_-^2}{E_2^0} + \frac{\sigma_{12}^2}{2G_2^0(1-d)}\right] \quad (I.32)$$

Where

$$< a >_+ = a \ if \ a > 0 \ et \ < a >_+ = 0 \ \ if \ a < 0$$
$$< a >_- = a \ if \ \ a < 0 \ et \ < a >_+ = 0 \ \ if \ a > 0$$

The thermodynamic forces associated with the damage variables can be deduced from the potential by partial derivation from the damage variables and are expressed as a function of the stresses in the fold as follows:

$$\begin{cases} Y_d = \frac{1}{2} \ \frac{\sigma_{12}^2}{G_{12}^0(1-d')^2} \\ Y_{d'} = \frac{1}{2} \ \frac{<\sigma_2>_+^2}{E_{12}^0(1-d')^2} \end{cases} \quad (I.33)$$

The evolution of damage is modelled by using two experimental laws linking the variables d and d‘ and the corresponding associated thermodynamic forces $\boldsymbol{Y_d}$ and $\boldsymbol{Y_{d'}}$. These laws take account of the loading history. It is therefore necessary to introduce the maximum values in time:

$$\begin{cases} \underline{Y_d}(t) = sup_{\tau<t}\left(Y_d(\tau)\right) \\ \underline{Y_{d'}}(t) = sup_{\tau<t}\left(Y_{d'}(\tau)\right) \end{cases} \quad (I.34)$$

These reflect the fact that the damage is dependent on a state of maximum stress during the entire history of the load. It will only evolve if this level is exceeded.

The author defines an equivalent thermodynamic force Y:

$$\underline{Y} = \underline{Y_d} + b.\underline{Y_d} \quad (I.35)$$

The coefficient b expresses the combination of shear and transversal tension. Finally, the laws of static damage evolution:

$$\begin{cases} d = \frac{<\sqrt{Y(t)}-\sqrt{Y_0}>_+}{\sqrt{Y_C}-\sqrt{Y_0}} \; si \; d > 1 \, , sinon \; d = 1 \\ d' = b'd \;\; si \; d' < 1 \; et \; Y'_d \, , sinon \; d' = 1 \end{cases} \quad (I.36)$$

The constants $\boldsymbol{Y_c}$, $\boldsymbol{Y_0}$, and $\boldsymbol{b'}$ depend on the material.

I.4.6. Model (CDM) for composite materials [26]

A new formulation of the damaged elastic behaviour of composite materials is expressed within the framework of Damage Mechanics. The originality of this modelling lies in the combination of variables of different natures describing the state of damage of the material. Depending on the compromise between the reinforcement and the matrix, the defects can be oriented either by the microstructure, translated by a family of scalar variables, or by the loading, which leads to the use of tensorial variables. This model can be used to describe all the essential phenomena observed in composites: initial anisotropy, induced anisotropy (i.e. the effects of damage on elastic behaviour), defect evolution laws, closure effects in relation to residual deformations, etc. This model is specific to ceramic matrix composites.

I.4.7. Van Paepegem and Degrick model [27]

This model shows the degradation of the normalised Young's modulus as a function of the normalised number of cycles. It shows 3 stages in the evolution of (E/E_0). The proposed model is based on the sum of two functions. The damage rate is written as:

$$\frac{\partial d}{\partial N} = f_i(\sigma, d, \dots) + f_p(\sigma, d, \dots) \quad (I.37)$$

$\boldsymbol{f_i}$ describes the first stage of damage in composites, while the second and third stages of damage are taken into account through the $\boldsymbol{f_i}$ the authors propose :

$$f_i(\sigma, d, \dots) = C_1(\sigma^*)^m . e^{-C_2 d} \quad (I.38)$$

Where damage $\boldsymbol{d}$ is a scalar value between 0 and 1, C1 and C2 are material constants, σ^* is the measured stress, m is a parameter. The second function $\boldsymbol{f_p}$ is written as:

$$f_p(\sigma, d, \dots) = C_3(\sigma^*)^n \quad (I.39)$$

Where $\boldsymbol{C_3}$ is a material constant and $\boldsymbol{n}$ is a parameter.

I.4.8. Sedrakian model [28]

variable and is written as follows:

$$\varphi = \frac{\alpha_{11}}{1-\beta_{11}} Y_{11}^{\beta 11} + \frac{\alpha_{22}}{1-\beta_{22}} Y_{22}^{\beta 22} + \frac{\alpha_{12}}{1-\beta_{12}} Y_{12}^{\beta 12} + \frac{\alpha_{13}}{1-\beta_{13}} Y_{13}^{\beta 13} + \frac{\alpha_{23}}{1-\beta_{23}} Y_{23}^{\beta 23} \quad (I.40)$$

I.4.9. Nouri model [19]

The author has proposed an extension of Sedrakian's model [20] in order to incorporate the characteristic damage kinetics of reinforced thermoplastics, which makes it possible to take into account the rapid fall in the elastic characteristics of the material during the first cyclic loadings. The modifications are based on the idea of enriching the functional translating the dissipation potential $\boldsymbol{\varphi}$. This has been rewritten by adding five exponential terms. The number of parameters in the damage law was thus doubled:

$$\varphi = \frac{a_{ij}}{1+B_{ij}} Y_{ij}^{\beta_{ij}} + \gamma_{ij} \frac{\gamma_{ij}^2}{2} e^{-\lambda_{ij}.N} \quad (I.41)$$

I.4.10. Thollon model [31]

The model, based on cumulative damage, is used to describe the evolution of damage under static and fatigue loading. The evolution of static damage depends on the maximum loading and takes into account the coupling between tension and shear. The evolution of fatigue damage depends on the maximum loading but also on the amplitude of the loading. The range of validity of this model is limited to the failure of the first ply and does not describe delamination. The author has presented a unified behaviour model that can be used to describe the failure of laminated composites made up of unbalanced woven plies under static and fatigue loading. A law for the evolution of fatigue damage as a function of the number of cycles can be defined:

$$\frac{\partial d_i^f}{\partial N} = C < (\Delta Y_i)^a (Y_i)^\beta - \left(Y_{0f}\right)^{\alpha+\beta} >_+ \quad for\ i = 1{,}2\ and\ 12 \quad (I.42)$$

With $\Delta \boldsymbol{Y}_I = \boldsymbol{Y}_{max} - \boldsymbol{Y}_{min}$ over the cycle and Y_{0f} the endurance limit.

During cyclic loading, the evolution of fatigue damage implies a growth in cumulative damage and can therefore, via the equivalent force Y, provoke an evolution in static damage. If monotonic loading is imposed after this cyclic loading, the continuity of the damage is ensured. The models mentioned above are summarised in Table (1).

Tab.I.1. Synthesis of the principal models of composite damage.

Authors - year	*Damage variable formulation*	*Materials*	**Experimental test**
Miner-1945	$d = \sum \left(\frac{n_i}{N_{fi}} \right)$	Material in general	Linearity of accumulation Independence from loading history
Chang-1980	$d = 1 - \frac{E}{E_0}$ $\frac{\partial d}{\partial N} = A \frac{\Delta \varepsilon^b}{(1-d)^{-1}}$	Unidirectional composite	Uniaxial loading Linearity of accumulation at imposed deformation
Chaboche-1988	$\frac{\delta d}{\delta N} = f_F(\sigma_M, \bar{\sigma}, d, T)$	Material in general	Accumulation dependent on σ_u only, Damage evolution insufficient.
Lin Ye-1989	$\frac{\partial a}{\partial N} = C \left(\frac{\sigma_{max}^2}{d} \right)^n$	Composite materials	Uniaxial loading Stress formulation
Ladevèze-1992	$d = \frac{< \sqrt{Y(t)} - \sqrt{Y_0} >_+}{\sqrt{Y_C} - \sqrt{Y_0}}$ $d' = b'd$	Unidirectional composite	Constraint formulation Two-stage evolution
Maire-1997	$d = \frac{\Delta E}{E_0}$ $d = \frac{\sqrt{E_0} - \sqrt{E}}{\sqrt{E_0}}$	Composite with brittle matrix, ceramic, concrete, organic	Tensor damage (order 4) Combination of energy and deformation equivalence
Van Paepegem-2002	$\frac{\partial d}{\partial N} = C_1 (\sigma^*)^m . e^{-C_2 d} + C_3 (\sigma^*)^m$	Composite materials	Stress formulation Uniaxial loading Delamination neglect
Sedrakian-2002	$d = 1 - \frac{E}{E_0}$ $\varphi = \frac{a_{ij}}{1 + B_{ij}} Y_{ij}^{\beta_{ij}}$	Thermosetting matrix composite, orthotropic configuration	Damage evolution in two stages
Nouri-2009	$\varphi = \frac{a_{ij}}{1 + B_{ij}} Y_{ij}^{\beta_{ij}} + \gamma_{ij} \frac{Y_{ij}^2}{2} e^{-\lambda_{ij} . N}$ $d = 1 - \frac{E}{E_0}$	Reinforced thermoplastic composite	Neglect of viscosity effect, loading speed and frequency
Thollon-2010	$\frac{\partial d_i^f}{\partial N} = C < (\Delta Y_i)^a \, (Y_i)^\beta - \left(Y_{0f} \right)^{\alpha+\beta} >_+$	Thermoset matrix composites from unidirectional to balanced wovens	Limited to the first fold break

I.5.Fatigue parameters influencing the kinetics of damage

Many variables are commonly used to define fatigue loading this variables related to mechanical stress and that reflect environmental conditions. The most commonly used parameters for characterizing fatigue load (mechanical) are shown in Figure I-12 in the case of imposed sinusoidal stress .Some of these variables are more influential than others.

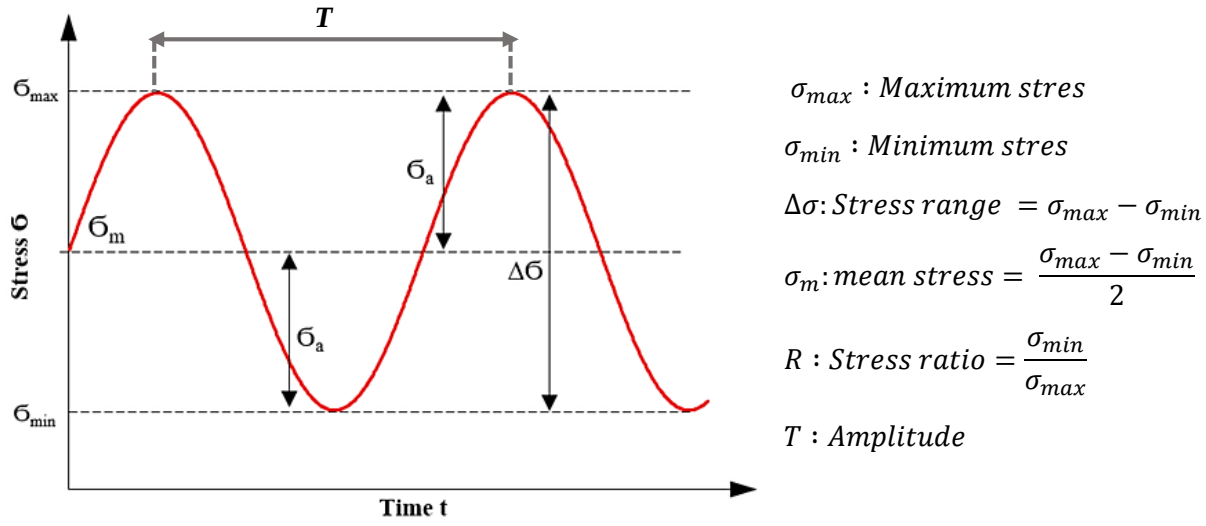

Fig.I.12. Presentation of the parameters of a fatigue mechanical loading

I.5.1.Maximum stress

Linhone 1996 **[31]** and Reifsnider ,1998 **[32]** present curves of loss of modulus of textile composites stressed in fatigue at different maximum load levels.They show that the maximum stress has an important influence on the evolution of the damage. whene the maximum stress is greater the,the damage development is mor faster (Figure I-13,).

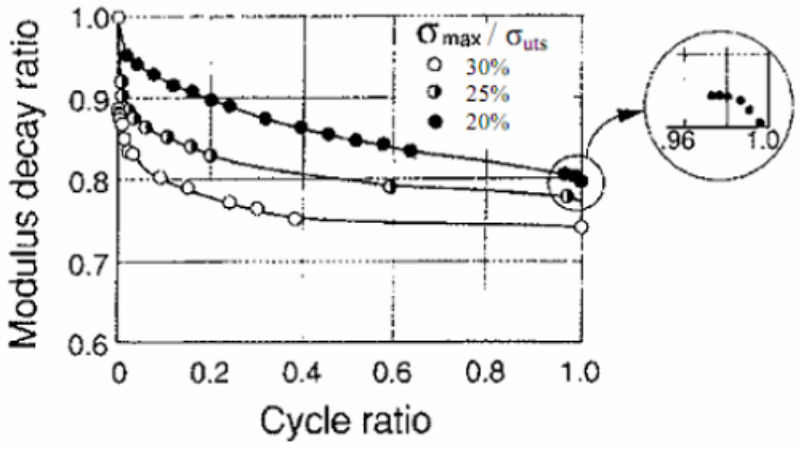

Fig.I.13. Evolution of the fatigue modulus according to different loading levels [32]

I.5.2.Load report

This load report allows three types of fatigue tests to be described (uniaxial): traction-traction fatigue tests (TT) with 0 <Rσ <1, alternating traction-compression (TC) fatigue tests with -∞ <Rσ <0 and compression-compression fatigue tests (CC) with 1 <Rσ <+ ∞.

The work of [33,34,35] on glass / epoxy woven fabrics in TT show that the Rσ ratio has little influence on the service life for tests in the axes, but a lot of influence during off-axis tests, where the effects of damage on the mechanical behavior are more important.

I.5.3-Frequency and Temperature

Pandita et al [36] (for 2D woven fabrics) and Kelkar and Whitcomb [37] (for braided fabrics) give the same observation for the frequency, tested in ranges going from 0.5Hz to 5Hz ,they concluded, that whene the frequency is higher the off-axis influence tends to decrease the life of the material. Perreux and Thiébaud [38] study the influence of frequency (from 0.02Hz to 5Hz) on the number of cycles at break of a UD [± 55] glass / epoxy ply laminate (Figure I-14).

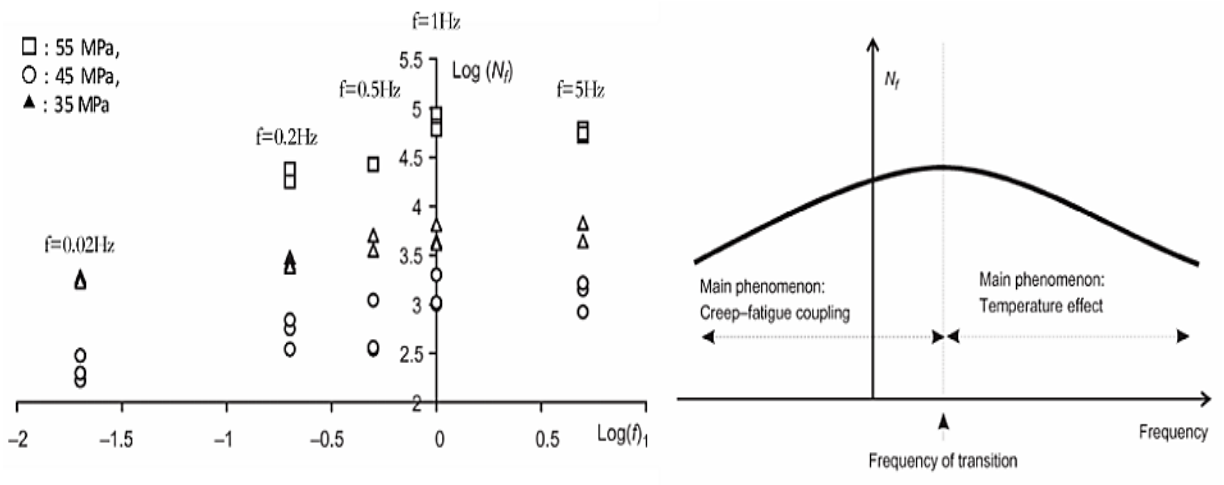

Fig.I.14. Effect of frequency on the number of failure cycles [38]

They show that the effect of frequency is linked to two phenomena with contradictory actions on the service life (defined in number of cycles): temperature and fatigue-creep coupling. When the frequency is higher, the energy dissipation linked to the viscous phenomena of the matrix causes an increase in the temperature of the specimen during the fatigue tests (a phenomenon which is greatly amplified in the presence of damage).

I.5.4. Effect of Humidity

Perreux and Thiébaud [39] show that humidity plays an important role in the lifestime of glass / epoxy laminates by testing specimens which have been immersed for different periods in water (between 15 days and 18 months). Humidity can have two actions that decrease lifetime: swelling, adding internal stresses, and degradation by aging.

I.6. Fatigue damage of composites and it's effect

The cyclic loading creates damage in to composites. When the number of cycles performed (n) is less than the life of the structure (N_f), it is important to quantify this damage in order to estimate the residual life of the structure. This is because the residual strength of the material decreases as the fatigue test continues**.**

The most studied indicators to characterize the damage progress of the material during the fatigue test are the evolution of deformation and modulus ,residual strength and crack density. As an indication, work having focused on the evolution of these indicators in the life of structures, are listed in Tab.I.2

Table I.2. Classification of previous work by topic resarch.

Topic Research	References
Module / rigidity	[40] [41] [42] [43] [44] [45] [46] [47] [48] [49] [50] [51] [52] [53] [54].
Hysteresis energy, amortization	[47] [50] [55] [56] [59] [60] [61] [62]
Deformations characteristics	[44] [45] [46] [52] [63] [64] [65] [66] [67].
Residual resistance	[68] [70] [71] [72] [73] [74] [75]
Crack density	[40] [76] [77] [78] [79] [80] [81] [81] [83] [84] [85] [86].

I.7. Models to predict lifetime

The first studies on the modeling of fatigue phenomena in composite materials consisted in transposing the knowledge acquired in metallic materials to composite materials. These were then empirical methods, based on failure criteria, which made it possible to address any mechanical behavior of stacking, while hiding the physics of the damage.

I.7.1. Macroscopic approaches (global)

The macroscopic approaches does not take into consideration the damage mechanisms but make it possible to predict the number of cycles N_f from which failure occurs under a fixed and given fatigue loading. These data are based on the use of WÖHLER curves, also called S-N curves or endurance curves. The WÖHLER curves, initially developed for metallic materials, are used to determine the service life Nf (number of cycles to failure) according to the amplitude of the uniaxial cyclic stress, for a load ratio R=MAX-MIN and a fixed frequency f (FIG. 2.28). These curves are obtained by uni-axial fatigue tests under cyclic amplitude loads constant.

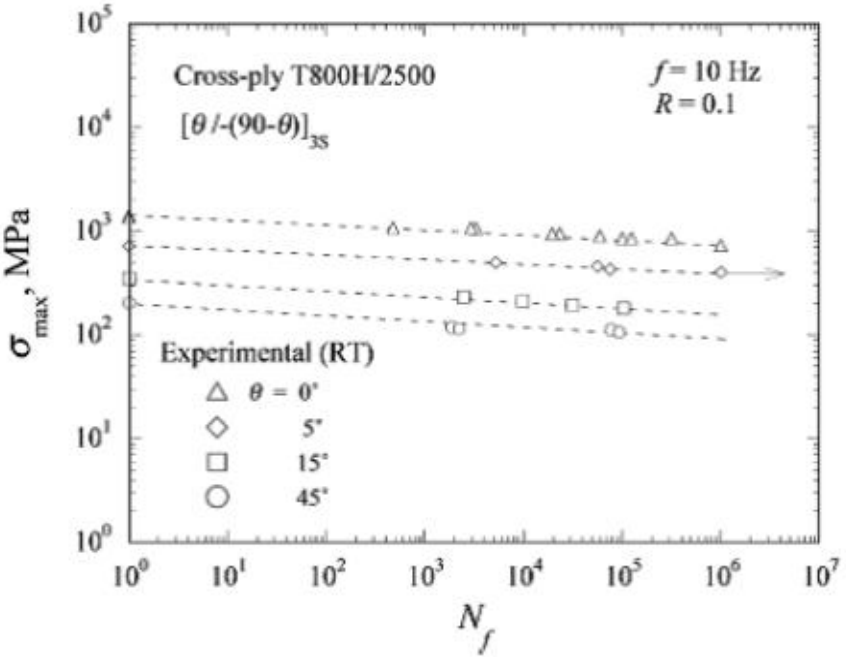

Fig.I.28. WÖHLER curves of a cross-ply laminate composite for different orientations [87]

-Use of a failure criterion

One of the first fatigue criteria for composite materials was proposed by HASHIN and ROTEM [88]. They describe the fiber failure (Equ. I.43) and matrix cracking.

$$\sigma_A = \sigma_A^u \qquad (I.43)$$

$$\left(\frac{\sigma_T}{\sigma_A^u}\right)^2 + \left(\frac{\tau}{\tau^u}\right)^2 = 1 \qquad (I.44)$$

Where $\sigma_A$and $\sigma_T$are respectively the stresses in the axis of the fibers and perpendicular to the fibers, τ is the shear stress, σ_A^u , σ_A^u and τ^u are respectively the ultimate stresses in axial traction , traction in the transverse direction and shear .The ultimate stresses are identified for fixed triplet (σ ,*R, N*) .The criterion is identified use the curves (S-N) obtained for cyclic uni-axial tests tensile on a uni-axial laminate in out of there axis direction.

This criterion dose not take into account the gradual nature of the damage and dose not give physical meaning to the damage.

Moreover this criterion is only valid for unidirectional composites with the condition of being able to differentiate the two types of damage et time of failure .The main criticism that can be do it with the different approaches that we have just presented lies in the fact that they require a large number of experimental data for each material, stack or type of loading. Moreover, these approaches are difficult to extend to the multi-axial case. Finally, they do not give any physical meaning to the damage and obscure the progressive nature of the latter. On the other hand, these approaches have the advantage of being very simple to implement and require very little information on the damage mechanisms

I.7. 2-Phenomenological approaches

-Residual Rigidity

These models based on the use of residual Rigidity aim to describe the degradation of the elastic properties of a material subjected to fatigue loading.

SIDOROFF and SUBAGIO [89] propose a uni-axial model developed in the context of unidirectional composite materials loaded in the direction of the fibers. The model is written in deformations, they introduce a damage variable D and separate the fields of tension and compression

$$\sigma_{11} = E(D)\varepsilon_{11} \qquad (I.45)$$

$$E(D) = E_0(1-d) \quad \text{(I.46)}$$

$$\frac{dD}{dN} = \begin{cases} \frac{\alpha(\Delta\varepsilon_{11})^c}{(1-D)^b} & traction \\ 0 & compression \end{cases} \quad \text{(I.47)}$$

$$D = 1 - \frac{E}{E_0} \quad \text{(I.48)}$$

With E_0 is the longitudinal Young modulus of undamaged material, a, b and c three constant characteristics of the material are identified. σ And ε the uni-axial stress and strain respectively, $\Delta\varepsilon$ amplitude of the strain. the model is identified by a 3-point bending test.

The parameter a plays the role of a scaling factor. It is identified by smoothing the curve representing the evolution of rigidity $\frac{E}{E_0}$ according to $\frac{E}{E_{90}}$ where E_{90} corresponds to the value of E for a falling in stiffness equal 10% .The parameter b controls the degradation process and c is identified by smoothing the curve $\sigma_{max} = f(N_{90})$. The modeling propose does not give information on the state of damage of the material, moreover it does not allow to consider the influence of the load ratio *R* and the frequency *f*.

PHILIPPIDIS and VASSILOPOUDOS [90], for glass / epoxy laminates, propose a standard law of stiffness drop that they compare to approaches based on the use of S-N curves.

I.7. 3. Progressive damage models

In this part we are interested in progressive damage models based on a static model. There are models of this type for UD laminates [91-103] have also extended their model to the case of 2D woven ply laminates.

UD Laminates - The fatigue model developed at LMA-Marseille [92] for laminates is an extension of the "damage meso-model for laminates".Diffuse damage (fiber / matrix decohesion and incipient delamination) is described in the mesmodel through two damage variables:

d' for the degradation of the transverse Young's modulus and d for the degradation of the shear modulus. The driving forces ($Y_{d'}$et Y_d) associated with these damage variables are written as a function of the components of the stress. Under cyclic loading, there is a superposition of two contributions, static and fatigue, the contribution of fatigue being dependent on the maximum loading and the damages d and d 'saturating at 1:

$$\begin{cases} d = d_s + d_f \\ d = d'_s + d'_f \end{cases} \quad \text{(I.49)}$$

$$d = \frac{\langle \sqrt{Y} - \sqrt{Y_0} \rangle_+}{\sqrt{Y_C} - \sqrt{(Y_0}} \quad \text{(I.50)}$$

With

$$Y(t) = \sup(Y_d(\tau) + bY_{d'}(\tau)) \quad \text{(I.51)}$$

$$d'_s = b' d_s \quad \text{(I.52)}$$

$$\frac{\partial d_f}{\partial N} = g * \langle \sqrt{Y_f} - \sqrt{Y_{0f}} \rangle_+ \quad \text{(I.53)}$$

With

$$Y_f(t) = \sup(Y_d(\tau) + bY_{d'}(\tau)) \quad \text{(I.54)}$$

$$d'_f = b' d_f \quad \text{(I.55)}$$

With Y the equivalent driving force taking into account the coupling between transverse traction / shear, Y_0 is the threshold of static damage, Y_{0f} the threshold of damage by fatigue, Y_c is the critical driving force related to the static kinematic slope , Y_f corresponds to the driving forces in fatigue , b is the parameter of transverse tension / shear coupling , b' is the ratio between the shear damage and the transverse damage and g is a material parameter.

2D Woven - The fatigue models presented in [93] and [97] are the respective extensions of the static models for balanced 2D woven [91] and for 2D woven in general [99] . [97], the damage level d_i^{ud} is introduced:

$$\frac{\partial d_f}{\partial N} = \langle a_f . \left(Y d_2^{UD^*}\right)^o . (\Delta Y d_2^{UD^*})^{\,p} + b_f . \left(Y d_{12}^{UD^*}\right)^q . (\Delta Y d_{12}^{UD^*})^{\,r} - Y_0^F \rangle_+ \quad \text{(I.56)}$$

$$\Delta Y d_I^{UD^*} = \frac{\left[\max_{\tau \in cycl\,(t)}(\sigma_i^{UD^*}) - \min_{\tau \in cycl\,(t)}(\sigma_i^{UD^*})\right]}{2E_i^{UD}(1 - a_I^{UD})^2} \quad \text{(I.57)}$$

The parameter Y_0^f corresponds to the material damage threshold and the coefficients (a_ρ , b_ρ , o , p , q , r) are material parameters.

The shear damage is assumed to be equal to the transverse damage. The law which governs the inelastic strains stays unchanged under cyclic loading.

I.8. Conclusion

Based on the critical review of damage models, fatigue parameters and life prediction methods presented in this first chapter, the experimental study (Chapter II) systematically examines the behaviour of composite tubes under three loading regimes: tension only, fatigue only and combined tension-fatigue loading.

The key formulae presented in Chapter I feed into the predictive framework of Chapter III, where they are integrated into a unified fatigue life model capable of handling all three loading scenarios. The model will explicitly account for flaw-induced failure transitions, enabling adaptive life predictions for composite pipes under real service conditions.

References

1. Zaid Allal, Hassan N. Noura, Ola Salman, Flavien Vernier, Khaled Chahine, A review on machine learning applications in hydrogen energy systems. International Journal of Thermofluids 26 (2025) 101119
2. Krishna Reddi Krishna Reddi , Neha Rustagi , Erika Gupta Techno-economic analysis of conventional and advanced high-pressure tube trailer configurations for compressed hydrogen gas transportation and refueling. International Journal of Hydrogen Energy Volume 43, Issue 9, 1 March 2018, Pages 4428-4438
3. Stinchbomb WW, Bakis CE. Fatigue behavior of composite laminates. Compos Mater 1991;4:10580
4. Nicolas Revest. Fatigue Behavior of thick tieces in composite materials. . National School of Mines of Paris, 2011. Français. . pastel-00677076.
5. Violeau, D. Une stratégie de calcul pour l'analyse à l'échelle "micro" des endommagements jusqu'à rupture des composites stratifiés. PhD thesis, Ecole Normale Supérieure de Cachan, 2007.
6. Gamstedt, E. and Sjören, B.. Michromechanisms in tension-compression fatigue of composite laminates containing transverse plies. Composites Sciences and echnology, vol. 59 :167–178, (1999).
7. Violeau, D. (2007). A computational strategy for the micro-scale analysis of damage to failure in laminated composites .PhD thesis, Cachan Higher Normal School.
8. Thionnet, A., Chambon, L., and Renard, J. (2002). A theoretical and experimental study to point out the notion of loading mode in damage mechanics: Application to the identification and validation of a fatigue damage modelling for laminates composites. International journal of solids and structures, vol.24 :147–154.
9. Pipes, R. and Pagano, N. (1970). Interlaminar Stress in Composite Laminates under Uniform Axial Tension. Journal of Composite Materials, vol.7
10. Puppo, A. and Evensen, H. (1970). Interlaminar shear in laminated composites under generalised plane stress. Journal of Composite Materials, vol. 4 :204–220.
11. Ye, L. and Yang, B. (1988). A boundary layer approach to interlaminar stresses in composite with curved edges. Journal of Reinforced Plastics and Composites, vol. 7 :179–198.

12. Engrand, E. (1981). A boundary layer approach to the calculation of transverse stresses along free edges of a symmetric laminated plate of arbitrary width under in-plane loading. Composite Structures, vol. 198 :247–261.

13. Caron, J., Diaz Diaz, A., Carreira, R., Chabot, A., and Ehrlacher, A. (2006). Multi-particle modelling for the prediction of delamination in multilayered materials. Composites Sciences and Technology, vol. 66 :755–765.

14. Camanho, P.-P. and Dàvilla, C.-G. (2002). Mixed-mode decohesion finite elements for the simulation of delamination in composite materials. In NASA/TM 2002-211-737.

15. Gamstedt, E. and Sjören, B. (2002). An experimental investigation if sequence effect in block amplitude loading of cross-ply composite laminates. International Journal of Fatigue, vol. 24 :437–446.

16. Blassiau, S., Thionnet, A., and Bunsell, A. (2008). Micromechanisms of load transfer in a unidirectional carbon-fibre epoxy composite due to fibre failures. Part 3 : Multiscale reconstruction of composite behavior. Composite Structures, vol. 83 :312–323

17. Kim, J., Kim, C., and Song, D. (2003). Strength evaluation and failure analysis of unidirectional composites using Monte Carlo simulation. Materials. Science and Engineering A, vol. 340 :33–40.

18. J. Degrieck, W.V. Paepegem, " Fatigue Damage Modelling of Fibrereinforced Composite Materials ", Applied Mechanics Reviews, vol.54 (4), pp.279-300, 2001.

19. H.Nouri, " Modélisation et identification de lois de comportement avec endommagement en fatigue polycyclique de matériaux composite a matrice thermoplastique ", Thèse de l'École Nationale Supérieure d'Arts et Métiers, Sciences des Métiers de l'Ingénieur, le 29 juin 2009.

20. L.M. Kachanov. " Introduction to Continuum Damage Mechanics ", Martinus Nijhoff, 1986.

21. J.P.Cordebois, F.Sidoroff, " Anisotropic damage in elasticity and plasticity, ", Journal of Theoretical and Applied Mechanics, pp. 45–60, 1982.

22. J.J. Marigo, " Mechanics of anelastic solids - Formulation of a damage law for an elastic material ", C.R, Acad. Sci, vol.292, Série II, pp.1309- 1312, 1981.

23. M.A. Miner, " Cumulative damage in fatigue ", Journals of Applied Mechanics, vol.67, pp.159-164, 1945.

24. P. Nimdum, " Fatigue design of thick composite railway structures, ", Doctoral thesis from the School of Mines in Paris, March 2009.

25. J.L.Chaboche, P.M.Lesne, " A non-linear continuous fatigue damage model ", Fatigue Fract, Engng Mater, Struct, vol.11, pp.1-17, 1988.

26. Y.Lin, " On fatigue damage accumulation and material degradation in composite materials ", Composites Science and Technology vol.36, pp.339-350, 1989.

27. P.Ladveze, L.Dantec, " Damage modelling of the elementary ply for laminated composites ", Composites Science and Technology vol.43, pp.257-267, 1992.

28. J.F.Maire, J.L.Chaboche, " A New Formulation of Continuum Damage Mechanics (CDM) for Composite Materials ", Aerospace Science and Technology, N° 4, pp.247-257, 1997.

29. W.V.Paepegem, J.Degrieck, " A new coupled approach of residual stiffness and strength for fatigue of fibre-reinforced composites ", International Journal of Fatigue, vol.24 (7), pp.747-762, 2002.

30. A.Sedrakian, T.Benzineb, J.L.Billoet, " Contribution of industrial composite parts to fatigue behaviour simulation ", International Journal of Fatigue vol.24, pp.307–318, 2002.

31. C.Linhone, 'A damageable elastoplastic behaviour model for laminated composite structures', Aerospace Research, No. 2, pp. 119-135, 1996.

32. K.L.REIFSNIDER, " Durability and damage tolerance of fibrous composite systems ", Handbook of Composites, edited by S.T. Peters, vol.35, pp.794-809, 1998.

33. Y.Thollon, C.hochard, " Damage to glass/epoxy laminate composites under static and fatigue loads, 18th French Mechanics Congress, Grenoble, 27–31 August 2007.

34. Y. Thollon C. Hochard ,A generalized damage model for woven ply laminates under static and fatigue loading conditions January 2010 International Journal of Fatigue 32(1):158-165

35. Fujii T., Amijima S., et Okubo K. (1993) Microscopic fatigue processes in a plain-weave glass-fibre composite, Composites Science and Technology, vol.49, no.4, pp.327-333

36. Ding Y.Q., Yan Y., McIlhagger R., et Brown D. (1995) Comparison of the fatigue behaviour of 2-D and 3-D woven fabric reinforced composites,Journal of Materials Processing Technology, vol.55, pp.171-177

37. Kelkar A.D. et Whitcomb J.D. (2009)Characterization and Structural Behavior of Braided Composites, Rapport , No.DOT/FAA/AR-08/52

38. Pandita S.D., Huysmans G., Wevers M., et Verpoest I. (2001) Tensile fatigue behaviour of glass plain-weave fabric composites in on- and off-axis directions, Composites Part A: Applied Science and Manufacturing, vol.32, no.10, pp.1533-1539

39. Hochard C., Payan J., et Bordreuil C. (2006) A progressive first ply failure model for woven ply CFRP laminates under static and fatigue loads, International Journal of Fatigue, vol.28, no.10, pp.1270-1276

40. Hochard C. et Thollon Y(2010) . A generalized damage model for woven ply laminates under static and fatigue loading conditions, International Journal of Fatigue, vol.32, no.1, pp.158-165

41. Pandita S.D., Huysmans G., Wevers M., et Verpoest I. (2001) Tensile fatigue behaviour of glass plain-weave fabric composites in on- and off-axis directions, Composites Part A: Applied Science and Manufacturing, vol.32, no.10, pp.1533-1539

42. Kelkar A.D. et Whitcomb J.D. (2009) Characterization and Structural Behavior of Braided Composites, Rapport , No.DOT/FAA/AR-08/52

43. Perreux D. and Thiébaud F. (2003) Fatigue in filament-wound structures, Fatigue in composites: Science and technology of the fatigue response of fibre-reinforced plastics edited by B. Harris, Chapter 24, pp. 644–657

44. Talreja R. Fatigue of Polymer Matrix Composites. In: Talreja R, Manson JAE , editors. Fatigue of polymer matrix composites. Elsevier Science, pp. 529–552 , 2001.

45. AFNOR. A 03-405 : Metallic Products-Fatigue Testing-Statistical Data Processing, 1991.

46. Yang JN, Jones DL, Yang SH, Meskini A. A Stiffness Degradation Model for Graphite/Epoxy Laminates. Journal of Composite Materials. Vol. 24, pp. 753-770, 1990.

47. Wu WF, Lee LJ, Choi ST. A Study of Fatigue Damage and Fatigue Life of Composite Laminates. Journal of Composite Materials. Vol. 30, pp. 123-137, 1996. 225

48. Subramanian S, Reifsnider KL and Stinchcomb WW. A cumulative damage model to predict the fatigue life of composite laminates including the effect of a fibre-matrix interphase. International Journal of Fatigue. Vol. 17, N° 5, pp. 343-351, 1995

49. Vallons K, Zong M, Lomov SV, Verpoest I. Carbon composites based on multi-axial multi-ply stitched preforms – Part 6. Fatigue behaviour at low loads: Stiffness

degradation and damage development. Composites: Part A. Vol. 38, pp. 1633–1645, 2007.

50. De Monte M, Moosbrugger E, Quaresimin M. Influence of temperature and thickness on the off-axis behaviour of short glass fibre reinforced polyamide 6.6 – cyclic loading. Composites: Part A. Vol. 41, pp. 1368-1379, 2010.

51. Renz R, Szymikowski R. Locally resolved hysteresis measurement of advanced glass-mat thermoplastic composites. International Journal of Fatigue. Vol. 32, pp. 174–183, 2010.

52. Gilbert JL, Ney DS, Lautenschlager EP. Self-reinforced composite poly(methy1 methacrylate): static and fatigue properties. Biomoterials. Vol. 16, pp. 1043-1055, 1995.

53. Tate JS, Kelkar AD. Stiffness degradation model forbiaxial braided composites under fatigue loading. Composites: Part B. Vol. 39,pp. 548–555, 2008.

54. Wu Z, Wang X, Iwashita K, Sasaki T, Hamaguchi Y. Tensile fatigue behaviour of FRP and hybrid FRP sheets. Composites: Part B. Vol. 41, pp. 396-402, 2010.

55. Keller T, Tirelli T, Zhou A. Tensile fatigue performance of pultruded glass fiber reinforced polymer profiles. Composite Structures, Vol. 68, pp. 235–245, 2005.

56. Plumtree A, Melo M, Dahl J. Damage evolution in a [±45]2S CFRP laminate under block loading conditions. International Journal of Fatigue. Vol. 32, pp. 139-145, 2010.

57. Petermann J, Schulte K. The effects of creep and fatigue stress ratio on the long-term behaviour of angle-ply CFRP. Composite Structures. Vol. 57, pp. 205-210, 2002**.**

58. Dyer KP and Isaac DH. Fatigue behaviour of continuous glass fibre reinforced composites. Composites Part B. Vol. 29B, pp. 725–733, 1998.

59. Xiong JJ, Shenoi RA. A two-stage theory on fatigue damage and life prediction of composites. Composites Science and Technology. Vol. 64, pp. 1331-1343, 2004.

60. Goel A, Chawla KK, Vaidya UK, Chawla N, Koopman M. Characterization of fatigue behavior of long fiber reinforced thermoplastic (LFT) composites Materials characterization. Vol. 60, pp. 537-544, 2009.

61. Tan TF, Dharan CKH. Cyclic Hysteresis Evolution as a Damage Parameter for Notched Composite Laminates. Journal of Composite Materials.2010 Vol. 44, pp. .1990-1977

62. Brodowsky HM, Jenschke W, Mader E. Characterization of interphase properties: Microfatigue of single fibre model composites. Composites: Part A . Vol. 41, pp. 1579–1586, 2010.

63. Kenny JM, Marchetti M. Elasto-plastic behavior of thermoplastic composite laminates under cyclic loading. Composite Structures. Vol. 32, pp. 375-382;1995 .

64. Pegoretti A, Ricco T. Fatigue crack propagation in polypropylene reinforced with short glass fibres. Composites Science and Technology. Vol. 59, pp ,1062-1055 . 1999.

65. Momenkhani K, Sarkani S. A New Method for Predicting the Fatigue Life of Fiber-reinforced Plastic Laminates. Journal of Composite Materials. Vol. 40, pp .1971-1892, 2006.

66. Drozdov AD. Cyclic viscoelastoplasticity and low-cycle fatigue of polymer composites. International Journal of Solids and Structures. Vol. 48, pp. 2026-2040, 2011.

67. Clark SD, Shenoi RA, Allen HG. Modelling the fatigue behaviour of sandwich beams under monotonic, 2-step and block-loading regimes. Composites Science and Technology. Vol. 59, pp. 471-486, 1999.

68. Mallick PK, Zhou Y. Effect of mean stress on the stress-controlled fatigue of a short E-glass fiber reinforced polyamide-6,6. International Journal of Fatigue. Vol. 26, pp. 941-946, 2004.

69. Ruggles-Wrenn MB, Hetrick G, Baek SS. Effects of frequency and environment on fatigue behavior of an oxide–oxide ceramic composite at 1200 °C. International Journal of Fatigue. Vol. 30, pp. 502–516, 2008.

70. Ruggles-Wrenn MB, Christensen DT, Chamberlain AL, Lane JE, Cook TS. Effect of frequency and environment on fatigue behavior of a CVI SiC/SiC ceramic matrix composite at 1200°C. Composites Science and Technology. Vol. 71, pp. 190–196, 2011

71. Reis PNB, Ferreira JAM, Antunes FV, Costa JDM. Flexural behaviour of hybrid laminated composites. Composites: Part A. Vol. 38, pp. 1612-1620, 2007.

72. Tai NH, Ma CCM, Wu SH. Fatigue behaviour of carbon fibre/PEEK laminate composites. Composites. Vol. 26, pp. 551-559, 1995.

73. Philippidis TP, Passipoularidis VA. Residual strength after fatigue in composites: Theory vs. experiment. International Journal of Fatigue. Vol. 29, pp. 2104–2116, 2007.

74. Van Paepegem W, Degrieck J. A new coupled approach of residual stiffness and strength for fatigue of fibre-reinforced composites. International Journal of Fatigue. Vol. 24, pp. 747–762, 2002.

75. Epaarachchi JA, Clausen PD. A new cumulative fatigue damage model for glass fibre reinforced plastic composites under step/discrete loading. Composites: Part A. Vol. 36, pp. 1236–1245, 2005.

76. Yang JN, Liu MD. Residual Strength Degradation Model and Theory of Periodic Proof Tests for Graphite/Epoxy Laminates. Journal of Composite Materials. Vol. 11, pp. 176-203, 1977.

77. Thwe MM, Liao K. Durability of bamboo-glass fiber reinforced polymer matrix hybrid composites. Composites Science and Technology. Vol. 63, pp. 375–387, 2003.

78. Berthelot JM, Le Corre JF. Statistical analysis of the progression of transverse cracking and delamination in cross-ply laminates. Composites Science and Technology. Vol. 60, pp. 2659-2669, 2000.

79. Berthelot JM, Leblond P, El Mahi A, Le Corre JF. Transverse cracking of cross-ply laminates: Part 1. Analysis. Composites: Part A. Vol. 27A, pp. 989-1001, 1996.

80. Berthelot JM, El Mahi A, Leblond P. Transverse cracking of cross-ply laminates: Part 2. Progressive widthwise cracking. Composites Part A. Vol. 27 A, pp. 1003-1010, 1996**.**

81. Smith LV, Weitsman YJ. Sea water effects on the fatigue response of polymeric composites. In: A.H. Cardon, H. Fukuda, K Reifsnider. Progress in durability analysis of composites systems. A.A. Balkema, rottrtdam, Brookfield. pp. 217-223, 1996

82. Thomas C. Etude des mécanismes d'endommagement des composites fibres de carbone/matrice polyamide : application à la réalisation de réservoirs de stockage de gaz sous haute pression de type IV. Thèse de doctorat. École Nationale Supérieure des Mines de Paris, 2011.

83. Hoang NT, Gamby D, Lafarie-Frenot MC. Predicting fatigue transverse crack growth in cross-ply carbon–epoxy laminates from quasi static strength tests by using iso-damage curves. International Journal of Fatigue. Vol. 32, pp. 166–173, 2010.

84. Gassan J, Dietz T. Fatigue behavior of cross-ply glass-fiber composites based on epoxy resins of different toughnesses. Composites Science and Technology. Vol. 61, pp. 157-163, 2001.

85. Ogasawara T, Ishikawa T, Yokozeki T, Shiraishi T, Watanabe N. Effect of on-axis tensile loading on shear properties of an orthogonal 3D woven SiC/SiC composite. Composites Science and Technology. Vol. 65, pp. 2541–2549, 2005.

86. Bechel VT, Fredin MB, Donaldson SL, Kim RY, Camping JD. Effect of stacking sequence on micro-cracking in a cryogenically cycled carbon/bismaleimide composite. Composites: Part A. Vol. 34, pp. 663–672, 2003.

87. Gagel A, Lange D, Schulte K. On the relation between crack densities, stiffness degradation, and surface temperature distribution of tensile fatigue loaded glass-fibre non-crimp-fabric reinforced epoxy. Composites: Part A. Vol. 37, pp. 222–228, 2006.

88. Reisfnider KL, Talug A. Analyses of fatigue damage in composite laminates. Int. Journal Fatigue. Vol.1, pp. 3-1, 1980.

89. Tate J.S. et Kelkar A.D. (2008) Stiffness degradation model for biaxial braided composites under fatigue loading, Composites Part B: Engineering, vol.39, no.3, pp.548-555.

90. Hashin, Z. and Rotem, A. A , Fatigue Failure Criterion for Fiber-Reinforced Composite Materials. Journal of Composite Materials, 7, 448-464. (1973).

91. Thionnet A., Chambon L., et Renard J. A theoretical and experimental study to point out the notion of loading mode in damage mechanics: Application to the identification and validation of a fatigue damage modeling for laminates composites, International Journal of Fatigue, 2002.vol.24, pp.147-154.

92. Abdelal G.F., Caceres A., et Barbero E.J. (2002) A micro-mechanics damage approach for fatigue of composite materials, Composite Structures, vol.56, no.4, pp.413-422.

93. Lubineau G. On a damage mesomodel for laminated composites: micro-meso relationships, possibilities and limitations, Doctoral Thesis (2002), Thèse de Doctorat, Cachan Higher Normal School .

94. Gornet L. et Ijaz ,High Cycle Fatigue Damage Model for Delamination Crack Growth in CF/Epoxy Composite Laminates, International Journal of Damage Mechanics 2011, vol.20, no.5, pp.783-807 .

95. Revest N. (2011Fatigue behaviour of thick composite parts, Doctoral Thesis, National School of Mines of Paris - Materials Centre .

96. Payan J. et Hochard C. Damage modelling of laminated carbon/epoxy composites under static and fatigue loadings, International Journal of Fatigue, 2002. vol.24, pp.299-306.

97. Hochard C., Payan J., et Bordreuil C. (2006) A progressive first ply failure model for woven ply CFRP laminates under static and fatigue loads, International Journal of Fatigue, vol.28, no.10, pp.1270-1276.

98. Hochard C. et Thollon Y. (2010) A generalized damage model for woven ply laminates under static and fatigue loading conditions, International Journal of Fatigue, vol.32, no.1, pp.158-165.

99. Thollon Y. et Hochard C. (2009) A general damage model for woven fabric composite laminates up to first failure, Mechanics of Materials, vol.41, no.7, pp.820-827.

100. Mohammadreza Bahadori : PROGRESSIVE FAILURE MODELING OF COMPOSITE MATERIALS LEVERAGING MULTISCALE NON-DESTRUCTIVE EVALUATION DATA" thesis ,Drexel University March 2022.

101. P. Liu and J. Zheng :Recent developments on damage modeling and nite element analysis for composite laminates: A review," Materials & Design, vol. 31,no. 8, pp. 3825,3834, 2010

102. X. Lu, M. Ridha, B. Chen, V. Tan, and T. Tay, \On cohesive element parameters and delamination modelling," Engineering Fracture Mechanics, vol. 206, pp. 278 ,296. 2019

103. Boyina, G. R. T., Rayavarapu, V. K., & V. V., S. R. Continuum damage mechanics based failure prediction and damage assessment in laminated composite structures. Mechanics Based Design of Structures and Machines, (2023).52(4), 2255–2283. https://doi.org/10.1080/15397734.2023.2177860

CHAPTER II:

MATERIALS AND

EXPERIMENTAL PROCEDURE

II.1. Introduction

The aim of this chapter is to draw definitive conclusions on the variables influencing the mechanical behavior of composite tubular structures, with a focus on key mechanical properties such as stiffness, strength, and fatigue life. The experimental design involves testing cylindrical Glass/Epoxy composite specimens under three distinct loading conditions: static loading, cyclic loading, and combined loading. Initial tensile tests, conducted at 100% of the ultimate tensile strength, provide a foundational understanding of the material's behaviour under static conditions, establishing baseline properties such as ultimate tensile strength and deformation characteristics. Building on these insights, this study extends the investigation to cyclic and combined loading scenarios, which are more representative of real-world applications where composite structures are subjected to repetitive and complex stresses.

The cyclic loading tests are conducted at multiple stress amplitudes (40%, 60%, and 80% of the ultimate tensile strength) to evaluate the material's fatigue life and damage progression under varying load levels. These tests aim to quantify the relationship between stress amplitude, number of cycles to failure, and the initiation of damage mechanisms. Additionally, combined loading tests, which involve cyclic fatigue followed by tensile loading to failure, are designed to assess the material's residual strength and damage tolerance after exposure to repetitive stresses. These tests provide critical insights into the progressive degradation of mechanical properties and the interaction between different damage mechanisms, such as matrix cracking, delamination, and fiber fracture.

By estimating critical parameters such as stress at failure, number of cycles to failure, and residual strength after cyclic damage, this study aims to enhance our understanding of the material's performance under both static and dynamic loading. The findings will contribute to a quantitative framework for assessing the durability and reliability of composite structures, particularly in applications involving repetitive or cyclic loading. Ultimately, this work seeks to provide valuable insights for optimizing the design and use of composite materials, ensuring their safe and efficient performance in demanding engineering applications.

II.2. Experimental protocol

II.2.1. Composite tubes fabrication

The prototypes of this experimental part were manufactured by MAHYTEC (Dole, France) and financed by the UHBC Laboratory of Control, Measurement and Mechanical Simulation. The tubes were manufactured by filament winding (Figure II.1). The tubes are characterised by six composite layers with the same thickness for each layer. Table 1 shows the mechanical properties of the Glass/Epoxy composite used in the manufacture of the specimens. Table 2 shows the dimensions and stacking sequence of the composite tubes.

Figure II.1. Filament winding process (DMA)

Tab II.1. Mechanical Properties of Glass / Epoxy.

	E_x[GPa]	E_y[GPa]	E_z[GPa]	v_{xy}	v_{yz}	v_{xz}	G_{xy}[GPa]	G_{yz}[GPa]	G_{xz}[GPa]
G/E	55	21	21	0.268	0.495	0.268	8.2677	9	9

Tab II.2. Composite tube properties

Length	300 mm
Internal diameter	60 mm
Layer thickness	0.25 mm
Layers number	6
Stacking sequence	±55°

II.2.2. Specimen preparation

Preparing the specimens for tensile and fatigue tests should be done by gluing the gauges to the outer wall of the different specimens of the composite tube (see Figure II.2). The purpose of this step is to measure the axial and hoop strains induced by static and cyclic axial tensile load.

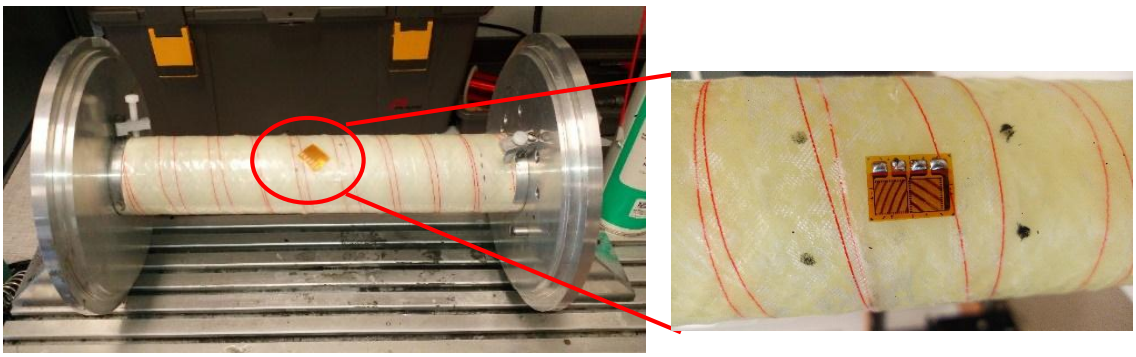

Fig II.2. Location of the strain gauges

The different types of gauges used in this series of experiments are shown in Figure II. 3. The 1D gauges allow obtaining only axial strains. The 2D gauges allow obtaining only axial and hooping strains. The 3D allows obtaining axial and hooping strain depending on its position on the outer wall of the tube specimen.

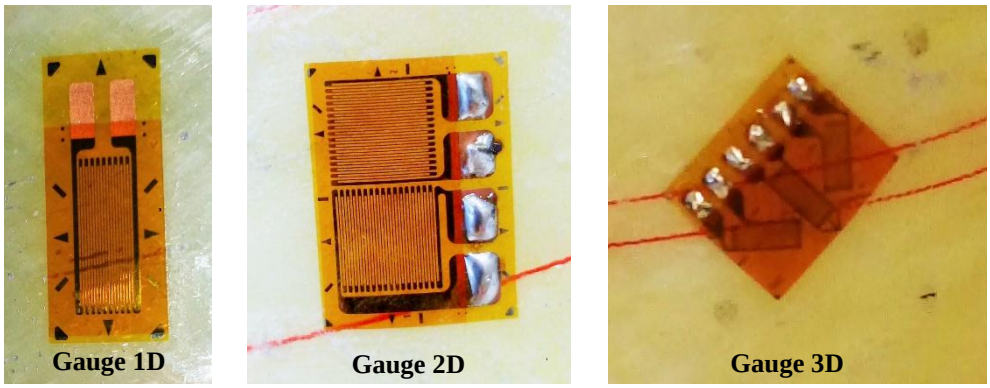

Fig.II.3. Strain gauges

II.2.3.Measuring strains (Use of gauges)

Gauges are mainly used in tests where pressure is the dominant stress. In this case, the mode of rupture is brutal and generates a blast effect capable of throwing the extensometer and therefore damaging or destroying it. To measure the strain, we use strain gauge .

The bonding protocol used consists of 3 stages, which can be divided into elementary operations:

Identification of the bonding zones

1 .Selection of measuring points

2 .Marking the tube directions (tube axis and circumferential axis)

Preparation of the surface

3 .Polishing and smoothing the bond area with fine sandpaper .

4 .Clean by degreasing

5 .Chemical etching (phosphoric acid)

6 .The etching is neutralised (ammonia water) .

Fixing the gauges

7 .A catalyst is applied to the gauge to improve the quality of the bond .

8. The gauge is bonded, the adhesive used is M Bond 200 based on cyanoacrylate ester ($C_5H_5NO_2$).

II.2.4. Description of the testing machine (Multiaxial testing machine)

In order to determine the mechanical properties of the specimens in static and fatigue behavior, a hydraulic tensile testing machine INSTRON -8501 is used, which is presented by Fig II.**4**. This machine allows measuring tensile strength, compressive strength, shear strength, flexural strength, ductility, hardness, impact strength, fracture toughness, creep and fatigue. The description of this machine is given in Tab II.3.

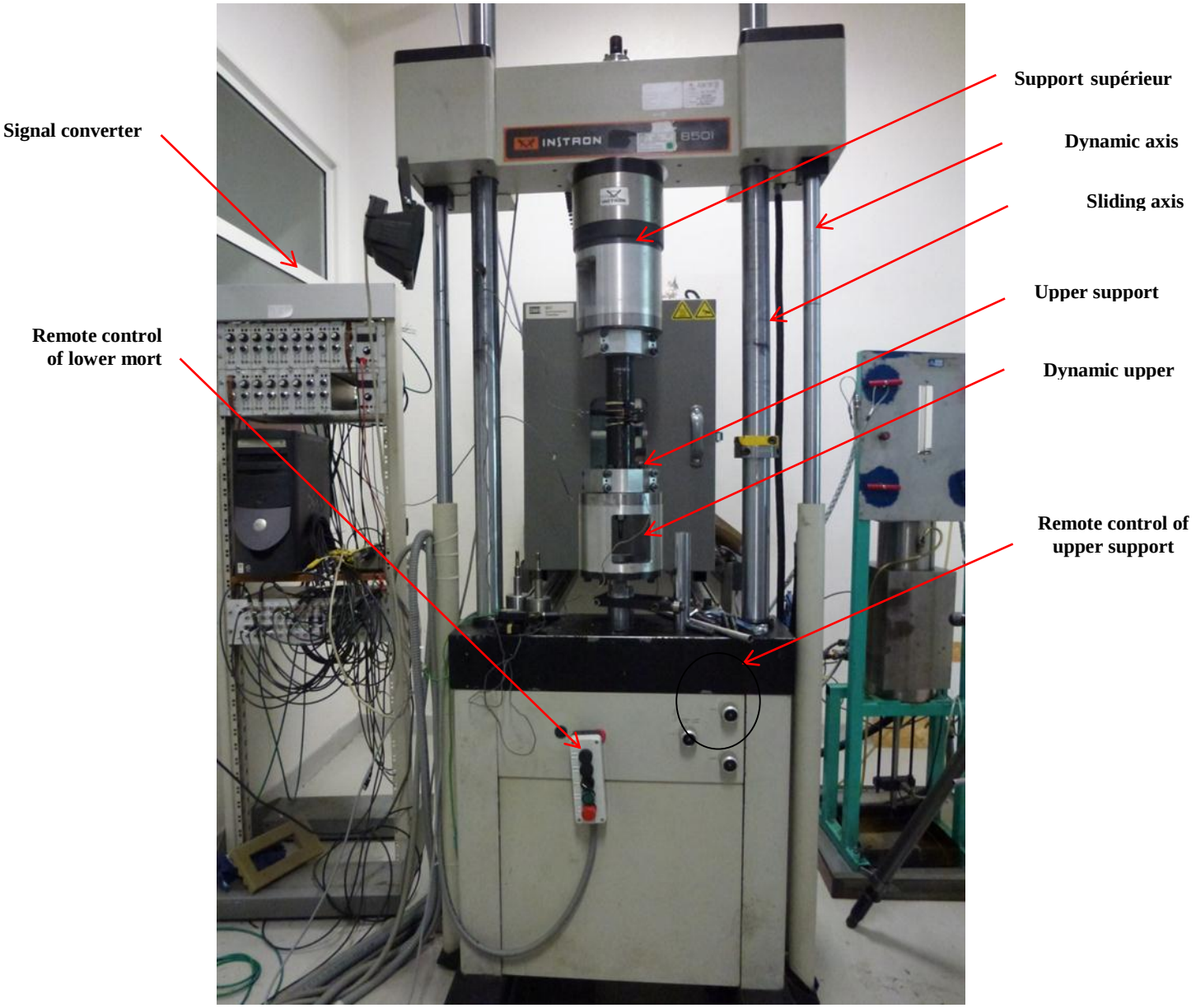

Fig II.4. Tensile machine INSTRON -8501 (DMARC)

Type	8501
Constructor	INSTRON
Power unit	Hydraulic system
Cyclic load waveforms	Sine, triangle, square
Characteristics	Load control, displacement, elongation. (extensometer) Electronic control.
Capacities	Dynamic force 100 kN Effective cylinder stroke ± 70 mm
Formes exemples	Cylindrical, cross section rectangular
Pilotage	"TEMA test" software on Windows: Traction - Compression Fatigue (cycles)

Tab II.3. Testing machine presentation

II.2.5. Mounting of test pieces

The assembly of the specimen is the most important step in the experimental protocol, as it ensures the safety and the good leak-tightness of the loaded tubes (simple or cyclic test), which guarantees good experimental measurements. Fig II.5 shows the six steps for mounting the composite tube specimen on the machine.

II.2.6. Stress tensile caracterisation

The static or fatigue test consists in the application of a tensile or cyclic uniaxial load to a specimen made of composite material. In order to define the ultimate stress in the static test or the number of cyclic fractures in the fatigue test, the expression of the stress induced by the type of loading is significant. Force is applied to the specimen to measure the response of the composite specimen in terms of stress. The TEMA controller is used to monitor the load as a function of the recorded deformations (see fig II.6).

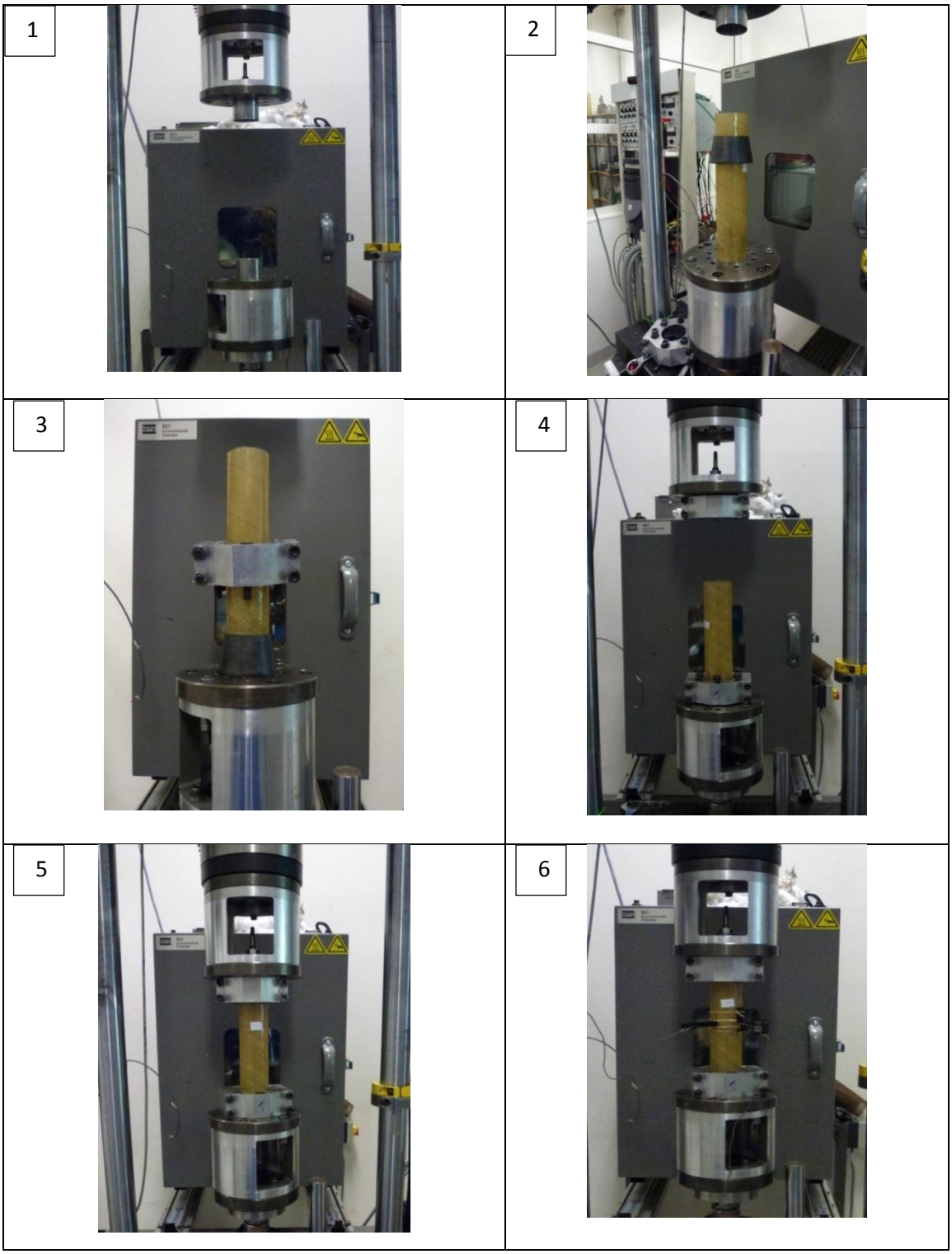

Fig II.5. The six steps of composites specimens mounting

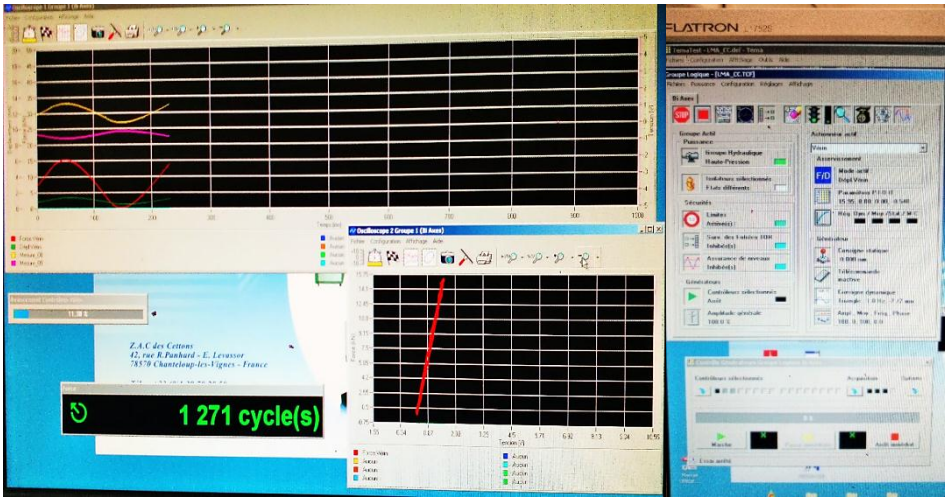

Fig II.6.The Piloting software TEMA controller

II.2.7. Fatigue test caracterisation

The main objective of the fatigue testing performed as part of this thesis is to determine the expected service life of the cyclically loaded specimens in terms of the number of cycles based on the ultimate stress obtained during simple tensile loading.

The fatigue test depends on main parameters as σ_{max}, σ_{min}, σ_{mean}, R and f. The test consists in applying to a specimen a cyclic uniaxial loading around a mean stress σ_{mean}. The type of loading is characterized by the load ratio R of the stress σ_{max} and σ_{min} per cycle, as shown in Figure II.7. In the literature, the R values generally studied are between a range of $0|<R<1$ [1].

$$\begin{cases} \sigma_{amplitude} = \sigma_{max} - \sigma_{min} \\ \sigma_{moyen} = (\sigma_{max} - \sigma_{min})/2 \\ R = \dfrac{\sigma_{min}}{\sigma_{max}} \\ f = \dfrac{1}{T} \end{cases}$$

Establishing the fatigue response curve of a material requires performing tests at several stress levels, generally in the wide range of stress-cycle data between 10% and 100% stress level of the ultimate stress σ **[2]**.

Due to the limited number of composite specimens, the samples were tested at stress levels of 80%, 60%, and 40% of the ultimate tensile strength until failure.

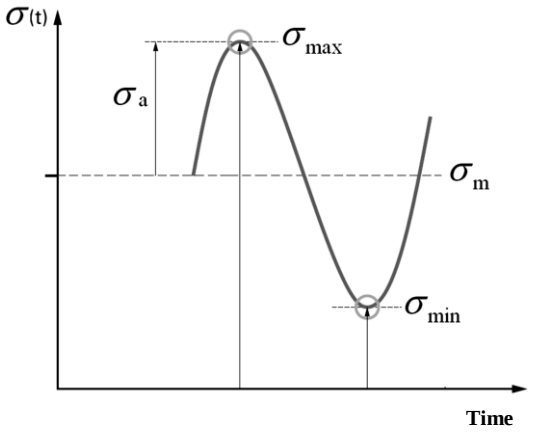

Fig II.7. Load parameters of a fatigue test

II.3 Experimental protocol

This experimental protocol aims to characterize the mechanical behavior of 08 cylindrical composite specimens subjected to three types of loading: monotonic tension until rupture, cyclic fatigue in tension until rupture, and a combined fatigue-tension sequence (fatigue damage followed by tensile testing until rupture). Tensile tests will determine intrinsic mechanical properties (elastic modulus, tensile strength, strain at rupture), while cyclic fatigue tests will provide data on fatigue performance (S-N curve) and failure mechanisms (crack propagation, delamination). The fatigue-tension combination will quantify the degradation of mechanical properties after cyclic damage, assessing the remaining potential of the material, i.e., its ability to withstand loads post-fatigue. This approach will predict residual lifespan and optimize the use of composites in critical applications.

	Experimental test types							
	Tensile test to failure	***Cyclic tensile test to failure***			***Cyclic Tensile Test At 80% of Ultimate Tensile failure + Tensile test to failure***		***Cyclic Tensile Test At 60% of Ultimate Tensile failure +Tensile test to failure***	
Experimental parameters		At 80% of the failure limit	At 60% of the failure limit	At 40% of the failure limit	1/2 of the Nf cycle	1/3 of the Nf cycle	1/2 of the Nf cycle	1/3 of the Nf cycle
Searched properties	Failure limite	Number of cycles to failure	Number of cycles to failure	Number of cycles to failure	Remaining potential	Remaining potential	Remaining potential	Remaining potential
Number of samples tested	01	01	01	01	01	01	01	01

Tab II.4. Experimental protocol

II.3 Experimental results and analysis

II.3.1-Pure Tensile test analysis

The main objective of this tensile failure test is to determine the tensile strength limit. This experimental data will make it possible to carry out a series of cyclic tests at force levels of 40%, 60% and 80% of this defined tensile limit.

The figure shows the distribution of axial stress as a function of axial and hoop strain for a pipe caused by a stacking sequence. The result is a good reflection of the mode of loading of the composite tube with an axial elongation and a circumferential contraction. The alignment of the two curves is characterised by an elastic phase until the elastic limit is reached, followed by a plastic phase until the total failure of the tube. This second phase reflects visco-elastic behaviour, followed by viscoplasticity, accompanied by progressive damage initiation. Final damage occurred at a tensile load of 25 KN.

The loss of rigidity, which characterises the strain trends, reflects primarily the degradation of the material properties of the composite and a displacement of the tube ends under the effect of the applied tensile load. If the test is not interrupted, the cylindrical shape of the specimen is transformed into a hyperboloid geometric configuration as shown in Fig.9. Where it can be seen that two damage zones are located away from the ends of the composite tube.

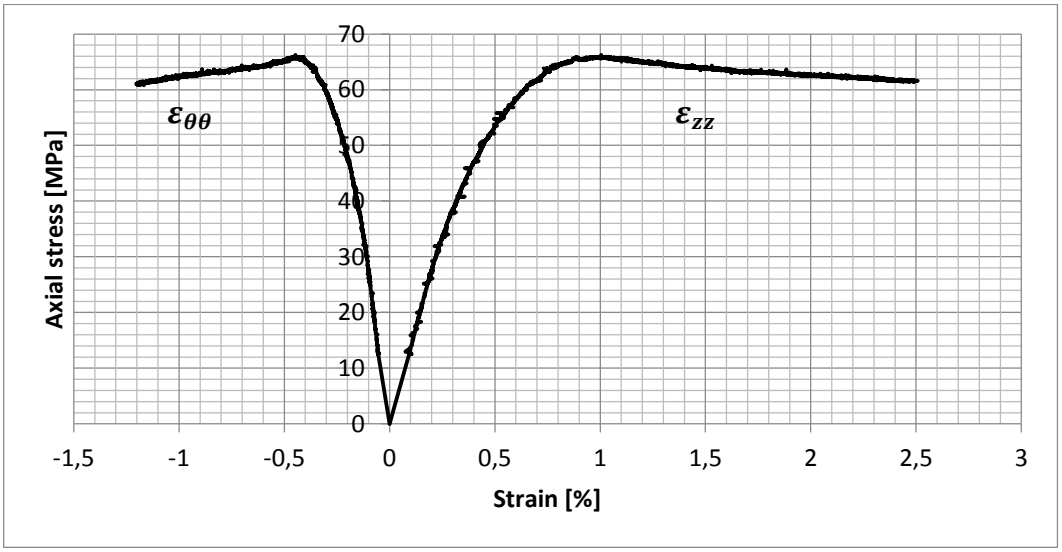

Fig II.8. Axial Stress - Strain of a Glass /Epoxy pipe $[\pm 55]_3$.

Fig II.9. Epoxy /glass composite tube before and after a tensile test.

Compared to the previous work of Farines [3] presented in the table belwo, the stress failure obtained for same specimen with 08 layers and six for us, the difference beteween our stress failure 65,34 [MPa] (25,4 [KN]) and 72.4 MPa for Farines is justified by difference of the number of layer.

Tab.II.5. Summary of tensile tests for tubes with 8 layers [+55] [3].

Tube n°	Stress at failure (MPa)
1	69,8
2	71,4
3	76, 4
Average	**72, 4**

II.3.2 - Cyclic tensile test to failure

Based on the tensile test results, the tensile strength limit is approximately 25 KN. The cyclic test series are performed at 40%, 60% and 80% of this limit, as shown in the table II.5.

Tab II.6.Ultimate load.

Ultimate load	80%	60%	40%
25,5 KN	**20 KN**	**15KN**	**10 KN**

II.3.2.1 – Cyclic test at 80% of ultimate load

The force applied for cyclic loading is 20 KN for a frequency equal to 5 Hz, as shown in the Fig.II.10. The cyclic loading parameters, ratio R, maximum and minimum forces are defined as follows:

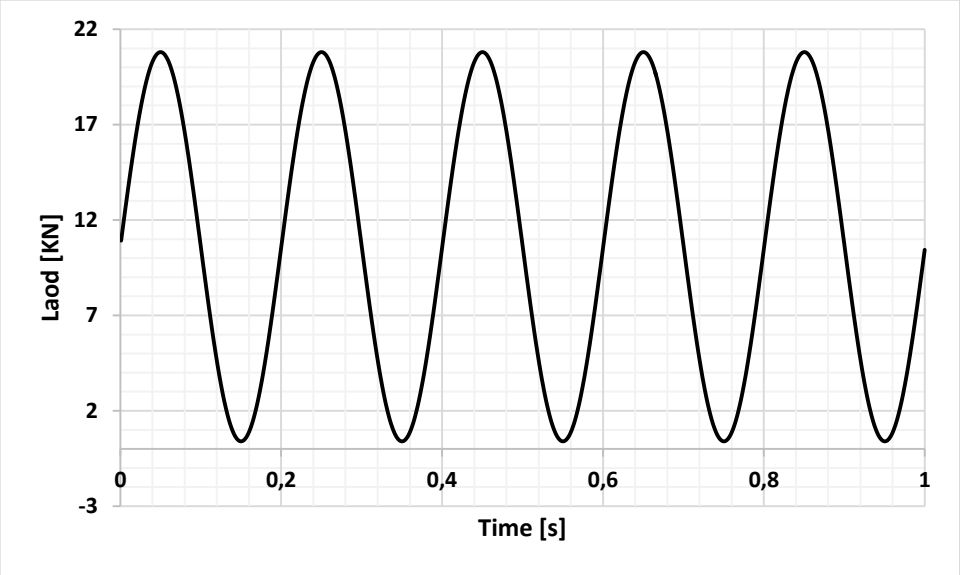

Fig II.10.Tensile force curve for 80% of UTL.

The **Fig. II.11**shows the state of the composite tubular structure before and after cyclic tensile loading, with areas of damage occurring away from the fastener ends. Fracture is characterised by the appearance of a macro crack along the coiling direction of the structure, accompanied by localised delamination. If the test is not interrupted, the shape of the specimen becomes that of a single layer hyperboloid.

Fig II.11. Epoxy /glass composite tube before and after a tensile test

The fatigue test, showed by Fig.12 revealed a stable axial stress plateau at 52.31 MPa sustained for 525 cycles (105 s at 5 Hz), followed by specimen rupture at 615 cycles—a 14.6% deviation from the expected cycle count. This discrepancy exceeds typical experimental variability and suggests potential influences from load-frequency instability or instrumental limitations in cycle detection.

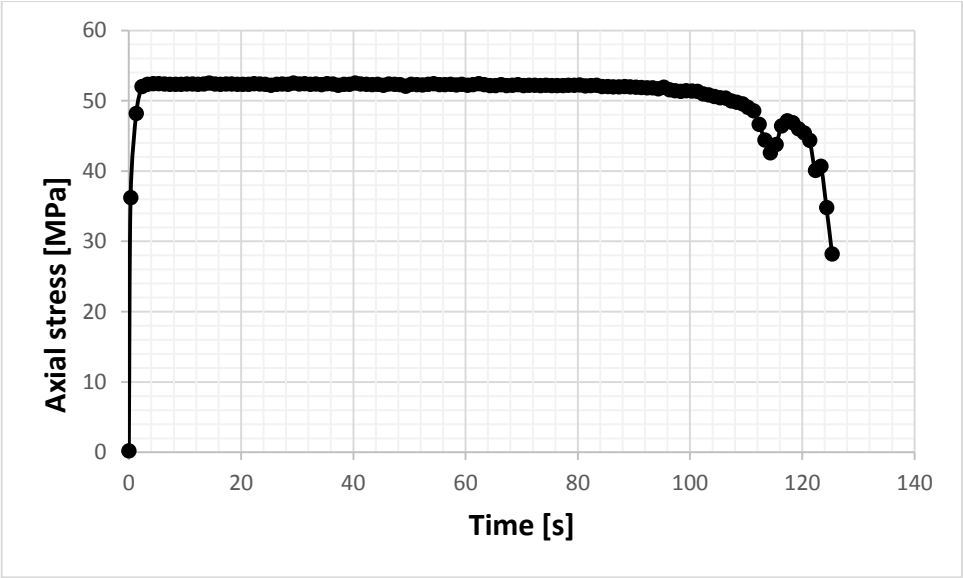

Fig II.12. Axial strain - axial stress of a Glass /Epoxy pipe $[\pm 55]_3$

In the same context, the following figures show the evolution of the axial and hoop strains as a function of time loading. The axial strain together with the circumferential shrinkage characterise both figures with more deformation in the loading direction at a rate 10 times greater than in the circumferential direction. This finding can be explained by the choice of filament winding angle, which has a negative effect on the stiffness of the structure in this loading mode.

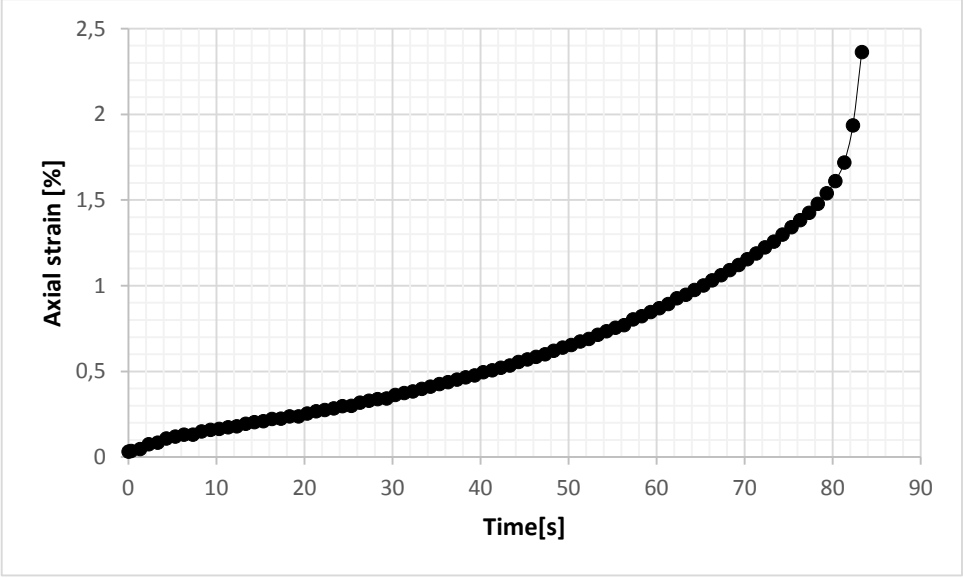

Fig II.13.Axial strain - Time of a Glass /Epoxy pipe $[\pm 55]_3$

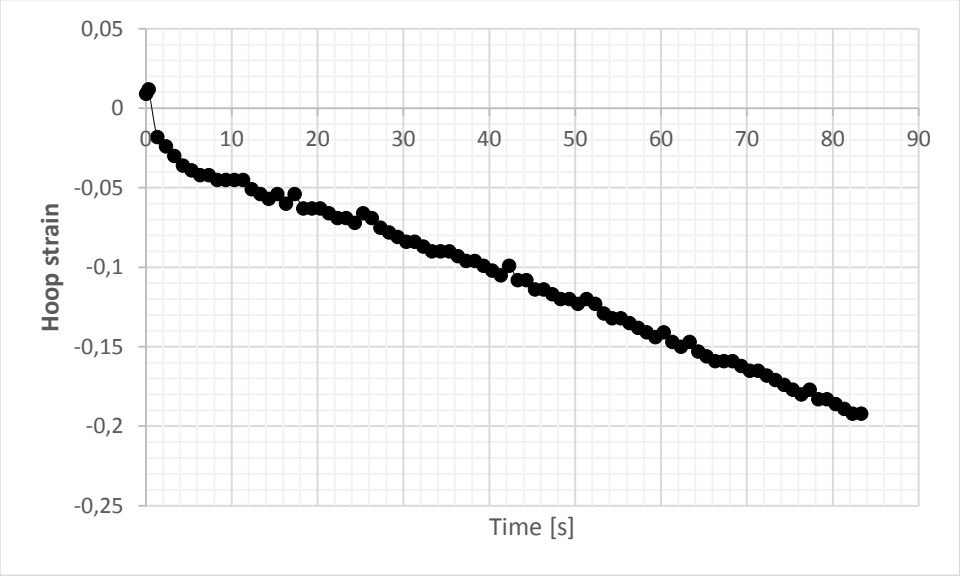

Fig II.14. Hoop strain - Time of a Glass /Epoxy pipe $[\pm 55]_3$

For a given number of cycles, the figure below shows the evolution of the axial stress as a function of the axial and circumferential strains during each load cycle. This limitation of the graph for the total number of cycles recorded, which is 615, makes it easier to understand and evaluate the results obtained. The compression of the load/unload points in the first cycles reflects the viscoelastic phase of the behavior. Once the cycles start to grow, plastic deformation of the material begins. The loss of rigidity characterises the failure of the specimen, leading to a significant displacement of the ends of the tube and hence the degradation of the original structure. All the maximum points of the cycles represent the law of behaviour of the composite material.

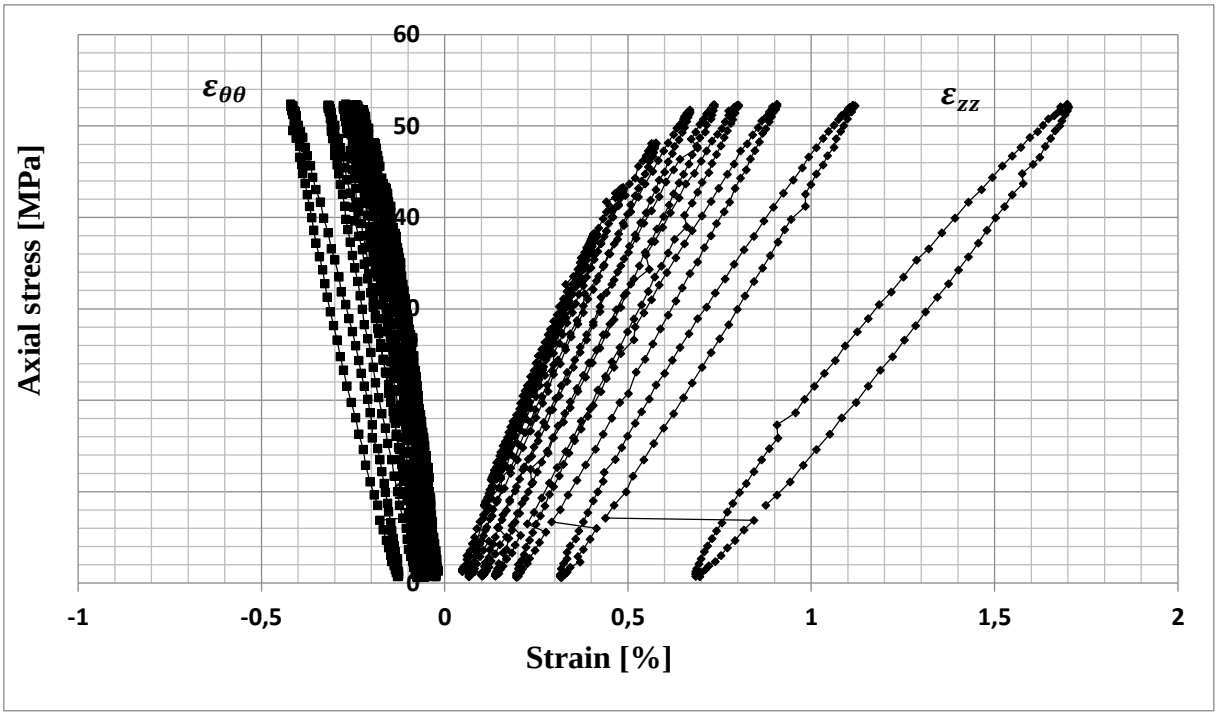

Fig II.15. The stress-strain curve of a Glass /Epoxy pipe $[\pm 55]_3$

II.3.2.2 - At 60% of ultimate load

The cyclic loading force is 15 KN at a frequency of 5 Hz, as shown in the figure II.16. The parameters of the cyclic loading, the ratio R and the maximum and minimum forces are expressed in the figure below as follows:

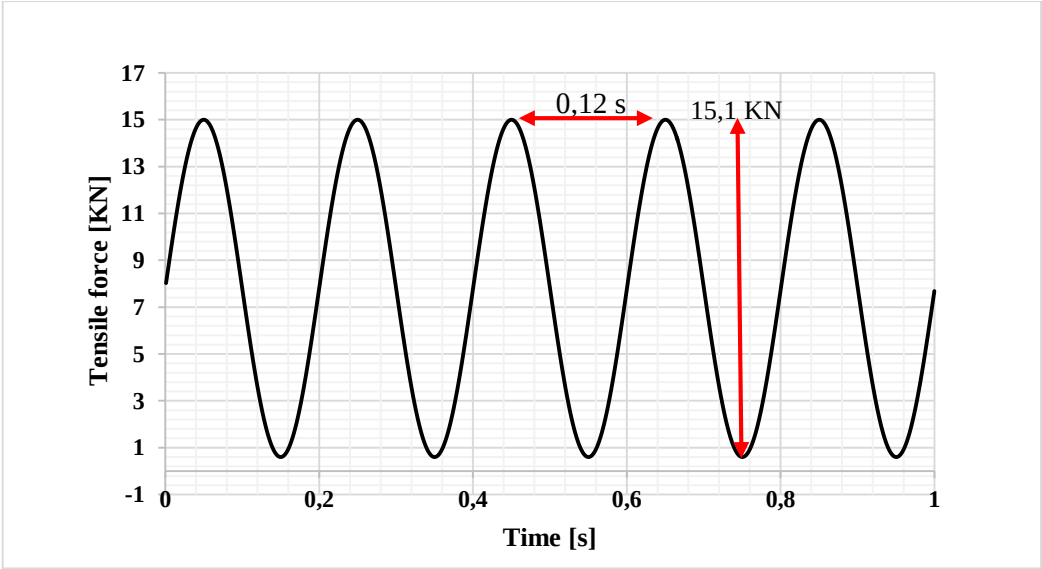

Fig II.16.Tensile force curve

Figure II.17 shows a composite tubular structure before and after cyclic tensile loading at 60% of ultimate load, with damaged areas away from fixing ends. The fracture in this test is

characterised by the appearance of a macro-crack in the direction of the winding of the structure, accompanied by a localised delamination, similar to the situation described in section II.3.2.1 at 80% of the ultimate load. On the other hand, it can be seen that there is no damage to the fibers, only to the matrix, accompanied by the formation of delamination.

Fig II.17.Epoxy /glass composite tube before and after a tensile test

Figure II.18 shows a stable axial stress plateau at 40 MPa sustained for 7,800 seconds, corresponding to 39,000 cycles at a frequency of 5 Hz. The fatigue testing machine recorded 38,875 cycles until failure, representing a negligible deviation of 0.32%, likely due to minor frequency fluctuations or instrumental precision limits.

These results align with ASTM E466 standards, confirming the reliability of the testing methodology. The minimal deviation reinforces the robustness of the experimental setup and supports its use in optimizing the composite layup sequences under investigation. Furthermore, the data provide a foundation for validating predictive fatigue models through the development of S-N curves, enhancing future fatigue life estimations for this material system.

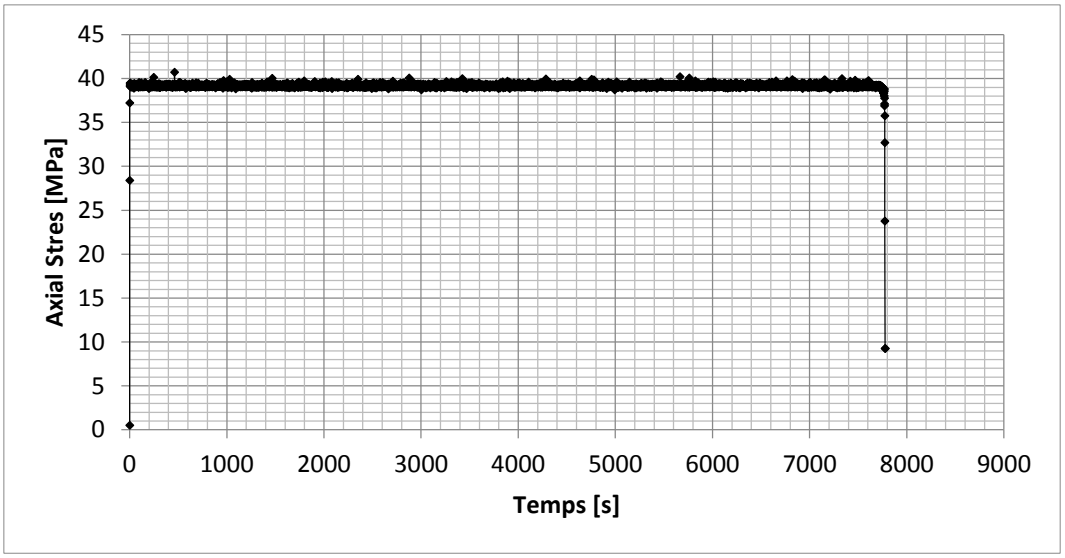

Fig II.18. Axial strain - axial stress of a Glass /Epoxy pipe $[\pm 55]_3$

Compared to 80% of the maximum load, the same response characterises the behaviour of the composite specimen at 60% of the maximum load, with a clear regression in terms of axial and hoop strains (Fig.II.19-II.20), which increases its lifetime. This finding can be explained by the shorter time to plastic behaviour in comparison to the 80 % load case.

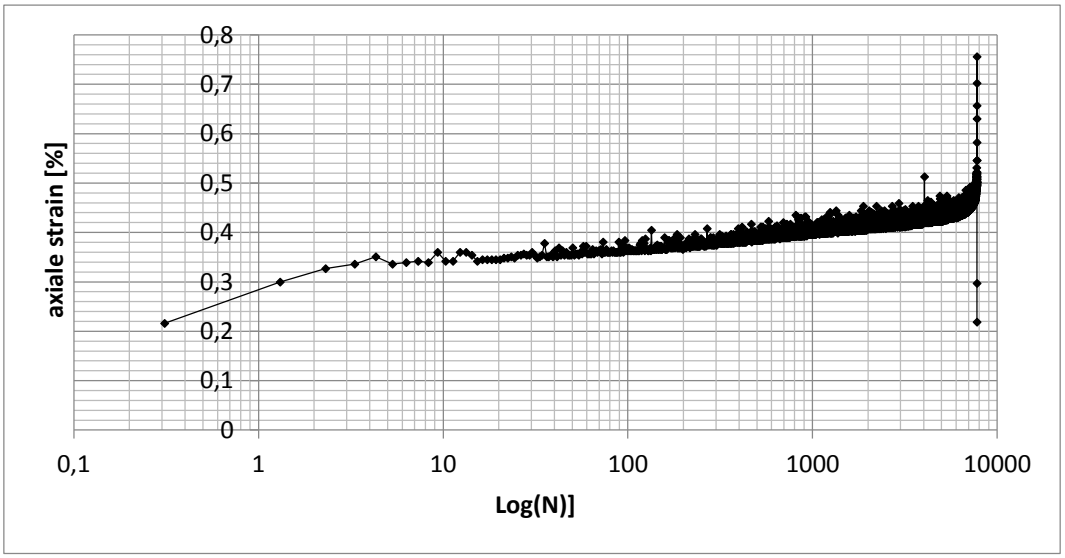

Fig II.19. Axial strain - Time of a Glass /Epoxy pipe $[\pm 55]_3$

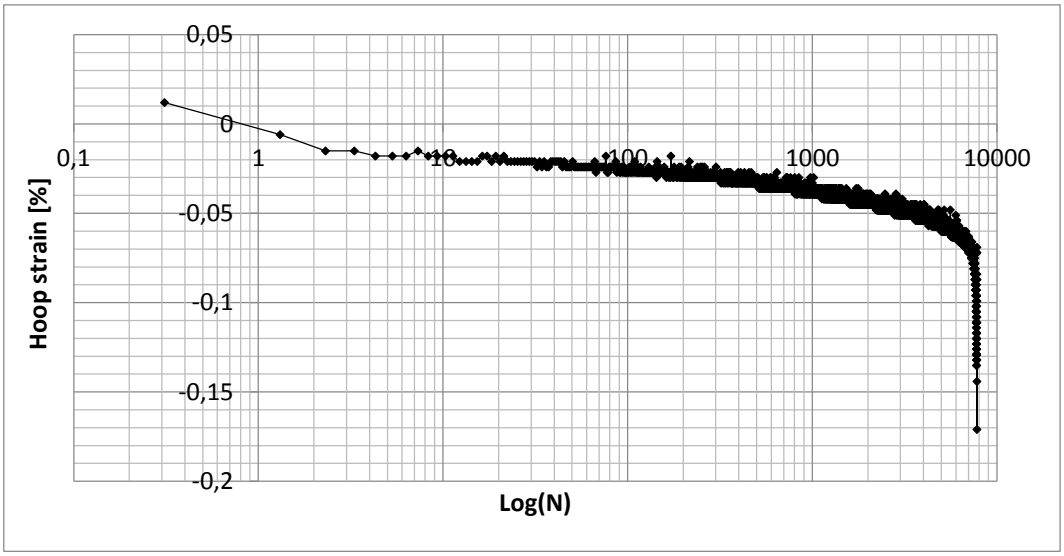

Fig II.20. Axial strain - Time of a Glass /Epoxy pipe $[\pm 55]_3$

The 60% load condition demonstrates a significantly higher number of cycles compared to the 80% load, reaching 38,875 cycles, which represents a 61% increase in fatigue life (Fig. II.21). This improvement can be attributed to the reduced internal stresses and delayed crack initiation at lower load levels, consistent with trends observed in S-N curves for composite materials. At a loading frequency of 5 Hz, this corresponds to a total testing time of 7 775 seconds (38 8755/5).

The extended fatigue life achieved with only 6 layers and a winding angle of 55° highlights the potential for optimizing composite tube designs for specific applications.

Furthermore, comparing the first and last cycles provides valuable insights into the accumulation of inelastic deformation and damage mechanisms. This analysis reveals how microstructural changes, such as matrix cracking or fiber-matrix debonding, evolve over time under cyclic loading. Understanding these mechanisms is critical for predicting long-term material behavior and improving the reliability of composite structures in real-world applications.

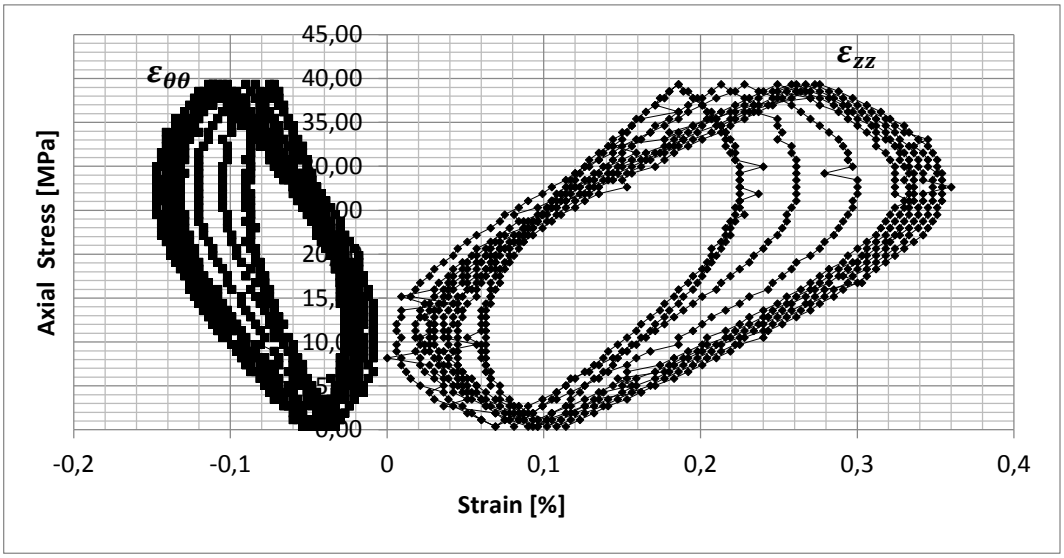

Fig II.21. Stress-strain curve of a Glass /Epoxy pipe $[\pm 55]_3$ under 60% of ultimate load.

II.3.2.3 - At 40% of ultimate load

For a load of 40% of the ultimate load, shown in Figure II.22, the failure stress is reached at 25.22 MPa, with a loss of rigidity until the specimen bursts. Figure II.23 shows the evolution of axial stress function the time of fatigue cyclic, which reach 6600 s number of cycles to failure obtained, which is of the order of 1594886 and corresponds to a lifetime of 73.83 hours. This result is clearly incomparable to those obtained for the 80% and 60% ultimate loads.

The figure II.23 presents the state of the composite specimen before and after cyclic loading at 40% of ultimate loading. The specimen is characterised by cracking with delamination between the layers. The cracking occurs after matrix damage and fibre fracture.

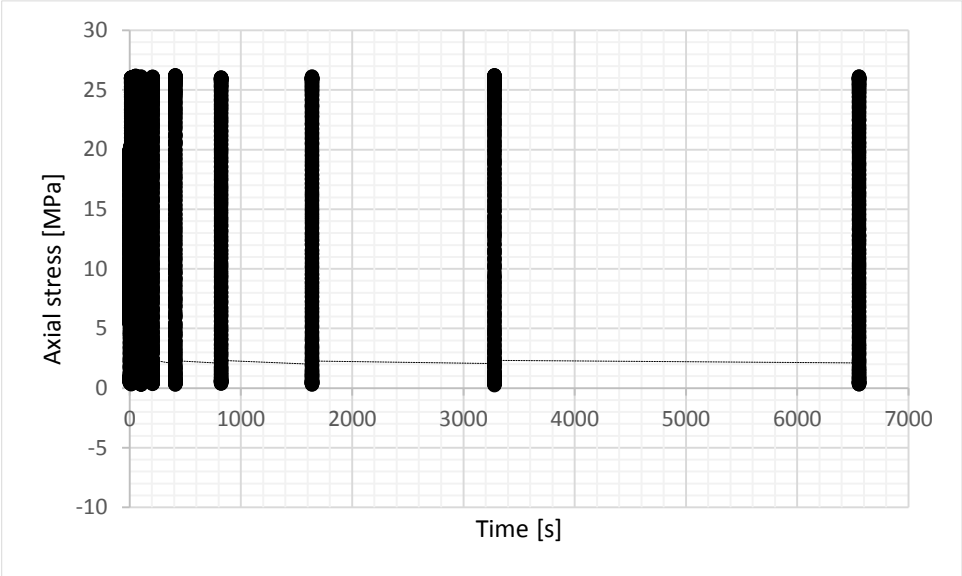

Fig II.22. Evolution of the axial stress of a Glass /Epoxy pipe $[\pm 55]_3$ 40% of ultimate load through time of fatigue cyclic.

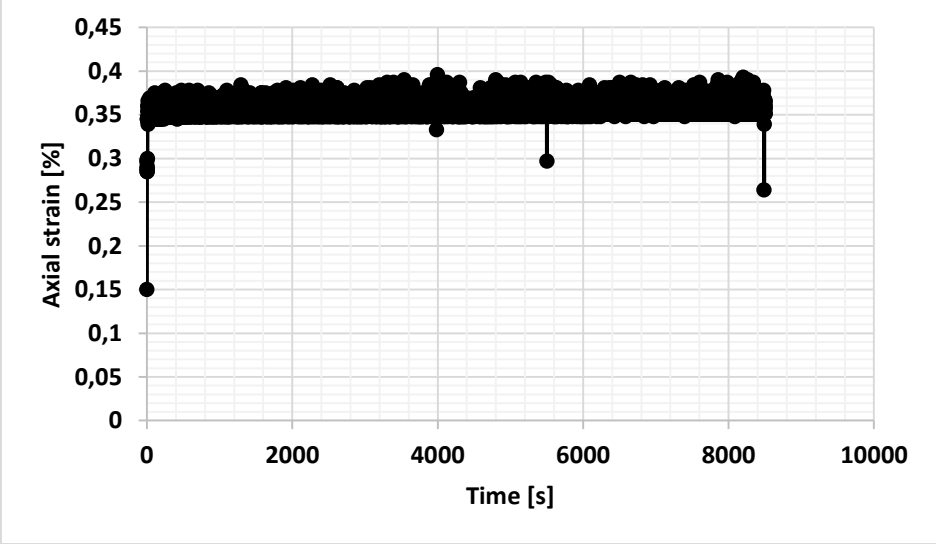

Fig II.22. Axial strain - axial stress of a Glass /Epoxy pipe $[\pm 55]_3$ 40% of ultimate load.

Fig II.23. Epoxy /glass composite tube before and after a tensile test

II.3.2.4 Synthesis of fatigue cycles

The table II.7. below present, the most result obtained in term of failure properties of composite tube under **4**0%, 60 and 80% of ultimate load, where a comparison is developed to the main results obtained for.

Tube n°	Ultimate load rate	Failure axial strain (%)	Failure hoop strain (%)	Failure cycle number (Nf)	Lifetime (s)	Lifetime Increase ratio (%)
1	80%	0,49	-0,17	615	123	-
2	60%	-	-	38875	7775	63,22
3	40%	-	-	1594886	318977,2	41,02

Tab II.7. Failure properties after 40, 60 and 80% of ultimate tensile load applied on composite tube.

II.3.3-Combined fatigue and axial tensile to failure

It is necessary to know the fatigue behavior of the material, in particular its life and damage variation, in order to determine experimentally the remaining potential of the material under tensile loading by plotting the Wohler curve. To this end, the study structure was subjected to two successive types of test. The cyclic fatigue tests under sinusoidal tension and followed by quasi-static tensile tests to failure. This third series of tests assesses the residual strength of the material after cyclic loading. At this stage, the composite structure has already accumulated damage and lost significant mechanical properties.

The table II.8. below gives a summary of the data from the roadmap of the four experimental tests mentioned below.

Tab.II.8. Cyclic fatigue tests parameters

			Tensile cycle number			
			Test 1 (Nf/2)	Test 2 (Nf/3)	Test 3 (Nf/2)	Test 4 (Nf/3)
Tensile loading (KN)	80%	20.4KN	308	205	-	-
		615				
	60%	15.1	-	-	11160	7440
		22320*				

* The 60% load test showed a change in the number of cycles after an initial fatigue test to failure in which the specimen failed after 5,767 cycles. On this basis, the number of cycles to failure for this second series of tests (combined) was recalculated by taking the average of the two values obtained, i.e. 38,875 cycles and 5,767 cycles.

This third section uses a plot of the variation in axial stress and strain as a function of the logarithm of the number of cycles, which simplifies the analysis of fatigue data, makes trends more visible and makes it easier to model and compare the performance of composite materials.

II.3.3.1. Cyclic Tensile Test At 80% of Ultimate Tensile failure followed by tensile test to failure

Case 1 - 1/2 of $N_{cycle-\ failure}$ - *20,4 KN Tensile force equal to and 308 cycles number*

The curves of Fig.II.24 depict the evolution of axial stress and strain during a cyclic fatigue test, conducted over 308 programmed cycles at a loading level corresponding to 80% of the rupture load (20.4 kN). Due to machine uncertainty, a total of 317 cycles, equivalent to 51 seconds, were recorded at the end of the fatigue loading. The results are plotted against the logarithm of the number of cycles to highlight the material's fatigue behavior. From the initial cycles, the composite enters an adaptation phase characterized by the onset of internal damage, such as microcracks and fiber/matrix debonding. These mechanisms lead to a gradual reduction in the material's stiffness, reflected by a continuous increase in axial strain.

During each cycle, axial stress rises sharply to 47.04 MPa during loading, accompanied by a simultaneous strain increase of 0.68%. This response demonstrates the material's ability to resist the applied load while accumulating irreversible damage-related deformations. In contrast, during unloading, axial stress stabilizes around 0.2 MPa, indicating partial relaxation of the composite. Meanwhile, axial strain shows minimal variation (0.09%), suggesting that internal damage reaches a temporary equilibrium.

As cycling progresses, damage accumulates, but the composite tends toward a stabilized state in terms of axial stress. This stabilization likely results from stress redistribution toward the fibers, which bear an increasing share of the load, and the limitation of microcrack propagation. However, despite this apparent stabilization, the progressive accumulation of strain may ultimately lead to sudden failure after a high number of cycles. The loading level, set at 80% of the rupture load, is moderate enough to avoid immediate failure but sufficiently high to induce gradual material degradation. The use of a logarithmic scale for the number of cycles effectively highlights the different phases of fatigue behavior, including initial adaptation and long-term stabilization.

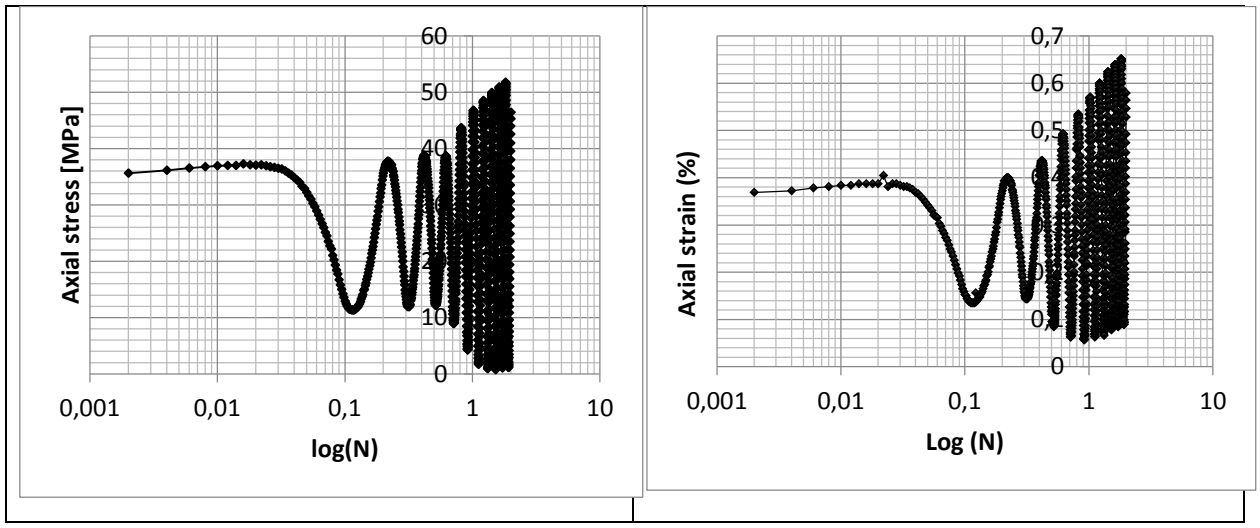

Fig.II.24 illustration of the variation of axial stress and strain as a function of the logarithm of the number of cycles, log(N), for a glass/epoxy pipe with a $[\pm 55]_3$ layup subjected to Nf/2 of cyclic tensile test at 80% of its ultimate tensile strength (UTS).

Figure II.25 illustrates the evolution of axial stress as a function of time for two distinct scenarios. The first scenario corresponds to pure tensile loading without prior fatigue testing, while the second represents tensile loading to failure following a fatigue test of 308 cycles, with results presented in Figure II.24.

The results confirm the impact of cyclic loading on the degradation of composite materials. Fatigue induces a progressive reduction in material stiffness, estimated at approximately **20%**, as well as significant evolution of internal damage. This degradation is primarily due to the accumulation of micro-damage mechanisms, such as matrix cracking, fiber-matrix debonding, and the initiation of transverse microcracks. These mechanisms gradually weaken the structure, reducing its load-bearing capacity.

Furthermore, the apparent stability of axial stress during pure tensile loading reflects the evolution of the damage process. This stability phase, characterized by limited stress variations, often corresponds to a period of slow damage propagation before a more pronounced degradation leading to failure. In contrast, the combined loading test (fatigue followed by tensile loading) exhibits a slower evolution with greater stiffness loss, eventually converging with the pure tensile loading curve at the point of intersection.

These results highlight the importance of a thorough analysis of the mechanical behavior of composites under fatigue. A deeper understanding of degradation mechanisms will enhance the prediction of material lifespan and optimize their design for critical structural applications

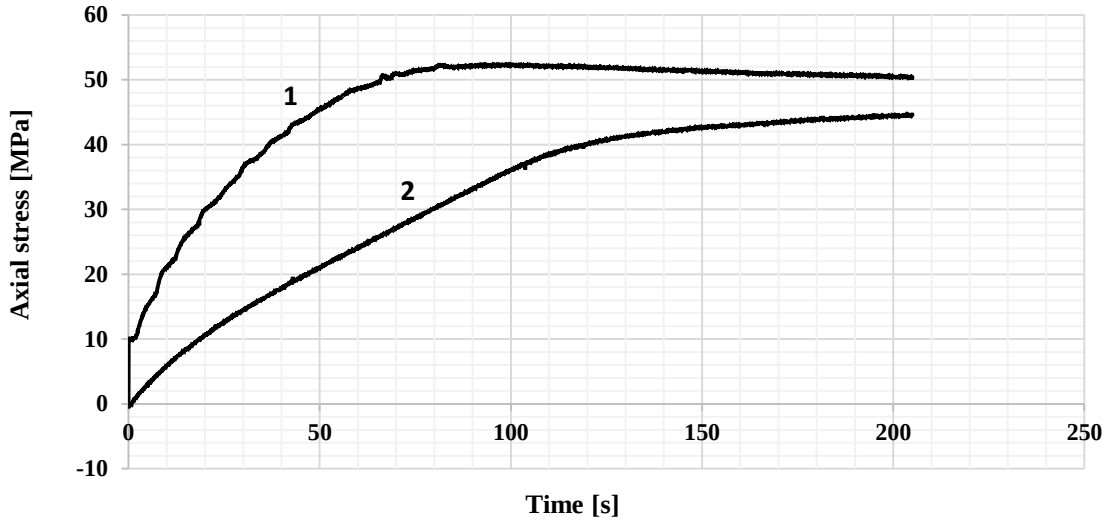

Fig.II.25 Comparative Analysis of Axial Stress Behavior in a $[\pm 55]_3$ Glass/Epoxy Pipe: Pure Tensile Loading vs. Cyclic Tensile Fatigue Followed by Tensile to Failure at 80% of its ultimate tensile strength (UTS)

The figure II.26 illustrates the variation of axial stress as a function of axial and circumferential strains. The obtained curves reflect the mechanical behavior of a cylindrical composite structure subjected to tensile loading until failure, following a programmed fatigue loading of 308 cycles. The observed axial elongation, accompanied by circumferential contraction, aligns with the Poisson effect, a characteristic phenomenon in both isotropic and anisotropic materials.

The analysis of the results reveals a nonlinear response, typical of composite materials. This nonlinearity is attributed to the progressive initiation of damage within the glass/epoxy matrix. Specifically, internal degradation mechanisms, such as matrix cracking and fiber-matrix debonding, develop under the applied load. These damage mechanisms gradually reduce the material's stiffness, leading to an increase in strain for a given stress level.

Furthermore, the apparent stability of axial stress around **48 MPa**, despite the evolving strains, indicates the continuous progression of damage until failure. This phenomenon underscores the importance of a detailed analysis of degradation mechanisms to improve the prediction of the lifespan of composite structures.

.

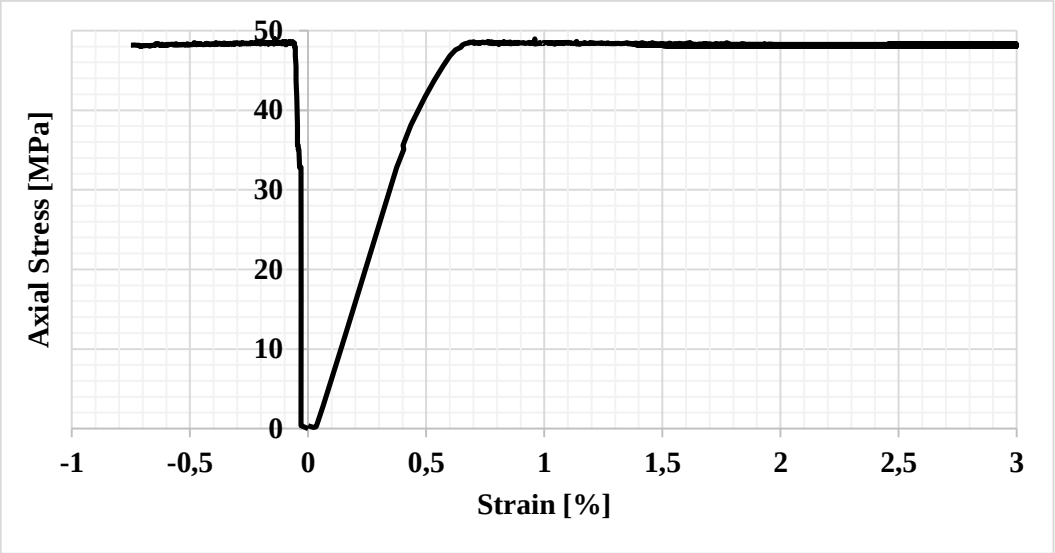

Fig.II.26 Axial Stress-Strain Response of a $[\pm 55]_3$ Glass/Epoxy Pipe Under combined 315 Cycles followed by tensile loading to failure.

Case 2 :* 1/3 du Ncycle *failure - 20,4 KN Tensile force and 205 cycles number

The curves in **Figure II.27** illustrate the evolution of axial stress and strain during a cyclic fatigue test conducted over 205 cycles at a loading level corresponding to 80% of the rupture load (20.4 KN). Due to machine uncertainty, a total of 210 cycles, equivalent to 42 seconds, were recorded at the end of the fatigue loading. These data are plotted against the logarithm of the number of cycles.

During each cycle, a sharp increase in axial stress is observed, reaching **47.04 MPa** during the loading phase, accompanied by a simultaneous strain increase of **0.49%**. This response reflects the material's ability to withstand the applied load while accumulating irreversible damage-related deformations. In contrast, during the unloading phase, axial stress stabilizes around **0.2 MPa**, indicating partial relaxation of the composite. Simultaneously, axial strain shows minimal variation (**0.063%**), suggesting that internal damage reaches a temporary equilibrium state.

The same behavior characterizes this second cyclic loading threshold, with progressive damage accumulation. Compared to the number of cycles at half the fatigue life (1/2 *Nf*), a **36% reduction in axial strain** is observed, highlighting the material's adaptation to cyclic loading and its gradual degradation over time.

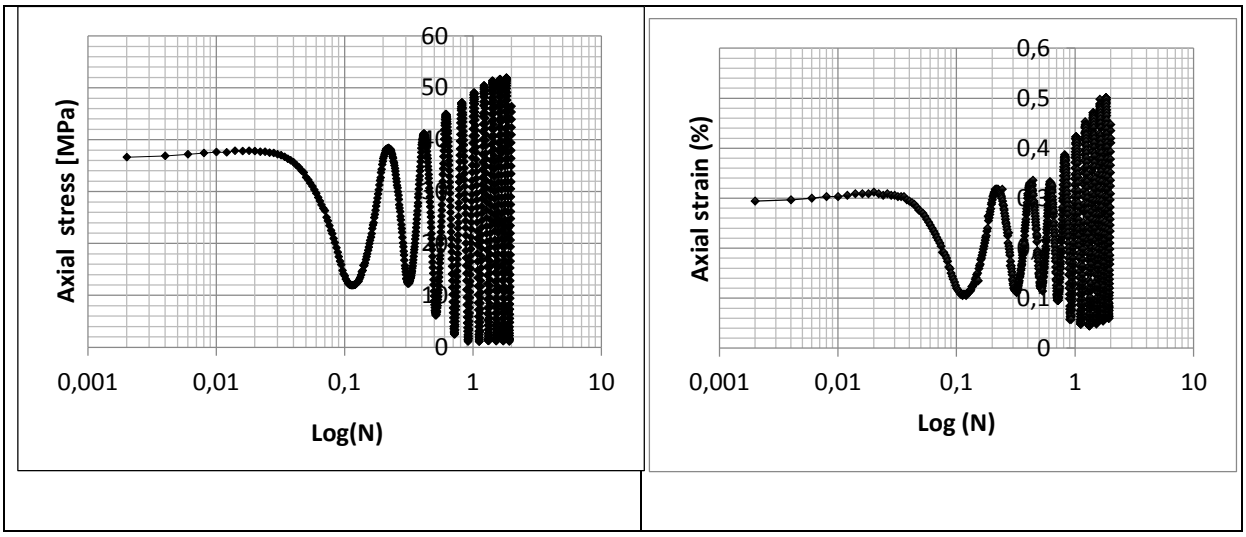

Fig.II.27 illustration of the variation of axial stress and strain as a function of the logarithm of the number of cycles, log(N), for a glass/epoxy pipe with a $[\pm 55]_3$ layup subjected to Nf/3 cyclic tensile test at 80% of its ultimate tensile strength (UTS)

To conclude this combined loading level (80%), the analysis of the results presented in **Figure II.28** highlights a nonlinear evolution of axial stress, which accurately reflects the applied tensile force. This nonlinearity is explained by the thinning of the specimen's surface during loading, indicating the progressive initiation of damage within the glass/epoxy matrix. Specifically, internal degradation mechanisms, such as matrix cracking and fiber-matrix debonding, develop under the applied load. These damage mechanisms gradually reduce the material's stiffness, leading to an increase in strain for a given stress level.

The results confirm the impact of cyclic loading rates on the degradation of composite materials. Fatigue induces a progressive reduction in material stiffness, which depends on the number of cycles applied to the studied composite structure. A stiffness loss between **9.62 and 24 MPa** is observed when comparing pure tensile behavior to combined loading after 308 programmed cycles. For the second observation, comparing pure tensile behavior to combined loading after 210 cycles, the stiffness loss ranges between **10 and 13 MPa**.

Furthermore, the apparent stability of axial stress during tensile loading also reflects the evolution of the damage process, regardless of the number of cycles applied. The three curves (pure tensile, combined loading after 308 cycles, and combined loading after 210 cycles) converge toward an intersection point, highlighting the material's progressive degradation and the influence of cyclic loading on its mechanical behavior

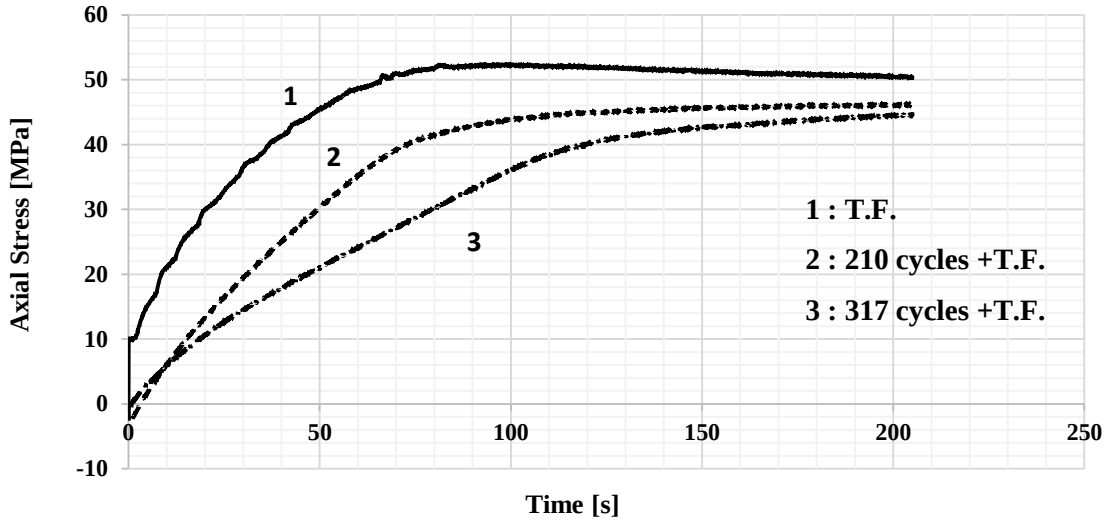

Fig. II.28 Comparative Analysis of the evolution of Axial Stress of $[\pm 55]_3$ Glass/Epoxy Pipe for: Pure Tensile Loading vs. Cyclic Tensile Fatigue for 317 cycles Followed by Tensile to Failure vs. Cyclic Tensile Fatigue for 210 cycles Followed by Tensile to Failure at 80% of its ultimate tensile strength (UTS)

II.3.3.2. Cyclic Tensile Test At 60% of Ultimate Tensile failure followed by Tensile test to failure

Figures II.29 and II.30 illustrate the evolution of axial stress and strain during cyclic fatigue tests conducted at 60% of the failure load (15.3 KN). Figure II.29 corresponds to a test performed over 11,160 cycles, while Figure II.30 represents a test with 7,410 cycles. In both cases, the data are plotted against the logarithm of the number of cycles to analyze trends over time.

Case 1 : 1/2 du Ncycle failure- : 15,3 KN Tensile force and 11160 cycles number

In the first case (Figure II.29), the composite initially enters an adaptation phase characterized by the onset of internal damage. This is followed by a marked increase in axial stress, reaching 8.24 KN during the loading phase, accompanied by a simultaneous rise in strain at a rate of 0.45. The test concludes with a stabilization of axial stress, even as damage continues to accumulate with progressive cycling. Notably, the strain at 60% of the ultimate load is lower than that recorded at 80%, indicating reduced deformation under lower stress levels.

These findings provide valuable insights into the material's fatigue behavior, which is critical for predicting its long-term performance and optimizing its use in applications requiring durability under cyclic loading conditions.

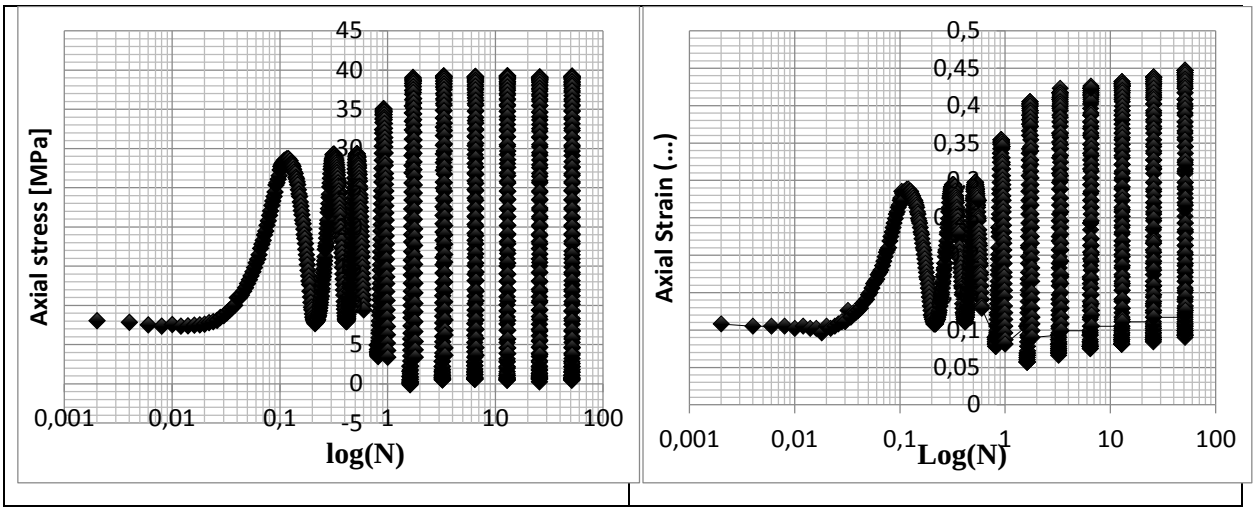

Fig.II.24 illustration of the variation of axial stress and strain as a function of the logarithm of the number of cycles, log(N), for a glass/epoxy pipe with a $[\pm 55]_3$ layup subjected to 2Nf/3 cyclic tensile test at 60% of its ultimate tensile strength (UTS)

Case 2: 1/3 du Ncycle failure - 15 ,3 KN Tensile force and 7410 cycles number

The second case (Figure II.30) exhibits similar behavior, with progressive damage development under cyclic loading. However, at half the number of cycles to failure (½ Nf), a 28% reduction in axial strain is observed compared to the first case. This suggests that the material's deformation response is not only influenced by the loading level but also by the duration of cyclic loading. These findings provide valuable insights into the material's fatigue behavior, emphasizing the importance of considering both load magnitude and cycle count when predicting long-term performance and optimizing composite materials for applications requiring durability under cyclic loading conditions.

These two cases of cyclic loading were subsequently subjected to tensile loading until failure. The results are summarized as follows: The figure compiles the nonlinear responses of the tubular structure under pure tensile tests and cyclic tests at 60% of the ultimate load, followed by tensile tests to failure at two predefined thresholds. This nonlinearity reflects the damage initiated during cyclic loading, which progressively reduces the material's stiffness, leading to an increase in strain for a given stress level.

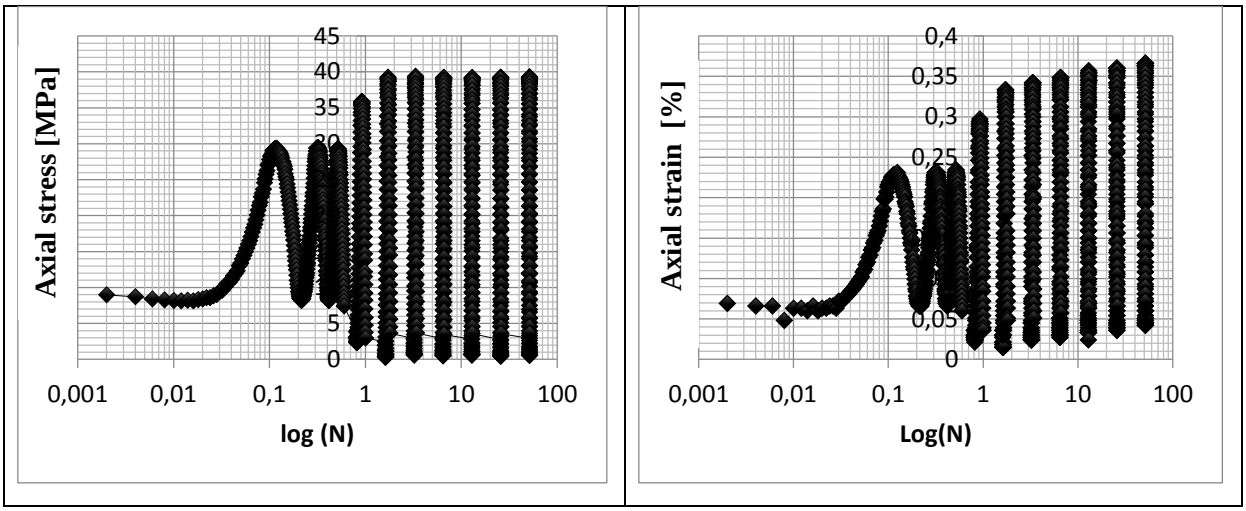

Fig.II.30 illustration of the variation of axial stress and strain as a function of the logarithm of the number of cycles, log(N), for a glass/epoxy pipe with a $[\pm 55]_3$ layup subjected to Nf/3 cyclic tensile test at 60% of its ultimate tensile strength (UTS).

The results confirm the impact of cyclic loading on the degradation of composite materials at the 60% load limit, specifically for 11,160 and 7,410 cycles. Fatigue causes a gradual reduction in the material's stiffness, which is directly influenced by the number of cycles applied to the composite structure. This behavior highlights the importance of considering both the magnitude of cyclic loading and the number of cycles when assessing the long-term performance and durability of composite materials.

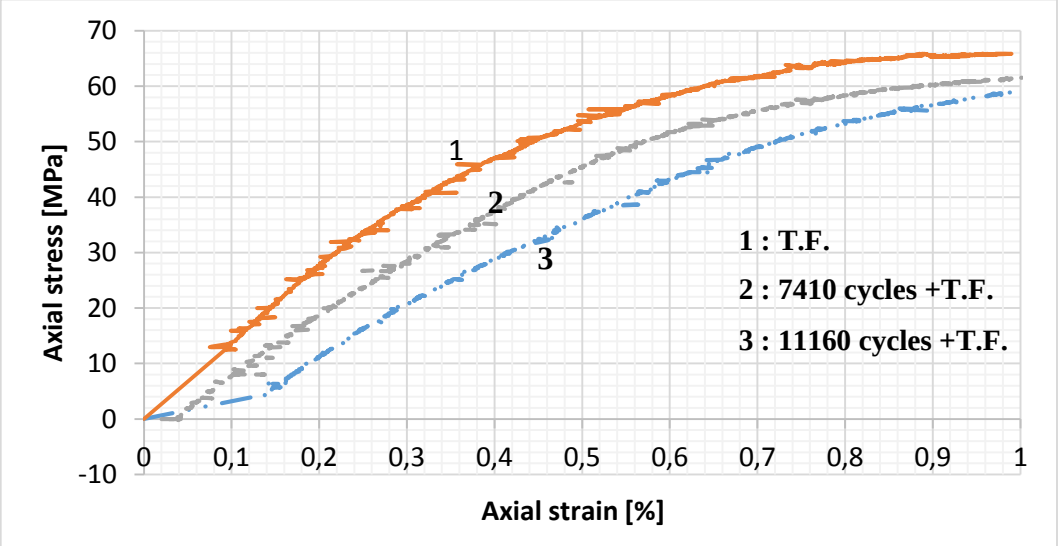

Fig. II.31. Axial Stress-Strain Response of a $[\pm 55]_3$ Glass/Epoxy Pipe Under pure tensile loading to failure and two level for cyclic loading, followed by tensile to failure.

II.3.4. Summary of Experimental Results

As presented in the table II.9. the experimental campaign, comprising eight tests, systematically investigates the mechanical behavior of the tubular composite structure under three distinct loading conditions: pure tensile loading until failure, cyclic fatigue loading, and combined loading. The fatigue tests were conducted at three levels—40%, 60%, and 80% of the ultimate load—to evaluate the material's response under varying stress amplitudes. The results reveal a nonlinear response characterized by progressive damage initiation and stiffness reduction, particularly under cyclic loading. At 60% of the ultimate load (15.3 kN), the number of cycles significantly influenced the material's degradation, with higher cycle counts leading to greater reductions in stiffness and increased strain. Similar trends were observed at 40% and 80% loading levels, albeit with varying degrees of damage accumulation and deformation. The combined loading tests further highlighted the interaction between prior fatigue damage and subsequent tensile loading, demonstrating a reduction in residual strength and deformation capacity. These findings underscore the importance of considering loading type, magnitude, and cycle count in the design and assessment of composite structures for applications involving complex loading scenarios.

	Type d'essai			**Données d'essai**		**Résultats**	
	Traction	**Cyclique**	**Cyclique-traction**	**Force appliqué**	**Nombre de cycles**	**Force rupture**	**Nombre de cycle-rupture**
Essai n°1	×	----------	----------	----------		**25,77kN**	
Essai n°2		×		**20,4 KN**			**N1=635**
Essai n°3		×		**15,1 KN**			**N2=38875**
Essai n°4		×		**10 KN**			**N3=1594886**
Essai n°5			×	**20,4 KN**	**317**	**22,34 KN**	
Essai n°6			×	**20,4 KN**	**211**	**23,39 KN**	
Essai n°7			×	**15,1 KN**	**11160**	**25,72 KN**	
Essai n°8			×	**15 ,1KN**	**7410**	**24,65 KN**	

Tab.II.9. Summary of Experimental Results from Pure Tensile, Fatigue (40%, 60%, 80%), and Combined Loading Tests on Tubular Composite Structures

II.4. Analysis of Damage in the Composite Specimen Under Combined Loading at 60% of the Ultimate Load

II.4.1. Evolution of the elastic modulus

In the same context, the expression of the elastic modulus during cyclic loading of the cylindrical composite structure, followed by pure tensile loading until failure—as shown in the figure II.32 below—reveals a progressive regression of this modulus. This regression, starting from an initial value of 10 GPa, reflects a loss of material stiffness, which is directly linked to the initiation and progression of internal damage within the composite structure.

The decline in the elastic modulus highlights the sensitivity of composite materials to damage under cyclic loading, which compromises the performance of composite structures in applications where dimensional stability and mechanical strength are critical.

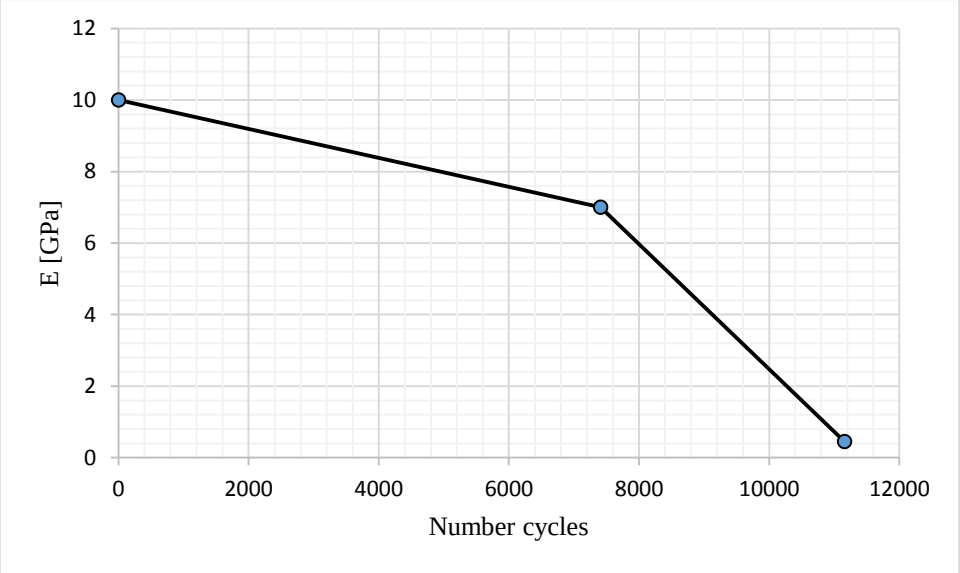

Fig. II.32. Variation of the longitudinal elastic module according to the number of cycle

II.4.2. Analysis of the Evolution of the Damage Coefficient

The progressive evolution of the damage coefficient with increasing cycle count clearly reflects the advancement of damage mechanisms within the composite material. This trend, which contrasts with the regression of the elastic modulus, highlights the continuous degradation of structural integrity under cyclic loading. By combining the analysis of the damage coefficient with that of the elastic modulus, it becomes possible to better understand the fatigue behavior of composites and optimize their design for demanding applications.

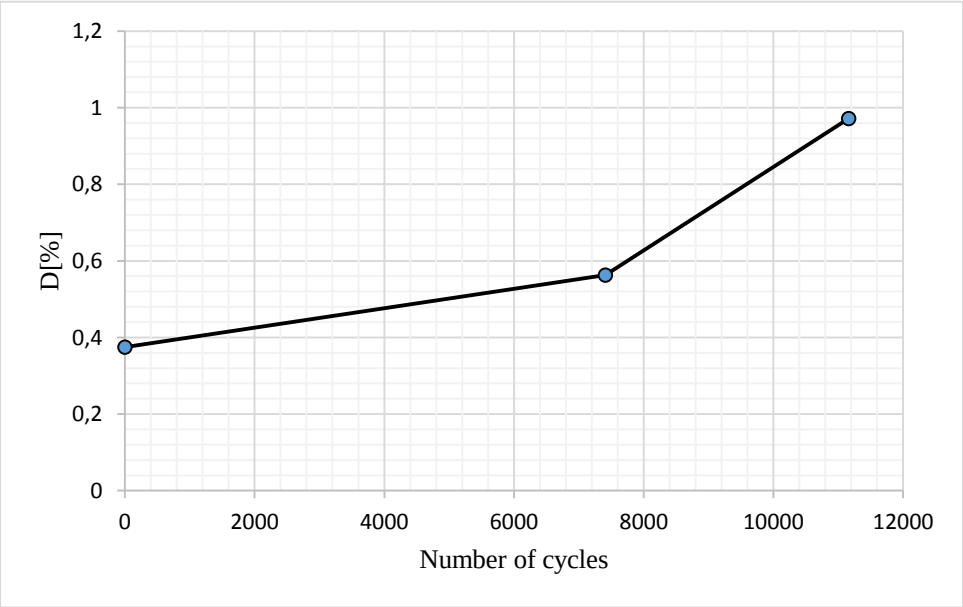

Fig.II.33. Variation of the damage parameter according to the number of cycle

II.4.3. Fracture Morphology for 60% Combined Loading

The figure II.34 presents the fracture morphology observed on a composite specimen subjected to fatigue loading, highlighting three primary damage mechanisms: (A) Matrix fracture, (B) Matrix/fiber delamination, and (C) Fiber fracture. These mechanisms, characteristic of composite materials under cyclic loading, illustrate the complexity of the material's progressive degradation and provide deeper insight into the causes of final failure.

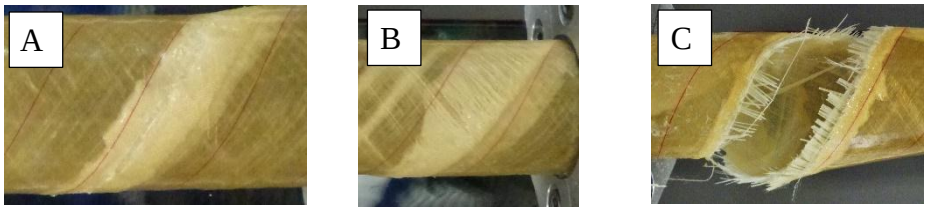

Fig.II.34. Different types of fracture
(A) Matrix fracture, (B) Delamination matrix fiber, (C) Fiber fracture,

II.4.3.1. Matrix Fracture (A):

- **Observation**: Figure (A) shows clear and localized cracks in the polymer matrix. These cracks typically appear perpendicular to the direction of the applied stress.
- **Mechanism**: Under cyclic loading, the matrix, being less resistant than the fibers, is the first site of damage initiation. Micro-cracks form due to repetitive stresses and gradually propagate.

- **Impact**: Matrix fracture reduces the material's ability to transfer loads between fibers, leading to stress redistribution and promoting other types of damage, such as delamination.

II.4.3.2. Matrix/Fiber Delamination (B):

- **Observation**: Figure (B) reveals a clear separation between the matrix and fibers, characterized by delamination zones. These zones often appear as interfacial cracks or localized debonding.
- **Mechanism**: Delamination results from stress concentration at the matrix/fiber interface, exacerbated by the presence of matrix cracks. Under cyclic loading, these interfacial stresses cause delamination to propagate.
- **Impact**: Delamination reduces the material's ability to transfer loads between layers, leading to a loss of stiffness and accelerated degradation of mechanical properties.

II.4.3.3. Fiber Fracture (C):

Observation: Figure (C) shows clear fractures of the fibers, often localized in areas of stress concentration. Fractures can be transverse or oblique, depending on fiber orientation and the direction of applied stress.

- **Mechanism**: Although fibers are highly resistant, they can fracture under repetitive cyclic stresses, particularly in areas where matrix damage and delamination have redistributed stresses.
- **Impact**: Fiber fracture is a critical mechanism, as it leads to an irreversible loss of the material's reinforcement capability. It often marks the final stage of degradation, resulting in complete structural failure.

II.4.3.4. Synthesis of Damage Mechanisms:

- **Degradation Sequence**: The observed fracture morphologies illustrate the typical degradation sequence of composites under fatigue loading: initiation of matrix cracks (A), propagation of delamination (B), and finally fiber fracture (C).
- **Interdependence of Damage Mechanisms**: These mechanisms are not independent; they interact and amplify each other. For example, matrix cracks promote delamination, which in turn concentrates stresses on the fibers, accelerating their fracture.
- **Impact on Fatigue Life**: The progression of these damage mechanisms explains the drastic reduction in fatigue life, as previously observed (1,800,000 cycles without damage vs. 900,000 cycles with damage).

II.4.4. Wöhler Curve Analysis

The Wöhler curve before damage describes the fatigue behavior of the composite material in its intact state, followed by tensile loading until failure, while the curve after damage reflects the degradation of its mechanical properties due to the initiation and propagation of damage. The shift of the curve toward shorter lifetimes and the potential change in its slope highlight the sensitivity of composites to fatigue and the importance of accounting for damage in their design and application (Fig.II.35).

It is observed that, in the absence of damage, the composite structure can withstand up to 1,800,000 cycles of cyclic loading, equivalent to a lifespan of approximately 4 days under the test conditions. However, in the presence of damage, this number of cycles drops significantly to 900,000 cycles, reducing the lifespan to only 2.60 days. This drastic reduction in lifespan, from 4 days to 2.60 days, underscores the devastating impact of damage on the material's mechanical properties.

This observation fully justifies the interpretation that fatigue must be rigorously considered in the design of composite structures. Indeed, the initiation and propagation of damage (matrix cracks, delamination, fiber fractures) under cyclic loading significantly reduce the material's ability to withstand repetitive stresses, compromising the durability and reliability of the structures.

This sensitivity to fatigue highlights the importance of adopting a robust design approach, including:

- **Optimization of design parameters** (stacking sequence, geometry, materials) to delay the onset of damage.
- **Implementation of monitoring systems** to detect damage early and prevent failures.
- **Use of predictive models** to estimate fatigue life and plan maintenance

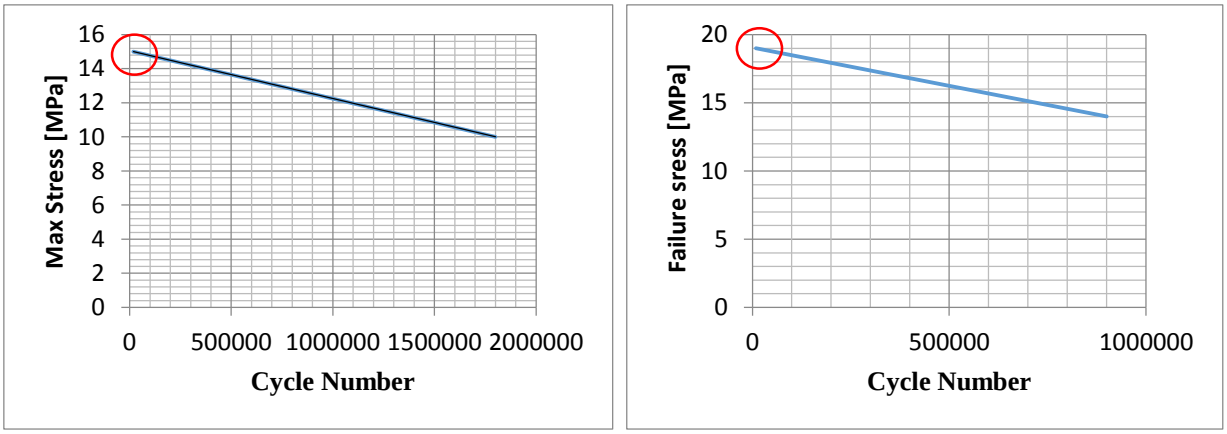

Wöhler curve **Remaining potential**

Fig.II.35 .S-N curve analysis

II.5. Conclusion

This chapter is centered around an in-depth experimental investigation aimed at characterizing the mechanical behavior of 08 cylindrical specimens made from a Glass/Epoxy composite material with a [±55°]3 stacking sequence. These specimens were subjected to three distinct loading modes, each designed to explore specific aspects of the material's mechanical response.

1. **Axial Tensile Test**:

   The first loading mode consists of a pure tensile test, where the specimen is loaded axially until failure. This test determined the ultimate tensile strength, which is approximately **25 kN**, as well as the failure strain and elastic modulus. These data are essential for understanding the material's ability to withstand static loads and undergo elastoplastic deformation before failure.

2. **Fatigue Test**:

   The second loading mode involves cyclic loading at three stress amplitudes (**40%, 60%, and 80%**) of the material's ultimate strength (**25 kN**). For each level, the number of cycles to failure (Nf) was determined, characterizing the fatigue life of the Glass/Epoxy composite cylindrical specimen. The results show a fatigue life of **634 cycles at 80%**, **38,875 cycles at 60%**, and **1,594,886 cycles at 40%**. These results highlight the material's sensitivity to stress amplitude, with a drastic reduction in fatigue life at higher stress levels.

3. **Combined Test: Fatigue Followed by Tensile Loading to Failure**:

   This more complex loading mode consists of two successive phases. First, the specimen is subjected to cyclic loading at two cycle thresholds (**Nf/2 and Nf/3**) for

stress amplitudes of **60% and 80%** of the ultimate strength. Subsequently, the specimen is subjected to a tensile test until failure to evaluate its residual strength after fatigue damage. The results revealed a significant loss of stiffness and strength, illustrating the impact of damage initiated during the fatigue phase.

A detailed analysis of the evolution of the elastic modulus, damage coefficient, and Wöhler curve was conducted for the **60%** stress amplitude, due to data availability. This analysis highlighted a progressive regression of the elastic modulus, decreasing from **10 GPa** to a lower value, as well as an increase in the damage coefficient with the number of cycles. These observations confirm the continuous degradation of structural integrity under cyclic loading.

The comparison between lifetimes before and after damage (**1,800,000 cycles vs. 900,000 cycles**) strikingly illustrates the need to consider fatigue as a critical factor in the design and use of composite materials. This reduction in lifespan, coupled with the loss of stiffness and strength, underscores the importance of adopting robust design strategies, such as optimizing design parameters (stacking sequence, geometry, materials) and implementing monitoring systems to detect damage early.

In conclusion, this experimental study provides valuable insights into the fatigue behavior of Glass/Epoxy composites and sheds light on the damage mechanisms that compromise their durability. Further analysis, including non-destructive characterization techniques (tomography, ultrasound, etc.), could enhance the understanding of damage initiation and propagation, as well as their impact on mechanical properties. These insights are essential for optimizing the design of composite structures and ensuring their reliability in applications subjected to repetitive cyclic loading.

Based on the experimental results, which have captured the behavior of the composite structure under various loading conditions, it is essential to develop a constitutive model that accounts for the different responses of the structure, including elasticity, plasticity, viscoplasticity, and damage prior to any tensile, fatigue, or combined loading. This perspective is the focus of the third chapter, where a comprehensive model will be proposed to predict the material's behavior under complex loading scenarios and to support the design of more reliable composite structures.

References

1. Stani CARBILLET Contribution to reliability calculations on composite structures . Thesis L'U.F.R DES SCIENCES ET TECHNIQUES DE L'UNIVERSITÉ DE FRANCHE-COMTÉ 2005.

2. W Ferdous , A Manalo , J Peauril, C Salih , K Raghava Reddy, P Yu, P Schubel, T Heyer: Testing and modelling the fatigue behaviour of GFRP composites – Effect of stress level, stress concentration and frequency .Engineering Science and Technology an International Journal . https://doi.org/10.1016/j.jestch.2020.01.001

3. Ludovic FARINES .Assessment of the remaining potential of glass/epoxy composite structures subjected to fatigue loads . Thesis L'U.F.R DES SCIENCES ET TECHNIQUES DE L'UNIVERSITÉ DE FRANCHE-COMTÉ 2007.

CHAPTER III:

ANALYTICAL MODEL AND MATHEMATICAL FORMULATION

III.1-Introduction

After all these mechanical tests presented in the previous chapter, we can conclude the type of mechanical behaviour of these composite tubes and all the physical phenomena that have to be passed during a static or cyclic loading. Based on all the information obtained in the previous chapter. This chapter proposes an approach to modelling the behaviour of composite tubes under static and fatigue loading. The previous chapter provided an understanding of the mechanical behaviour and the phenomechanical deformations under these two types of loading (tensile test and cyclic tensile test). Studying the mechanical behaviour of a composite structure involves determining the stress and strain field at each point in the structure. This chapter presents analytical modelling for static and cyclic loading. Firstly, the assumptions that define the limits of the model and the equations derived from them within the framework of the theory of elasticity are presented. In the case of constant amplitude fatigue loading, the initial load up to the maximum stress can be considered as static stress, the operation of which was explained in the previous subsection. The model then takes into account the increase in damage generated during the fatigue cycles. The operation of the model can therefore be divided into three main stages: (i) simulation of the initial static loading, (ii) calculation of the fatigue damage generated during a fatigue increment, during a block of N cycles and (iii) evaluation of the failure criterion.

III.2-Analysis of displacement, stress and strain

We consider a multilayer cylindrical structure with internal r_0 and external r as shown in Fig III.1.

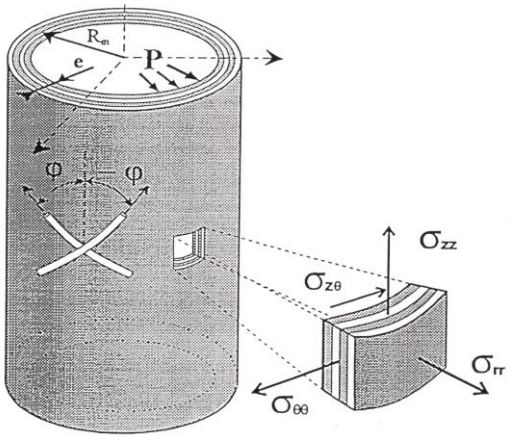

Fig III.1: stress state in a multilayer pipe

We define the cylindrical coordinates radial (r), circumferential (θ) and axial (z). If we consider the case where the structure is subjected to an axisymmetric thermomechanical load, and the hypothesis that the structure remains axisymmetric, we can write that the states of stresses and deformations are independent of the circumferential coordinate.

Moreover, the radial and axial displacements respectively depend only on z and r. From then on, the displacement field can be written in the following form:

$$\begin{cases} U_r = U_r(r) \\ U_\theta = U_\theta(r,z) \\ U_z = U_z(z) \end{cases} \quad \text{(III.1)}$$

In the context of a uniform loading, the deformation-displacement relationships for the structure consisting of k layers can be written for (k) layer :

$$\begin{cases} \varepsilon_r^{(k)} = \frac{\partial U_r^{(K)}}{\partial r}, \varepsilon_\theta^{(k)} = \frac{1}{r}\frac{\partial U_\theta^{(k)}}{\partial \theta} + \frac{U_r^{(k)}}{r}, \varepsilon_z^{(k)} = \frac{\partial U_z^{(K)}}{\partial z} \\ \gamma_{z\theta}^{(k)} = \frac{1}{r}\frac{\partial U_z^{(k)}}{\partial \theta} + \frac{\partial U_\theta^{(k)}}{\partial z}, \gamma_{z\theta}^{(k)} = \frac{\partial U_z^{(k)}}{\partial r} + \frac{\partial U_z^{(k)}}{\partial z} \\ \gamma_{\theta r}^{(k)} = \frac{1}{r}\frac{\partial U_r^{(k)}}{\partial \theta} + r\frac{\partial}{\partial r}\left(\frac{U_\theta^{(k)}}{r}\right) \end{cases} \quad \text{(III.2)}$$

Then, it is considered that the axial deformation is homogeneous transversely and longitudinally in the tube structure and that the rotation of the cylinder is independent of z. Then equations (II.2) are reduced to the following formulation $\left(\frac{\partial}{\partial \theta} = 0 ; \frac{\partial}{\partial z} = 0\right)$:

$$\begin{cases} \varepsilon_r^{(k)} = \frac{\partial U_r^{(k)}}{\partial r}, \quad \varepsilon_\theta^{(k)} = \frac{U_r^{(k)}}{r}, \quad \varepsilon_z^{(k)} = \frac{\partial U_z^{(k)}}{\partial z} = \varepsilon_0 \\ \gamma_{z\theta}^{(k)} = \frac{\partial U_\theta^{(k)}}{\partial z} = \gamma_0 r, \quad \gamma_{zr}^{(k)} = 0, \quad \gamma_{\theta r}^{(k)} = \frac{\partial U_\theta^{(k)}}{\partial r} - \frac{U_\theta^{(k)}}{r} \end{cases} \quad \text{(III.3)}$$

Or $\gamma_0$is the rotation of the tube per unit length.

As for equilibrium equations, in cylindrical coordinates, they take the following form:

$$\begin{cases} \frac{\partial \sigma_r^{(k)}}{\partial r} + \frac{1}{r}\frac{\partial \tau_{\theta r}^{(k)}}{\partial \theta} + \frac{\partial \tau_{zr}^{(k)}}{\partial z} + \frac{\sigma_r^{(k)} - \sigma_\theta^{(k)}}{r} = 0 \\ \frac{\partial \tau_{\theta r}^{(k)}}{\partial r} + \frac{1}{r}\frac{\partial \sigma_\theta^{(k)}}{\partial \theta} + \frac{\partial \tau_{z\theta}^{(k)}}{\partial z} + \frac{2\sigma_{\theta r}^{(k)}}{r} = 0 \\ \frac{\partial \tau_{zr}^{(k)}}{\partial r} + \frac{1}{r}\frac{\partial \tau_{z\theta}^{(k)}}{\partial \theta} + \frac{\partial \sigma_z^{(k)}}{\partial z} + \frac{\sigma_{zr}^{(k)}}{r} = 0 \end{cases} \quad \text{(III.4)}$$

This system is reduced to the formulation that follows the context of this study, namely:

$\left(\frac{\partial \sigma_{ij}}{\partial \theta} = 0 \ , \frac{\partial \sigma_{ij}}{\partial z} = 0\right)$:

$$\frac{d\sigma_r^{(k)}}{dr} + \frac{\sigma_r^{(k)} - \sigma_\theta^{(k)}}{r} = 0 \quad \text{(III.5)}$$

$$\frac{d\sigma_{\theta r}^{(k)}}{dr} + \frac{2}{r}\sigma_{\theta r}^{(k)} = 0 \quad \text{(III.6)}$$

$$\frac{d\tau_{zr}^{(k)}}{dr} + \frac{\tau_{zr}^{(k)}}{r} = 0 \quad \text{(III.7)}$$

From equations (2.6) and (2.7), we can deduce the following expressions:

$$\begin{cases} \tau_{\theta r}^{(k)} = \frac{A^{(k)}}{r^2} \\ \tau_{zr}^{(k)} = \frac{B^{(k)}}{r} \end{cases} \quad \text{(III.8)}$$

III.3-Laws of behavior

In this part, we are interested in defining the laws of behaviour of each layer of the structure studied. The constitutive behavior law of a layer of the structure under thermomechanical loading is expressed as indicated below:

$$\varepsilon = S\,\sigma + \alpha\, I\, \Delta T \quad \text{(III.9)}$$

$$\sigma = C(\varepsilon - \alpha\, I\, \Delta T) \quad \text{(III.10)}$$

Note that the temperature variation in the thickness is not considered in this study.

$$\varepsilon = \varepsilon^e + \varepsilon^{ve} + \varepsilon^p + \varepsilon^{vp} \quad \text{(III.11)}$$

3.3.1-Elastic behaviour

The composite is anisotropic and the description of its behavior requires keeping the φ orientation of its fibers (see Fig.III.2). For this, we define the Cartesian coordinate system (X, Y, Z) , the cylindrical coordinate system (r, θ, z) and the local coordinate system of the fiber (x, y, z) , where, x and y are the main axes longitudinal and transverse directions of the fibers respectively.

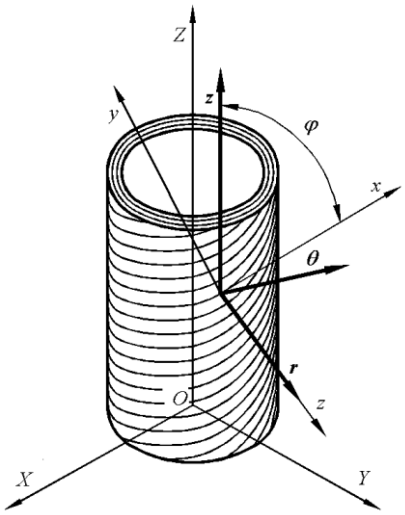

Fig III.2. Relationship between the cylindrical coordinates and the reference coordinates of the composite [33].

The elastic properties of this type of material are: $\boldsymbol{E_x}$ longitudinal module in fiber direction. $\boldsymbol{E_y}$ and $\mathbf{E_z}$ are the transverse modules in the directions of the y and z axes, respectively. $\boldsymbol{G_{xy}}$, $\boldsymbol{G_{xz}}$ and $\boldsymbol{G_{yz}}$ shear modulus. $\boldsymbol{\nu_{zy}}$ and $\boldsymbol{\nu_{zy}}$ are the Poisson coefficients in the x-z and x-y plane respectively. $\boldsymbol{\gamma_{xy}}$ is the shear strain in the x-y plane.

The fiber distribution for a unidirectional composite is similar in the Y and Z directions.

The material characteristics are equivalent in the Y and Z planes.

$$E_y = E_z \ , G_{xy} = G_{xz}$$

$$v_{xy} = v_{xy} \ , G_{xy} = \frac{E_y}{2 \times (1 + v_{xy})}$$

Filament winding fabrication mode imparts transverse isotropy to the reinforcement layers.

Figure 2.3 shows the coordinate system of the unidirectional. The components of the flexibility matrix are written as follows:

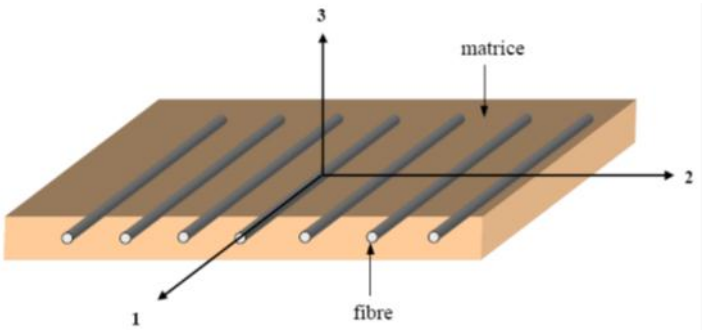

Fig. III.3. Coordinate system of unidirectional [22].

$$S^C = \begin{bmatrix} S_{11}^C & S_{12}^C & S_{13}^C & 0 & 0 & 0 \\ S_{21}^C & S_{22}^C & S_{23}^C & 0 & 0 & 0 \\ S_{31}^C & S_{32}^C & S_{33}^C & 0 & 0 & 0 \\ 0 & 0 & 0 & S_{44}^C & 0 & 0 \\ 0 & 0 & 0 & 0 & S_{55}^C & 0 \\ 0 & 0 & 0 & 0 & 0 & S_{66}^C \end{bmatrix} \quad \text{(III.13)}$$

$$\begin{cases} S_{11}^c = \frac{1}{E_x} \ , S_{12}^c = S_{13}^c = \frac{v_{xy}}{E_x} \\ S_{22}^c = S_{33}^c = \frac{1}{E_y} \ , S_{23}^c = \frac{v_{yz}}{E_y} \\ S_{44}^c = S_{55}^c = S_{66}^c = \frac{1}{G_{xy}} \end{cases} \quad \text{(III.14)}$$

$$E_y = E_z \ , v_{xy} = v_{xz}$$

The relations make it possible to express the strain vectors and that of stress in the fiber reference [17].

$$\acute{\varepsilon} = T_\varepsilon \varepsilon \quad \text{(III.15)}$$

$$T_\varepsilon = \begin{bmatrix} \cos^2\phi & \sin^2\phi & 0 & 0 & 0 & 2\sin\phi\cos\phi \\ \sin^2\phi & \cos^2\phi & 0 & 0 & 0 & -2\sin\phi\cos\phi \\ 0 & 0 & 1 & 0 & 0 & 0 \\ 0 & 0 & 0 & \cos\phi & -\sin\phi & 0 \\ 0 & 0 & 0 & \sin\phi & \cos\phi & 0 \\ -\sin\phi\cos\phi & \sin\phi\cos\phi & 0 & 0 & 0 & \cos^2\phi - \sin^2\phi \end{bmatrix} \quad \text{(III.16)}$$

$$\acute{\sigma} = T_\sigma \sigma \quad \text{(III.17)}$$

With :

$$T_\sigma = \begin{bmatrix} \cos^2\phi & \sin^2\phi & 0 & 0 & 0 & \sin\phi\cos\phi \\ \sin^2\phi & \cos^2\phi & 0 & 0 & 0 & -\sin\phi\cos\phi \\ 0 & 0 & 1 & 0 & 0 & 0 \\ 0 & 0 & 0 & \cos\phi & -\sin\phi & 0 \\ 0 & 0 & 0 & \sin\phi & \cos\phi & 0 \\ -2\sin\phi\cos\phi & 2\sin\phi\cos\phi & 0 & 0 & 0 & \cos^2\phi - \sin^2\phi \end{bmatrix} \quad \text{(III.18)}$$

Tab III.1. Thermodynamic variable for elastic behavior.

state variables		associated variables
visible	internal	
ε	ε^e	σ
		σ

III.3.2- Viscoelastic behavior

The epoxy matrices have viscoelastic behavior:

$$C_R = S_R^{-1} = \begin{bmatrix} 0 & 0 & 0 & 0 & 0 & 0 \\ 0 & \beta_{22}S_{22} & \beta_{23}S_{23} & 0 & 0 & 0 \\ 0 & 0 & \beta_{33}S_{33} & 0 & 0 & 0 \\ 0 & 0 & 0 & \beta_{44}S_{44} & 0 & 0 \\ 0 & 0 & 0 & 0 & \beta_{55}S_{55} & 0 \\ 0 & 0 & 0 & 0 & 0 & \beta_{66}S_{66} \end{bmatrix} \quad \text{(III.19)}$$

It is possible to write additional evolution equations:

$$\dot{\varepsilon}^{ve} = \sum_i \dot{\xi}_i \quad \text{(III.20)}$$

$$\dot{\xi}_i = -\frac{\partial \varphi_{ve}^*}{\partial \sigma} = -\frac{1}{\tau_i}(\xi_i - \mu_i S_R : \sigma) \quad \text{(III.21)}$$

The shape of the distribution of relaxation times is selected triangular rather than Gaussian(see Fig III.4).

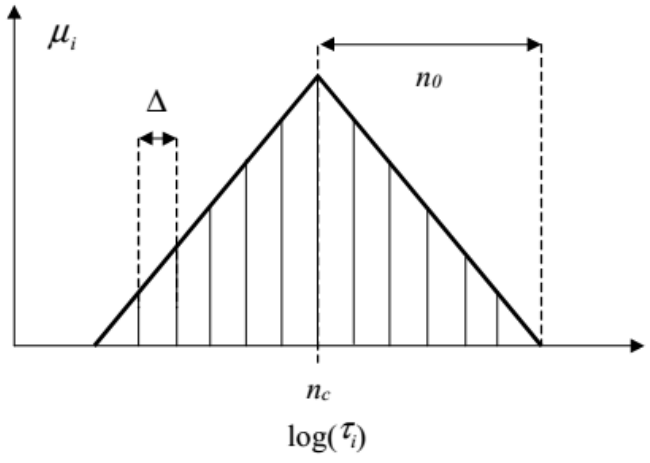

Fig III.4.Spectrum of relaxation time

Noting the number x of relaxation time, Δ the interval between time and pitch triangle, we obtain relaxation times:

$$\tau_i = 10^{n(t)} \tag{III.22}$$

Where:

$$\begin{cases} n(i) = n_c - n_i + (i-1)\Delta \\ \Delta = \frac{2n_0}{n_b - 1} \end{cases} \tag{III.23}$$

the weighting:

$$\begin{cases} \mu_i = +a[n(i) - (n_c - n_0)] \; pour \;\; n(i) \in [(n_c - n_0), n_c] \\ \mu_i = +a[n(i) - (n_c - n_0)] \;\; pour \;\; n(i) \in [, n_c \, , (n_c + n_0)] \end{cases} \tag{III.24}$$

The normalization of the spectrum gives:

$$\sum_{i=1}^{n_b} \mu_i = 1 \tag{III.25}$$

We then obtain the expression of slope:

$$a = \frac{2}{n_0(n_b - 1)} \tag{III.26}$$

Tab.III.2.Thermodynamic variable for viscoelastic

state variables		**associated variables**
visible	**internal**	
ε	ε^{ve} ξ_i	σ -σ x_i

III.3.3.Damaged

Damage describes the evolution of phenomena between the initial state, assumed to be intact, and the appearance of a macroscopic crack (see fig III.4).The damage considered in this work is related to the cracking of resin in the direction parallel to fibers. This type of cracking is assumed to change the compliance tensor. In this context, three damage parameters D_I, D_{II} and D_{III} are defined, and they characterize the lower transverse modulus E_2 and shear modulus G_{12} and G_{23}.

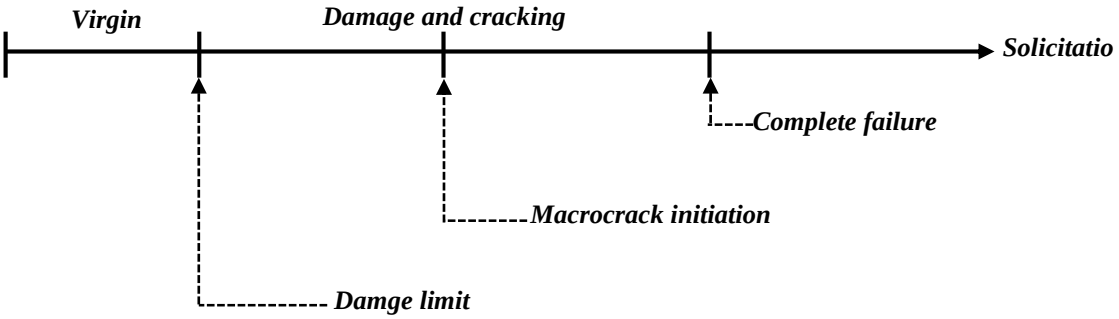

Fig III.5. Evolution of the state of materials

The damage is introduced by adding the damage contribution tensor H to the compliance tensor of compositeS^c. Then, the damaged compliance tensor $S^c$of a layer takes the form:

$$H = \begin{bmatrix} 0 & 0 & 0 & 0 & 0 & 0 \\ 0 & H_{22} & 0 & 0 & 0 & 0 \\ 0 & 0 & 0 & 0 & 0 & 0 \\ 0 & 0 & 0 & H_{44} & 0 & 0 \\ 0 & 0 & 0 & 0 & 0 & 0 \\ 0 & 0 & 0 & 0 & 0 & H_{66} \end{bmatrix} \quad \text{(III.27)}$$

The experimental analysis shows that the damage is due to the micro-cracking of the polymer matrix in the fibres direction x_1, perpendicularly to the transverse direction x_2 (see Fig. III.5).

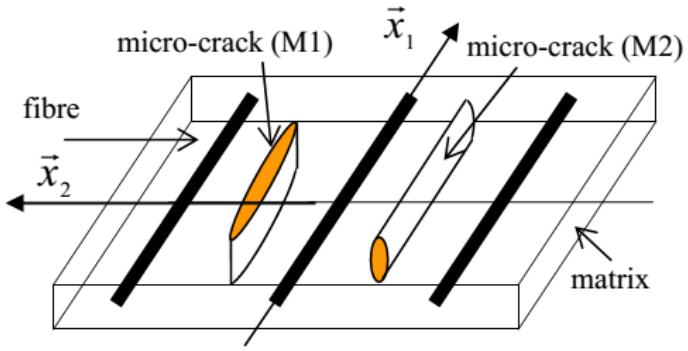

Fig III. 6.Micro-cracks orientation in the matrix

These three variables of damage can also be expressed in terms of flexibilities:

$$\begin{cases} D_I = 1 - \frac{S_{22}}{S_{22}+H_{22}} \\ D_{II} = 1 - \frac{S_{66}}{S_{66}+H_{66}} \\ D_{III} = 1 - \frac{S_{44}}{S_{44}+H_{55}} \end{cases} \quad \text{(III.28)}$$

According to [17] and relations D_I ,D_{II}etD_{III}allows to obtain:

$$\begin{cases} D_{II} = 1 - S_{66}\left[S_{66} + \frac{D_I}{(1-D_I)^{1/2}} \times (S_{11} \times S_{22})^{1/2}\right]^{-1} \\ D_{III} = 1 - S_{44}\left[S_{44} + \frac{D_I}{(1-D_I)^{1/2}} \times S_{22}\right]^{-1} \end{cases} \quad \text{(III.29)}$$

III.3.4. Plasticity

In the context of tests with high loading speeds, *glass / epoxy* type materials have shown the presence of irreversible and time-independent deformations. These are the plastic deformations.

The fibers being considered fragile elastic and the matrix being viscoelastic, the source of these deformations are not at the level of the constituents but in the process of degradation of the material. The damage will create micro cracks, voids with for main consequences the introduction of sources of friction within the structure. Two causes of plasticity can be distinguished: friction and damage. The first cause is mainly in shear, the second in the transverse direction.

III.3.4.1. Friction plasticity

This plasticity manifests itself mainly in shear and appears when the damage is triggered. According to the formalism of the associated plasticity, the potential φ^* p plays the role of indicator function of the convex f = 0.The global model developed in the laboratory provides a function of load adaptable to the monolayer:

$$f^p = \overline{\tilde{\sigma} - X} - R^P - Z_c \quad \text{(III.29)}$$

σ represents the equivalent stress and Z_c: the plasticity threshold. The variables of kinematic hardening X and of isotropic hardeningR^P are associated with the internal variables α and ε^p, where pε represents the cumulative plastic strain (Tab.III.3).

Tab.III.3. Thermodynamic variable for plastic

state variables		associated variables
visible	**internal**	
$\boldsymbol{\varepsilon}$	$\boldsymbol{\varepsilon^p}$ $\boldsymbol{\overline{\varepsilon}^p}$ $\boldsymbol{\sigma}$	$\boldsymbol{\sigma}$ $\boldsymbol{-\widetilde{\sigma}}$ $\boldsymbol{R^p}$ $\boldsymbol{X}$

The conventional choice of the cumulated plastic strain as internal variable makes it possible to check the equivalence:

$$(\tilde{\sigma} - X) : \dot{\varepsilon}^p = (\overline{\tilde{\sigma} - X})\dot{\bar{\varepsilon}}^P \tag{III.30}$$

By definition, the charging function has the following properties:

$$\begin{cases} f^p < 0 \;\Rightarrow\; \dot{\varepsilon}^p = 0 \\ f^p = 0 \;\; and \;\; \frac{\partial f^p}{\partial \tilde{\sigma}} \dot{\tilde{\sigma}} \leq 0 \Rightarrow \dot{\varepsilon}^p = 0 \\ f^p = 0 \quad and \; \frac{\partial f^p}{\partial \tilde{\sigma}} > 0 \;\Rightarrow\; \dot{\varepsilon}^p \neq 0 \\ f^p > 0 \;\; impossible \end{cases} \tag{III.31}$$

When the load is active, ie when both of the following conditions are true:

$$f^p = 0 \; and \; \frac{\partial f^p}{\partial \tilde{\sigma}} \dot{\tilde{\sigma}} > 0 \tag{III.32}$$

Plastic kinetics obtained by the laws of evolution:

$$\dot{\varepsilon}^p = \dot{\lambda}^p \frac{\partial f^p}{\partial \tilde{\sigma}} \tag{III.33}$$

$$\dot{\bar{\varepsilon}}^p = -\dot{\lambda}^p \frac{\partial f^p}{\partial R^P} = \dot{\lambda}^p \tag{III.34}$$

$$\dot{\alpha} = -\dot{\lambda}^p \frac{\partial f^p}{\partial X} = \dot{\varepsilon}^p \tag{III.35}$$

Where d is the Lagrange multiplier whose expression can be obtained by the consistency equation:

$$\dot{f}^p = 0 \tag{III.36}$$

The equivalent stress can be expressed in terms of an anisotropy tensor M

$$\bar{\tilde{\sigma}} = (\tilde{\sigma} : M : \tilde{\sigma})^{1/2} \quad \text{(III.37)}$$

With :

$$M = \begin{bmatrix} 0 & 0 & 0 & 0 & 0 & 0 \\ 0 & 0 & 0 & 0 & 0 & 0 \\ 0 & 0 & 0 & 0 & 0 & 0 \\ & & & \frac{Z_4^C}{Z_C} & 0 & 0 \\ & Sym & & & \frac{Z_5^C}{Z_C} & 0 \\ & & & & & 1 \end{bmatrix} \quad \text{(III.38)}$$

Equations (81) and (84) then make it possible to obtain the cumulated plastic strain rate:

$$\dot{\bar{\varepsilon}}^p = (\dot{\varepsilon}^p : M^{-1} : \dot{\varepsilon}^p)^{1/2} \quad \text{(III.39)}$$

Finally, we will write the load function in the form:

$$f^p = [(\tilde{\sigma} - X) : M : (\tilde{\sigma} - X)]^{1/2} - R^P - Z_C \quad \text{(III.40)}$$

The particularly simple form of the M anisotropy tensor comes from the fact that only shear can lead to plastic deformation of friction. It is postulated that the threshold of plasticity during a strain stress σ_6 is equal to c Z_6, noted Zc (respectively Z_4^C and Z_5^C for σ_4 and σ_5).

If it is postulated that the irreversible phenomena are triggered at the same moment as the damage, when the monolayer is blank, the convex f = 0 can be written in the space of the constraints in the form (67):

$$\frac{1}{2}\left[\frac{\sigma_2^2 - \sigma_4^2}{E_2} + \frac{\sigma_6^2}{\sqrt{E_1 E_2}}\right] - Y_c = 0 \quad \text{(III.41)}$$

In pure shear, we obtain

$$\sigma_6^2 - 2Y_c\sqrt{E_1 E_2} = 0 \quad \text{(III.42)}$$

The expression that gives the value of Z is :

$$Z_c = 2Y_c\sqrt{E_1 E_2} \quad \text{(III.43)}$$

Similarly, one can determine Z_4^C and Z_5^C .

Experimental observations have led to adopt laws of evolution of the variables hardening of the form:

$$X = X_1 + X_2 \tag{III.44}$$

$$\dot{X}_1 = \delta_1 \dot{\varepsilon}^p + \gamma_1 M : X_1 \dot{\varepsilon}^P \tag{III.45}$$

$$\dot{X}_2 = \delta_2 \dot{\varepsilon}^p \tag{III.46}$$

$$\dot{R}^P = 0 \tag{III.47}$$

These laws necessitate the identification of three parameters: γ_1, δ_2, δ_1.

The introduction of non-linear kinematic variables imposes the abandonment of the associated plasticity that is to say that the potential indicating the direction of the flow in the space of the force variables is no longer the potential pf, but a potential pF. Equations (84) are no valid. To preserve a free energy potential quadratic in α, one can choose the potential pF of the form:

$$F^P = F^P + \eta_x(X) + \eta_\alpha(\alpha) \tag{III.48}$$

With:

$$\eta_x(X) + \eta_\alpha(\alpha) = 0 \tag{III.49}$$

We can show that:

$$\eta_x(X) = \frac{\gamma_1}{2\delta_1} X_1 : M : X_1 \tag{III.50}$$

$$\eta_\alpha(\alpha) = \frac{\gamma_1 \delta_1}{2} \alpha_1 : M : \alpha_1 \tag{III.51}$$

This mathematical artifice makes it possible to continue to work using the formalism of the associated plasticity, even if the two potentials are not strictly identical.

Indeed, we have .We reach the flow laws:

$$\dot{\varepsilon}^p = \dot{\lambda}^p \frac{\partial F^P}{\partial \tilde{\sigma}} = \dot{\lambda}^p \frac{\partial f^P}{\partial \tilde{\sigma}} \tag{III.52}$$

$$\dot{\varepsilon}^p = -\dot{\lambda}^p \frac{\partial F^P}{\partial \tilde{\sigma}} = -\dot{\lambda}^p \frac{\partial f^P}{\partial R^P} = \dot{\lambda}^p \tag{III.53}$$

$$\dot{\sigma} = -\dot{\lambda}^p \frac{\partial F^P}{\partial X} \neq -\dot{\lambda}^p \frac{\partial f^P}{\partial X} \tag{III.54}$$

III.3.4.2. Damage plasticity

The second source of plasticity is the creation of voids by micro-cracking. These voids tend to increase the volume of the fold. This damage-related plasticity is expressed as transverse deformation, the amplitude of which is related to the micro-crack density $\boldsymbol{D_I}$ according to a linear relationship

$$\dot{\varepsilon}_2^p = \delta_3 \dot{D}_I \tag{III.55}$$

δ_3 Is a parameter to be identified.

To stay within the thermodynamic framework, we need to ensure that the potential for dissipation exists. Note $\phi_{pd}^*(\tilde{\sigma}, A_K)$ This potential, which operates as an indicator function for the convex $f^{pd} = 0$. Using (Equ 60), we can write the equivalence :

$$\dot{\varepsilon}_2^P = \dot{\lambda}^{pd} \frac{\partial f^{pd}(\tilde{\sigma}, A_K)}{\partial \tilde{\sigma}} = \delta_3 \dot{\lambda}^d \tag{III.56}$$

III.3.5. Viscoelasticity

The retarded plastic deformations ε are irreversible time dependent deformations .
We will assume that only crack friction can delay plasticity .We choose to define the viscoplastic potential ϕ as simply as possible with a power law similar to a generalised Norton's law:

$$\varphi_{vp}^* = \frac{k}{\eta+1}\left[\left\langle\left[(\tilde{\sigma} + X_3) : M : (\tilde{\sigma} + X_3)^{1/2}\right]\right\rangle - Z_C\right]^{\eta+1} \tag{III.57}$$

$\boldsymbol{K}$ and $\boldsymbol{\eta}$ are the parameters to be identified and $\boldsymbol{X_3}$ contains the kinematic hardening variables associated with internal variables $\boldsymbol{\alpha}_3$ (Tab III.4).

Tab III.4. Thermodynamic variable for viscoplastic.

state variables		associated variables
visible	internal	
ε	ε^{vp} α_3	$\tilde{\sigma}$ $-\tilde{\sigma}$ X_3

The retarded plastic deformation is derived from classical flow laws:

$$\dot{\varepsilon}^{vp} = \frac{\partial \varphi_{vp}^{*}}{\partial \tilde{\sigma}} \tag{III.58}$$

$$\dot{\alpha}_3 = \frac{\partial \varphi_{vp}^{*}}{\partial X_3} = \dot{\varepsilon}^{vp} \tag{III.59}$$

We choose the following linear kinetics, with δ a parameter to identify:

$$\dot{X}_3 = \delta \dot{\varepsilon}^{vp} \tag{III.60}$$

The analytical expression of the potentials for the modelling of dissipative phenomena has now been established. The general equations for inelastic behaviour, which are equations (III.56), can be written as:

$$\begin{cases} \dot{\varepsilon}^{in} = \lambda^d \frac{\partial f^d(Y, A_k)}{\partial \tilde{\sigma}} + \lambda^d \frac{\partial \varphi_{ve}^{*}(\tilde{\sigma}, A_k)}{\partial \tilde{\sigma}} + \lambda^d \frac{\partial f^d(\tilde{\sigma}, A_k)}{\partial \tilde{\sigma}} + \dot{\lambda}^{pd} \frac{\partial f^{pd}(\tilde{\sigma}, A_k)}{\partial \tilde{\sigma}} + \lambda^d \frac{\partial f^d(\tilde{\sigma}, A_k)}{\partial \tilde{\sigma}} \\ \dot{V}_K = -\lambda^d \frac{\partial f^d(Y, A_k)}{\partial A_k} - \frac{\partial \varphi_{ve}^{*}(\tilde{\sigma}, A_k)}{\partial A_k} - \lambda^p \frac{\partial f^d(\tilde{\sigma}, A_k)}{\partial A_k} - \dot{\lambda}^{pd} \frac{\partial f^d(\tilde{\sigma}, A_k)}{\partial \tilde{\sigma}} - \lambda^d \frac{\partial f^d(\tilde{\sigma}, A_k)}{\partial A_k} \end{cases} \tag{III.61}$$

Until now, the effect of temperature has not been considered. Introducing thermal deformation .Thermal deformation can be introduced in a very simple way:

$$\varepsilon = \varepsilon^e + \varepsilon^{in} + \alpha \Delta T \tag{III.62}$$

where $\boldsymbol{\alpha}$ is the dilatation tensor and ΔT is the temperature variation with respect to a reference temperature. The hypothesis of transverse isotropy allows this tensor to be expressed in terms of two expansion coefficients α_{11} and α_{22} . The effect of damage on these coefficients can be neglected to a first approximation.

To check the composite resistance, the TSAI-WU failure criterion is used. This criterion admits that composite failure is only reached when the following inequality is verified [III.17]:

$$F_{11}\left(\sigma_x^{(k)}\right)^2 + F_{22}\left(\sigma_y^{(k)}\right)^2 + F_{66}\left(\sigma_{yx}^{(k)}\right)^2 + 2F_{12}\sigma_y^{(k)}\sigma_x^{(k)} + F_1\sigma_x^{(k)} + F_2\sigma_y^{(k)} \leq 1 \tag{III.63}$$

$$\begin{cases} F_1 = \frac{1}{\sigma_{xU}} - \frac{1}{\sigma'_{xU}}, F_2 = \frac{1}{\sigma_{yU}} - \frac{1}{\sigma'_{yU}}, F_{11} = \frac{1}{\sigma_{xU} \times \sigma'_{xU}} \\ F_{22} = \frac{1}{\sigma_{yU} \times \sigma'_{yU}}, F_{66} = \frac{1}{\sigma_{yxU}^2}, F_{12} = -\frac{1}{2} \times \frac{1}{\sqrt{(\sigma_{xU} \times \sigma'_{xU}) \times (\sigma_{yU} \times \sigma'_{yU})}} \end{cases} \tag{III.64}$$

Or $\sigma_{xU}, \sigma'_{xU}, \sigma_{yU}, \sigma'_{yU}$ are the tensile stress in compression and in shear.

For a composite shell element of the cylindrical structure (see Figure2.2), the stress-strain relations of a layer k, for anisotropic materials, are given by [17].

$$\begin{Bmatrix}\sigma_Z\\ \sigma_\theta\\ \sigma_Z\\ \tau_{\theta r}\\ \tau_{zr}\\ \tau_{z\theta}\end{Bmatrix} = \begin{bmatrix}C_{11} & C_{12} & C_{13} & 0 & 0 & C_{16}\\ C_{21} & C_{22} & C_{23} & 0 & 0 & C_{26}\\ C_{31} & C_{32} & C_{33} & 0 & 0 & C_{36}\\ 0 & 0 & 0 & C_{44} & C_{45} & 0\\ 0 & 0 & 0 & C_{45} & C_{55} & 0\\ C_{16} & C_{26} & C_{36} & 0 & 0 & C_{66}\end{bmatrix}^{(k)} \begin{Bmatrix}\varepsilon_z - \alpha_z \Delta T\\ \varepsilon_\theta - \alpha_\theta \Delta T\\ \varepsilon_r - \alpha_r \Delta T\\ \gamma_{\theta r}\\ \gamma_{zr}\\ \gamma_{z\theta}\end{Bmatrix} \quad \text{(III.65)}$$

For a multilayer, the coefficients of thermal expansion $\alpha_r, \alpha_\theta, \alpha_z$ are determined using the following expression:

$$\{\acute{\alpha}\} = [T_\varepsilon]\{\alpha\} \quad \text{(III.66)}$$

That is to say,

$$\begin{pmatrix}\alpha_z\\ \alpha_\theta\\ \alpha_r\end{pmatrix}^{(k)} = \begin{bmatrix}\cos\varphi^2 & \sin\varphi^2 & \cos\varphi^2 \sin\varphi^2\\ \sin\varphi & \cos\varphi^2 & -\cos\varphi^2 \sin\varphi\\ 1 & 0 & 0\end{bmatrix}^{(k)} \times \begin{pmatrix}\alpha_x\\ \alpha_y\\ \alpha_z\end{pmatrix}^{(k)} \quad \text{(III.67)}$$

III.4. Formatting of the problem

Assumptions, equations of consistency and equilibrium as well as laws of behavior are defined. We can now determine the expressions of the displacement fields. Stress are expressed for each layer (k) using the following relationships

$$\begin{cases}\sigma_z^{(k)} = C_{11}^{(k)}\varepsilon_z + C_{12}^{(k)}\varepsilon_\theta + C_{13}^{(k)}\varepsilon_r + C_{16}^{(k)}\gamma_{z\theta}\\ \sigma_\theta^{(k)} = C_{21}^{(k)}\varepsilon_z + C_{22}^{(k)}\varepsilon_\theta + C_{23}^{(k)}\varepsilon_r + C_{26}^{(k)}\gamma\varepsilon_{z\theta}\\ \sigma_r^{(k)} = C_{31}^{(k)}\varepsilon_z + C_{32}^{(k)}\varepsilon_\theta + C_{33}^{(k)}\varepsilon_r + C_{36}^{(k)}\gamma_{z\theta}\\ \tau_{z\theta}^{(k)} = C_{61}^{(k)}\varepsilon_z + C_{62}^{(k)}\varepsilon_\theta + C_{63}^{(k)}\varepsilon_\theta + C_{66}^{(k)}\gamma_{z\theta}\end{cases} \quad \text{(III.68)}$$

Differential equations that travel should check the circumferential and radial displacements multilayer composite tubular structures in order to meetthe equilibrium of both internal and external efforts on each layer (k) are expressed by the equation system (3) [III.1,III.17]:

Where

$$N_1^{(k)} = \frac{C_{22}^{(k)}}{C_{33}^{(k)}} \qquad N_2^{(k)} = \frac{C_{12}^{(k)} - C_{13}^{(k)}}{C_{33}^{(k)}} \qquad N_4^{(k)} = \frac{C_{26}^{(k)} - 2\,C_{36}^{(k)}}{C_{33}^{(k)}}$$

$$\alpha_2^{(k)} = \frac{N_2^{(k)}}{1 - N_1^{(k)}} \qquad \alpha_4^{(k)} = \frac{N_4^{(k)}}{4 - N_1^{(k)}} \quad \text{(III.69)}$$

The solution of equation (16) depends on the value $\beta^{(k)} = \sqrt{N_1^{(k)}}$.

For $\beta^{(k)} = 1$:

$$U_r^{(k)} = D^{(k)} r + E^{(k)} / r + r \ln(r)\, N_2^{(k)} \varepsilon_0 + \alpha_4^{(k)} \gamma_0 r^2 \tag{III.70}$$

For $\beta^{(k)} = 2$:

$$U_r^{(k)} = D^{(k)} r^{\beta^{(k)}} + E^{(k)} r^{-\beta^{(k)}} + \alpha_2^{(k)} \varepsilon_0\ r + \frac{N_4^{(k)}}{2} \gamma_0 r^2 \ln(r) \tag{III.71}$$

For $\beta^{(k)} \neq 1$ (or 2):

$$U_r^{(k)} = D^{(k)} r^{\beta^{(k)}} + E^{(k)} r^{-\beta^{(k)}} + \alpha_2^{(k)} \varepsilon_0\ r + \alpha_4^{(k)} \gamma_0 r^2 \tag{III.72}$$

$D^{(k)}$, $E^{(k)}$, γ_0 and ε_0 are the integration constants for $k \in [1, w]$, ou $w = n_L + n_C$ and the total number of layers. The thickness of the liner is discretised into.n_L sub-layers and the number of composite layers is given by n_c.

III.5. Boundary conditions

The boundary conditions are continuity and conservation of volume on the one hand, and those imposed by the loading on the other. It will be assumed that there is no slip at the interfaces and that there is continuity of stresses and displacements. These boundary conditions are used to determine the integration constants introduced later.

In the following, the inner and outer radii are introduced.$R_{int}(k)$ and $R_{ext}(k)$ of each layer k. We note that:

$$R_{int}^{(k=1)} = r_0 \quad et \quad R_{ext}^{(k=w)} = r_a \tag{III.73-a}$$

The loading conditions of the inner and outer walls are presented as follows:

$$\sigma_r^{(k=1)}(r = r_0) = 0 \tag{III.73-b}$$

$$\sigma_r^{(k=w)}(r = r_a) = 0 \tag{III.73-c}$$

$$\tau_{\theta r}^{(k=1)}(r_0) = \tau_{zr}^{(k=1)}(r_0) \tag{III.73-d}$$

$$\tau_{\theta r}^{(k=w)}(r_a) = \tau_{zr}^{(k=w)}(r_a) \tag{III.73-e}$$

The condition of continuity of radial displacements is expressed by the relation:

$$\forall\, k \in\ [1, w-1], \quad U^{(k)}\left(r_{ext}^{(k)}\right) = U^{(K+1)}\left(r_{ext}^{(k)}\right) \tag{III.73-f}$$

La condition de contraintes radiales est exprimée par :

$$\begin{cases} \forall\, k\ \in\ [1, w-1], & \sigma_r^{(k)}\left(r_{ext}^{(k)}\right) = \sigma_r^{(k+1)}\left(r_{ext}^{(k)}\right) \\ & \tau_{zr}^{(k)}\left(r^{(k)}\right) = \tau_{zr}^{(k+1)}\left(r^{(k)}\right) \\ & \tau_{\theta r}^{(k)}\left(r^{(k)}\right) = \tau_{\theta r}^{(k+1)}\left(r^{(k)}\right) \end{cases} \tag{III.73-g}$$

The axial forces-internal pressure balancing condition with bottom effect

$$2\pi \sum_{k=1}^{w} \int_{r_{(k-1)}}^{r_k} \sigma_z^{(k)}(k) r^2 dr = \pi r_0^2 p_0 \tag{III.732-h}$$

Torsion torque balance:

$$2\pi \sum_{k=1}^{w} \int_{r^{(k-1)}}^{r^{(k)}} \tau_{z\theta}(r) r^2 dr = 0 \tag{III.73-i}$$

The boundary conditions enable us to write

$$\begin{cases} \tau_{\theta z}^{(k)} = 0 \\ \tau_{zr}^{(k)} = 0 \end{cases} \quad \text{et} \quad \begin{cases} \varepsilon_{\theta r}^{(k)} = 0 \\ \varepsilon_{zr}^{(k)} = 0 \end{cases} \tag{III.73-j}$$

Substituting equation (2.18) into equation (2.6) gives the integration constants :

$$A^{(k)} = B^{(k)} = 0 \tag{III.73-k}$$

This will allow us to write the solution to the followingU_θ as follows:

$$U_\theta = \gamma_0\, z\, r \tag{III.73-l}$$

for w $(w = n_L + n_C)$ layers of the storage solution, the number of unknowns, or integration constants of the system to be solved is equal to a $2(1-w)$ it's all about $D^{(k)}, E^{(k)}, \gamma_0\ et\ \varepsilon_0$ pour $k \in [1, w]$In the following, we write the components of the matrix A and the vector B of the equivalent linear problem such that:

$$X = A^{-1} \times B \tag{III.74}$$

Avec X qui définit le vecteur des constants d'intégration du système, tel que :

$$X = \left(D^{(1)}\, D^{(2)}\, .\, .\, .D^{(w)}, E^{(1)}\, E^{(2)}\, .\, .\, .E^{(w)}\, , \varepsilon_0\, , \gamma_0\right) \tag{III.75}$$

For a cylindrical structure with four layers, the system (III.74) can be written in detail:

Note: The components of the matrix A are shown in the Appendix.

$$\begin{bmatrix} D^1 \\ D^2 \\ D^3 \\ D^4 \\ E^1 \\ E^2 \\ E^3 \\ E^4 \\ \varepsilon_0 \\ \gamma_0 \end{bmatrix} = \begin{bmatrix} d_{11} & 0 & 0 & 0 & e_{11} & 0 & 0 & 0 & \alpha_{11} & \alpha_{12} \\ d_{21} & d_{22} & 0 & 0 & e_{21} & e_{22} & 0 & 0 & \alpha_{21} & \alpha_{22} \\ 0 & d_{32} & d_{33} & 0 & 0 & e_{32} & e_{33} & 0 & \alpha_{31} & \alpha_{32} \\ 0 & 0 & d_{43} & d_{44} & 0 & 0 & e_{43} & e_{45} & \alpha & \alpha \\ d_{15} & d_{52} & 0 & 0 & e & e & 0 & 0 & \alpha & \alpha \\ 0 & d_{62} & d_{63} & 0 & 0 & e & e & 0 & \alpha & \alpha \\ 0 & 0 & d_{73} & d_{64} & 0 & 0 & e & e & \alpha & \alpha \\ 0 & 0 & 0 & d & d & d & e & e & \alpha & \alpha \\ d_{91} & d_{92} & d_{93} & d_{94} & e_{91} & e_{92} & e_{93} & e_{94} & \alpha_{91} & \alpha_{92} \\ d_{101} & d_{102} & d_{103} & d_{104} & e_{101} & e_{102} & e_{103} & e_{104} & \alpha_{101} & \alpha_{102} \end{bmatrix} \times \begin{bmatrix} -P_0 \\ 0 \\ 0 \\ 0 \\ 0 \\ 0 \\ 0 \\ 0 \\ r_0^2 P_0 / 2 \\ 0 \end{bmatrix}$$

After determining the parameters d_{ij} , e_{ij} et a_{ij} the boundary conditions, the radial displacement and the strains and stresses are determined .

$D^{(k)}$, $E^{(k)}$, γ_0 and ε_0 are the constants of integration. The boundary conditions are on the one hand the continuity and conservation of volume, and secondly those imposed by the loading. Assume that there is no slip at the interfaces and that there is continuity of stresses and displacements. These boundary conditions to determine the constants of integration introduced later [1]. The internal radius of the multilayered cylindrical structure is of 30 mm, where the thickness of each composite layer is of 0.27 mm. The solutions are obtained by using the MATLAB software.

III.7. Algorithm resolution

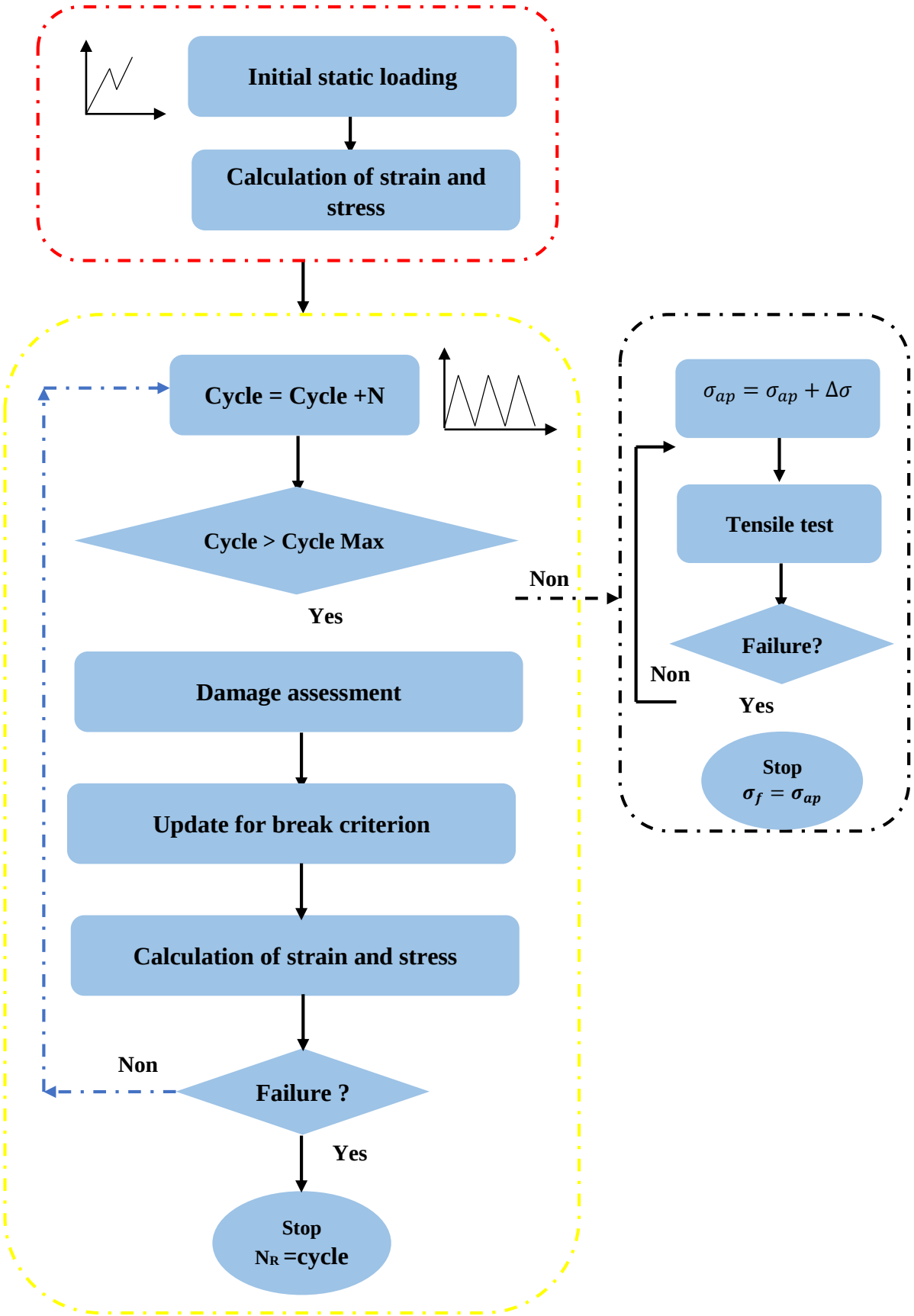

Fig .III.7. Algorithm resolutionFig.

III.8. Conclusion

A phenomenological model is developed to study the behaviour of organic matrix and long fibre laminates. The mechanical behaviour of a monolayer is proposed: viscoelastic-viscoplastic-visco-damaging. Damage is assumed to be due to the presence and growth of micro-cracks in the matrix. This anisotropic damage is then completely described by a single scalar variable . This model is used to predict the life under cyclic loading of composite tubular structures. To summarise for each fatigue increment (or block of cycles N), the model performs the following steps: (*i*) calculates the new diffuse damage value ,(*ii*) estimates the viscous deformations at the mean stress of the cycles ,(*iii*) gives assessment the mechanical strains and forces, and finally (*iv*) applies the failure criterion. All of the equations presented in this chapter, which constitute the analytical model, are solved and implemented using MATLAB, and the results are presented in the following chapter.

CHAPTER IV:

MODEL RESULTS AND DISCUSSION

IV.1-Introduction

In Chapter II, we defined a protocol for determining the mechanical response of a composite tube under two loading types: static and cyclic loading. The specimen is a long-fiber composite tube with six winding layers ($[\pm 55]_3$), measuring 60 mm (inner diameter), 62.3 mm (outer diameter), and 300 mm in length.

Based on the formulations from Chapter III, This chapter presents a detailed analytical investigation of Glass-Epoxy composite tubes subjected to quasi-static and cyclic tensile loading. The analysis begins with a description of the modeling procedure, followed by validation against experimental and numerical results, covering quasi-static and cyclic loading scenarios. The behavior of composite tubes under quasi-static tensile loading is examined, focusing on stress and strain distribution, damage evolution, and the degradation of the elastic modulus. Additionally, the analysis extends to cyclic tensile loading, evaluating stress-strain responses under repeated loading-unloading conditions.

IV.2 Data Analysis

In this analysis, all the pipes are made with six layers of pipes with glass/epoxy, the layers of these pipes have a property of opposite fibre orientation ($+\emptyset\ /-\emptyset$).The multi-layer pipes have an inner radius (r_0) of 60 mm, each layer thickness of 0.23 mm. It is assumed that the pipe is subjected to the tensile loading of 30 KN.

To show the results, the nondimensional quantities for the radial distance through the thickness are used. The non dimensional radial coordinate is defined as:

$$R = \frac{r - r_0}{r_a - r_0} \qquad (4.1)$$

The solutions are obtained by using the MATLAB numerical code. Tables 1 and 2 respectively present the material properties of a glass/epoxy composite, carbon/epoxy composite and aluminum liner. The used composite stacking sequences are presented in Table 3.

Tab IV. 1. Mechanical properties of composite material Glass/Epoxy [1.]

	E_x **[GPa]**	E_y **[GPa]**	G_{xy} **[GPa]**	ν_{yx}	α	β
G/E	**55**	**21**	**8.267**	**0,268**	**0.41**	**0.62**
C/E	**141.6**	**10.7**	**3.88**	**0.268**	**0.6**	**1**

Tab IV. 2. Different stacking sequences of the hybrid solution

Sequence	Winding angle	Sequence	Winding angle
Seq 1	$[\pm 50]_3$	Seq 2	$[\pm 50]_2+[+90]_2$
Seq 3	$[\pm 55]_3$	Seq 4	$[\pm 55]_2+[+90]_2$
Seq 5	$[\pm 60]_3$	Seq 6	$[\pm 60]_3+[+90]_2$

IV.3 Model validation

IV.3.1. Quasi-Static loading

IV.3.1.1 Tensile loading

Figure IV.1 presents the stress-strain distribution of the glass-epoxy composite tube under static tensile loading, with $[\pm 55]_3$ sequences. The modeled results demonstrate strong agreement with experimental data, particularly after incorporating viscous effects into the simulation, which reduced the analytical-experimental discrepancy. The strain distribution reveals a dominant axial strain component, exhibiting a 1.5:1 ratio relative to hoop strain.

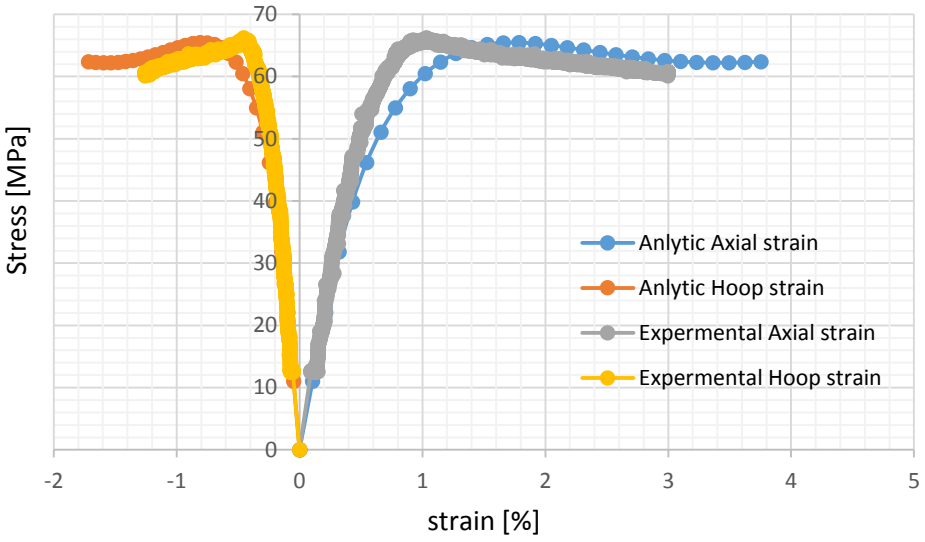

Fig IV.1.The distribution of stress through strain for a glass/epoxy pipe with a $[\pm 55]_3$ sequence

IV.3.1.2. Pure Internal pressure loading

The second step of model validation, it consists to compare the analytical results behavior of composite under pure internal pressure by experimental results obtained by Perreux et al. [1]. The figure IV.2 shows that there is good agreement between our current results and the experimental results for the type of loading. The results obtained show a non-linear pace from the beginning of the loading and this is due to the viscoelastic model. Another remark can be added, it is the loss of stiffness that characterises the stress-strain curve for its analytical approach or the experimental curve. This loss is due to the progressive damage built into the material and is based on incremental loading.

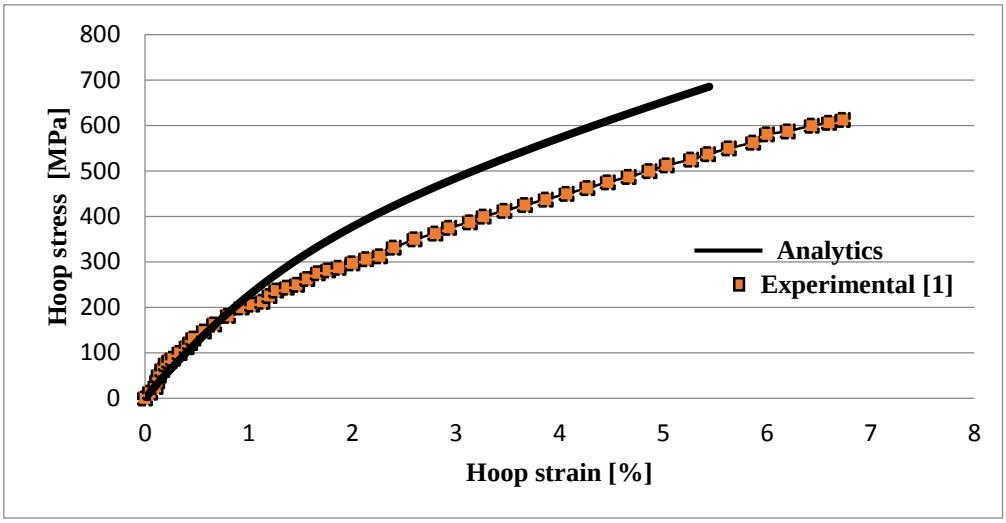

Fig . IV.2.Evolution of the circumferential stress versus circumferential strain (pure internal pressure time for a glass/epoxy pipe with a $[\pm 55]_3$ layup).

IV.3.1.3. Internal pressure loading with end effects

Figure IV.3 shows the variation of the stress in function of the strain along the hoop direction for internal pressure with the bottom end. The results of the developed model are compared with experimental analysis, led by Perreux et al. [1]. A good agreement is obtained between our current results and the experimental results for the type of loading.

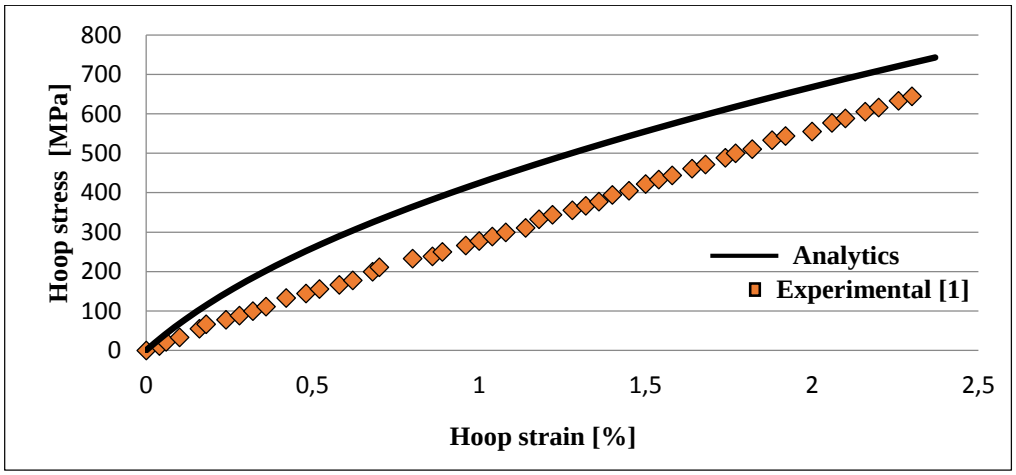

Fig . IV.3. Evolution of the circumferential stress versus circumferential strain (internal pressure with end effec time for a glass/epoxy pipe with a $[\pm 55]_3$ layup).

IV.4 Analysis of composite tube behavior under quasi-static tensile loading

IV.4.1 Stress and strain through the thickness

Figures IV.4, IV.5, and IV.6 present the variation of the axial, hoop, and shear stress components with respect to the non-dimensional radial coordinate RRR in a composite pipe subjected to a tensile load of 20 MPa. Four winding angles were analyzed: 30°, 40°, 55°, and 60°, with a layup consisting of six alternating plies.

It is evident that the stress distributions exhibit discontinuities across the thickness, particularly in the shear stress, which shows the most pronounced variation. These discontinuities arise from the abrupt changes in material properties between adjacent layers.

The axial stress is generally higher than the hoop stress, which reflects the tensile nature of the applied loading. The influence of fiber orientation is also notable: for winding angles greater than 50°, both axial and hoop stresses tend to decrease, while angles below 50° result in increased stress levels. Moreover, layups with lower winding angles (i.e., < 50°) exhibit higher sensitivity to shear stress, with magnitudes exceeding those of higher-angle configurations by more than 100%.

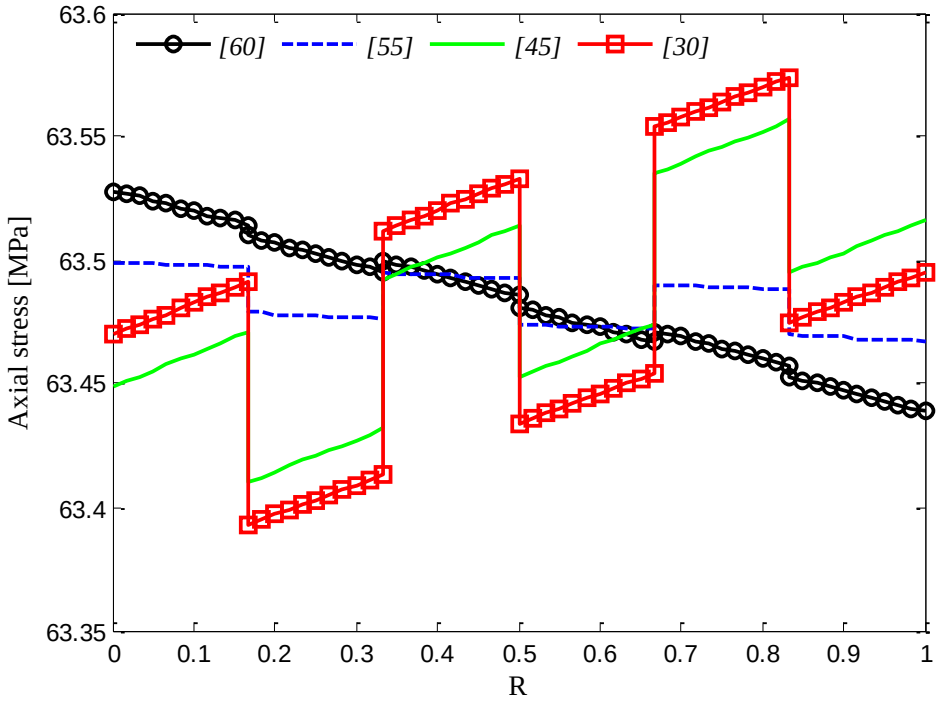

***Fig* . IV.*4*.The distribution of Axial stress through the non dimensional radial distance for a glass/epoxy pipe with a $[\pm 55]_3$ layups**

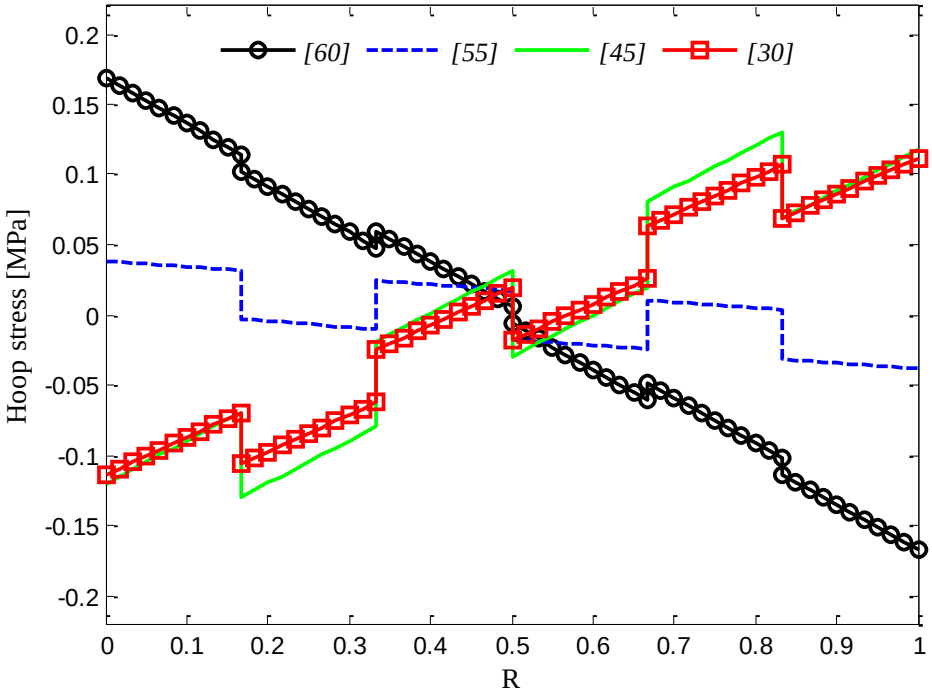

Fig .* IV.*5.The distribution of hoop stress through the non dimensional radial distance for a glass/epoxy pipe with a $[\pm 55]_3$ layup

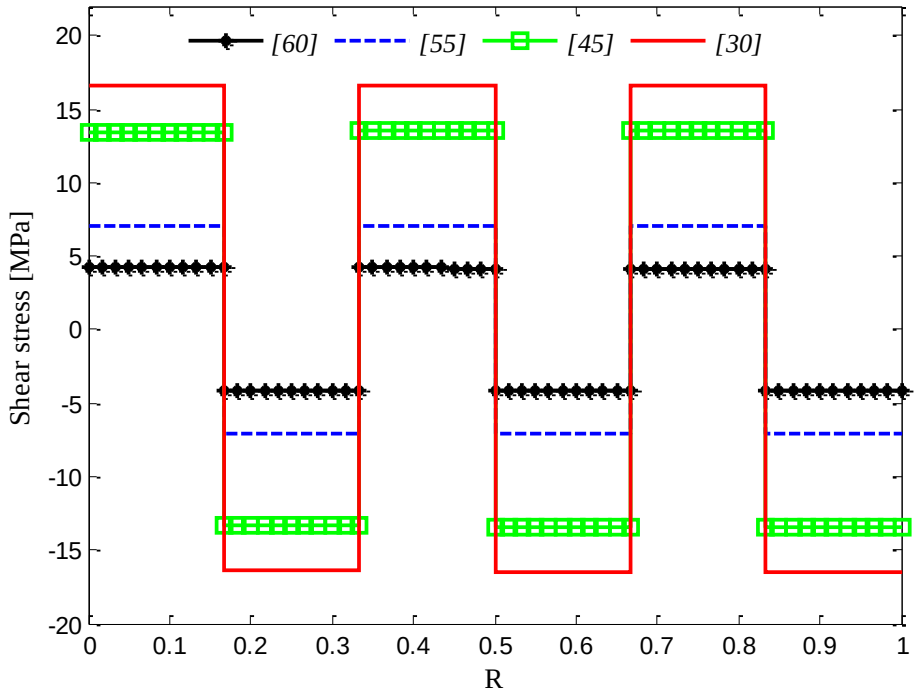

Fig. IV.6.The distribution of Shear stress through the non dimensional radial distance for a glass/epoxy pipe with a $[\pm 55]_3$ layup

Figures IV.7 and IV.8 illustrate the distribution of axial and hoop strain components along the non-dimensional radial coordinate R for composite tubular structures subjected to axial tensile loading. In contrast to the stress components shown in Figures IV.5 and IV.6, the strain components exhibit a continuous and smooth variation across the wall thickness, reflecting the strain compatibility between adjacent layers in the multilayered.

The axial strain remains positive throughout the multilayered, indicating uniform elongation along the loading direction, while the hoop strain is negative, corresponding to a contraction in the circumferential direction. This behavior is characteristic of axial tensile loading in anisotropic multilayered, where Poisson coupling effects play a significant role.

The observed strain magnitudes are in good agreement with the trends seen in the stress profiles. Higher axial strain values are observed for layups with ±55° and ±60° ply orientations compared to those with ±30° and ±40°. This can be attributed to the orientation of fibers being less aligned with the loading axis at higher angles, resulting in a lower axial stiffness and therefore higher axial strain under the same load.

Additionally, multilayered with high-angle plies exhibit increased in-plane shear strain contributions, which influence the overall axial deformation response due to the anisotropic nature of the composite material. These differences in deformation behavior may significantly affect the axial stiffness and structural integrity of the tubular component under service conditions, especially in applications where precise dimensional stability is critical.

In summary, the fiber orientation plays a critical role in determining the strain distribution and structural response of the composite tube. Layups with higher winding angles (above ±50°) lead to increased axial strains and potentially reduced stiffness, which must be carefully considered during the design phase for load-bearing applications

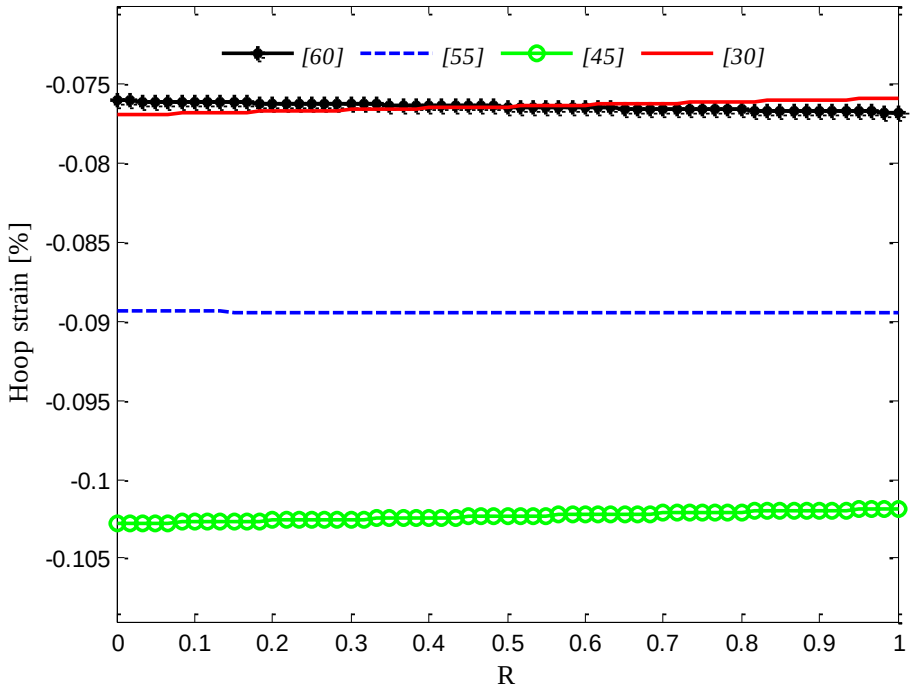

Fig . IV.7.The distribution of Hoop Strain through the non dimensional radial distance for a glass/epoxy pipe with a $[\pm 55]_3$ layup

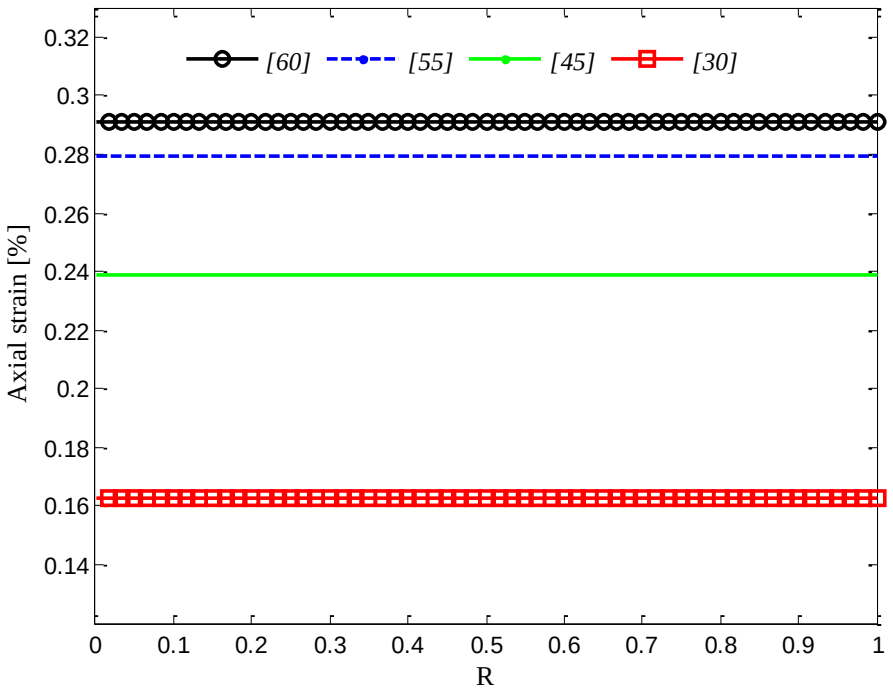

Fig . IV.8. Distribution of Axial Strain through the non dimensional radial distance for a glass/epoxy pipe with a $[\pm 55]_3$ layup

IV. 4. 2.Effect of the number of layers on the mechanical behaviour

Figure IV.9 presents the analytical response of the G/E (glass/epoxy) composite tube, showing the evolution of hoop stress as a function of hoop and axial strains for three tube configurations: Types A, B, and C. All three configurations share the same winding angle of ±55°, but differ in the number of layers—4, 6, and 8 plies, respectively.

The results indicate that increasing the number of layers enhances the structural rigidity of the composite tube under tensile loading. Specifically, the hoop stress at a given strain increases by approximately 30% when comparing the 4-ply configuration (Type A) to the 8-ply configuration (Type C). This improvement is attributed to the increased thickness and fiber volume fraction, which contribute to greater resistance against axial and hoop strains.

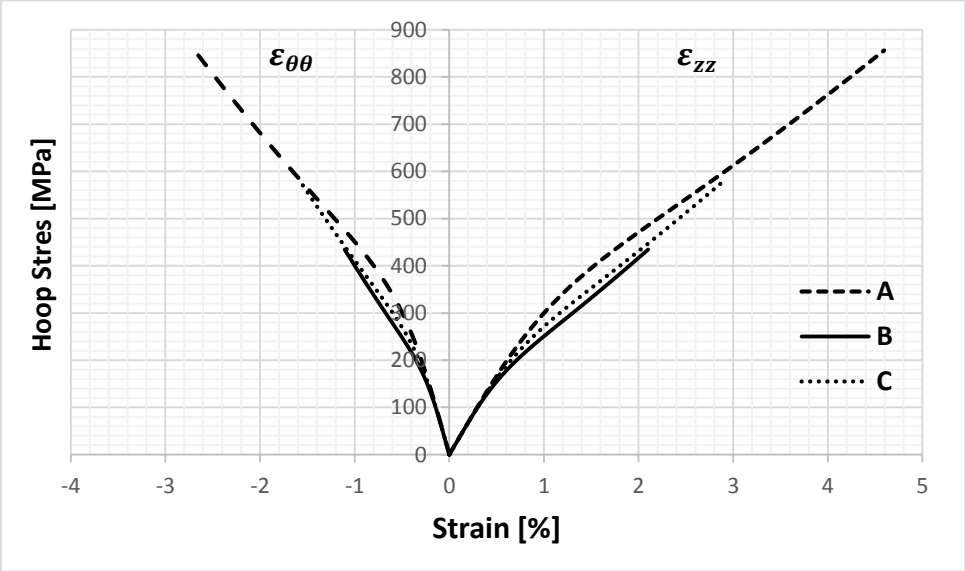

Fig .IV.9. Evolution of the Hoop stress versus strain (internal pressure with end effect time for a glass/epoxy pipe with a $[\pm55]_2$, $[\pm55]_3$, $[\pm55]_4$ layup).

IV.5. Effect of winding angle orientation on mechanical behavior

Figure IV.10 illustrates the distribution of hoop stress as a function of both axial and hoop strain for a composite tubular pipe subjected to internal pressure with end effect loading. The analysis includes six different winding angles: 30°, 40°, 45°, 50°, 55°, and 60°.

The results show that tubes with winding angles closer to the axial orientation (30° to 45°) exhibit greater circumferential deformation under the same loading conditions. On the other hand, the response curves of structures oriented beyond 45° show better behaviour in terms of deformation.

All curves demonstrate a non-linear stress–strain response, which reflects the constitutive behavior and material laws implemented in the analytical model developed in this study. The non-linearity may be attributed to progressive matrix cracking, fiber-matrix interaction, and anisotropic elastic behavior.

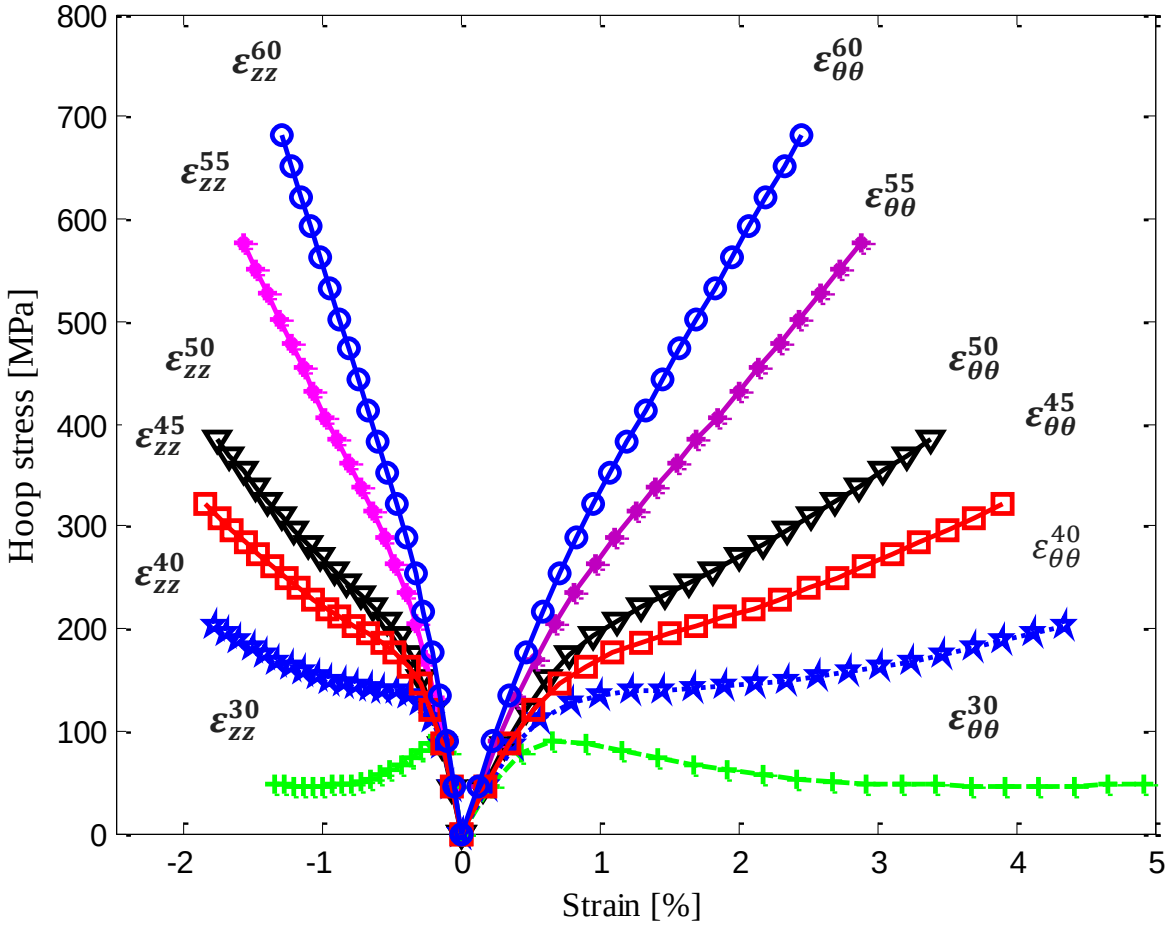

Fig .IV.10.Evolution of the Hoop stress versus strain (internal pressure with end effect time for a glass/epoxy pipe with a $[\pm30]_3$, $[\pm40]_3$, $[\pm45]_3$, $[\pm50]_3$, , $[\pm55]_3$, $[\pm60]_3$ layups).

In composite material design, the onset of damage is typically associated with a critical strain threshold, beyond which matrix cracking, fiber–matrix debonding, or delamination may occur. According to commonly accepted design standards for polymer matrix composites (e.g., ASTM D3039, ISO 527-4), axial strains exceeding approximately 2–3% in glass/epoxy multilayered are indicative of the transition from linear-elastic to damage-prone behavior.

Based on this criterion, the results presented in Figure IV.10 suggest that only configurations with winding angles of 55° and 60° remain within the safe deformation range under tensile loading, with maximum axial deformations of less than 3%. Conversely, tubes with winding angles of 30° to 50° exceed this critical deformation limit, making them more susceptible to early damage mechanisms. This highlights the importance of fiber orientation in tailoring the deformation capacity and structural resilience of filament-wound composite tubes.

IV.6. Damage evolution

Figure IV.11 illustrates the evolution of damage in a composite tubular structure subjected to axial tensile loading, based on a six-layer symmetric layup with the sequence $[\pm 55\circ]_3$. The onset of damage is observed at approximately 8 KN of applied load, indicating the initiation of micro-level degradation mechanisms such as matrix cracking or fiber–matrix debonding.

The damage progression follows a non-linear exponential trend, consistent with the behavior expected from progressive failure models in laminated composites. Beyond approximately 55 KN, a pronounced increase in damage sensitivity is observed, as indicated by a steep rise in the damage parameter. This rapid escalation suggests the transition from diffuse damage to more critical failure mechanisms, such as delamination or localized fiber breakage, which significantly compromise the structural integrity of the composite tube

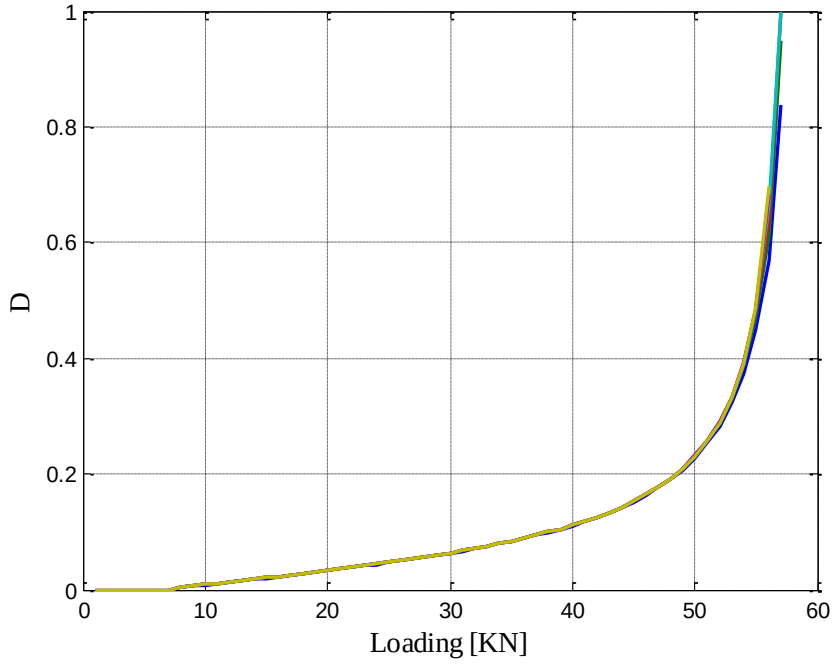

Fig .IV.11.The Evolution of damage through the tensile loading

IV.7 Stress and strain analysis for cyclic tensile loading

IV.7.1.The strain and stress evolution

Figure IV.12 presents the evolution of axial strain as a function of loading time for two cases: (A) without considering damage, and (B) with damage effects included. In case A, the axial strain remains relatively stable over time, reflecting the idealized elastic response of the undamaged composite structure.

In contrast, when damage is accounted for (case B), a noticeable increase in axial strain is observed as loading progresses. This behavior indicates the initiation and accumulation of progressive damage mechanisms within the multilayered composite pipe, such as matrix cracking, fiber–matrix debonding, and interlaminar degradation. The growing strain response underlines the material's loss of stiffness and structural integrity due to damage evolution throughout the laminate.

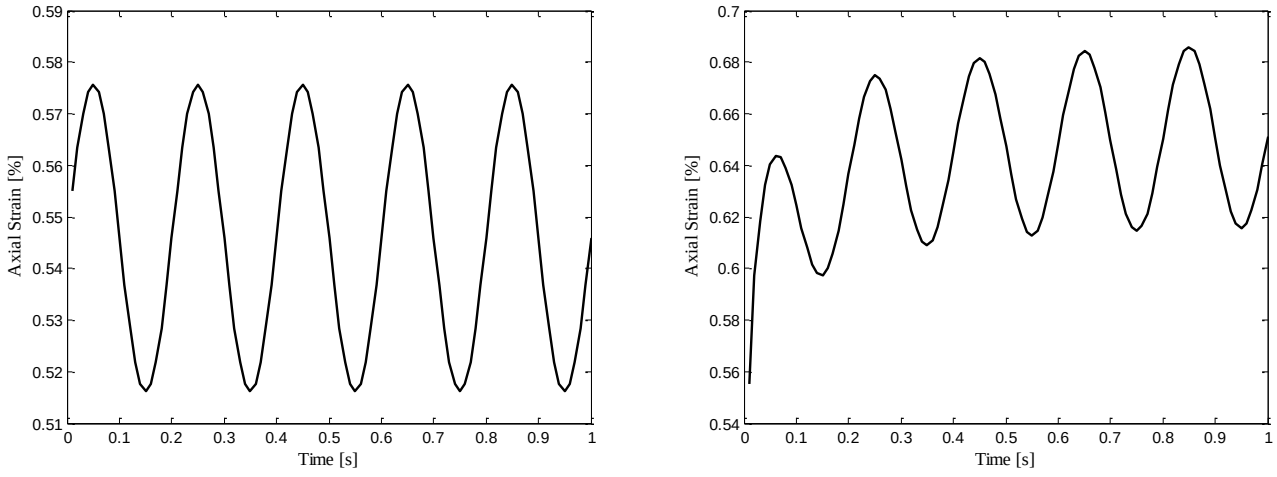

Fig . IV.11. The distribution of Axial strain through the time for a glass/epoxy pipe with a $[\pm 55]_3$ layup(A with damage B without damage).

In contrast, the hoop (circumferential) strain exhibits a gradual contraction throughout the tensile loading of the composite tubular structure (see figure IV.12).

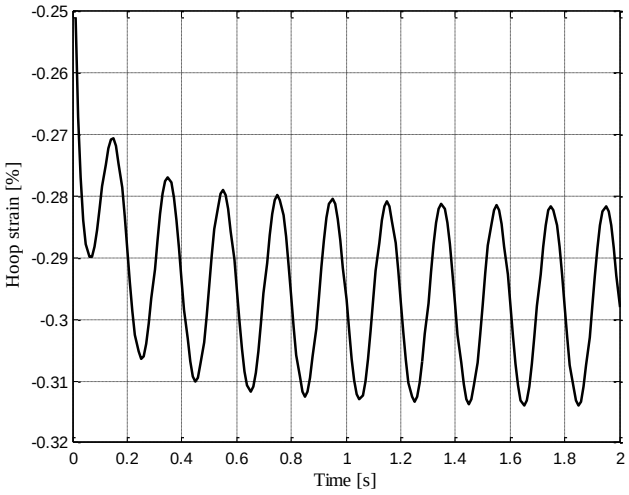

Fig . IV.12. The distribution of Hoop strain through the time for a glass/epoxy pipe with a $[\pm 55]_3$ layup

IV.7.2.The strain evolution performed at 40%, 60% and 80% of ultimed load.

As discussed in Chapter 2, cyclic loading tests were conducted at various loading rates relative to the failure stress. These values were then used to simulate the mechanical response of composite tubes under the same experimental conditions.The following figures show how axial strain evolves over time. Cyclic tests were performed at 40%, 60% and 80% of the ultimate load.

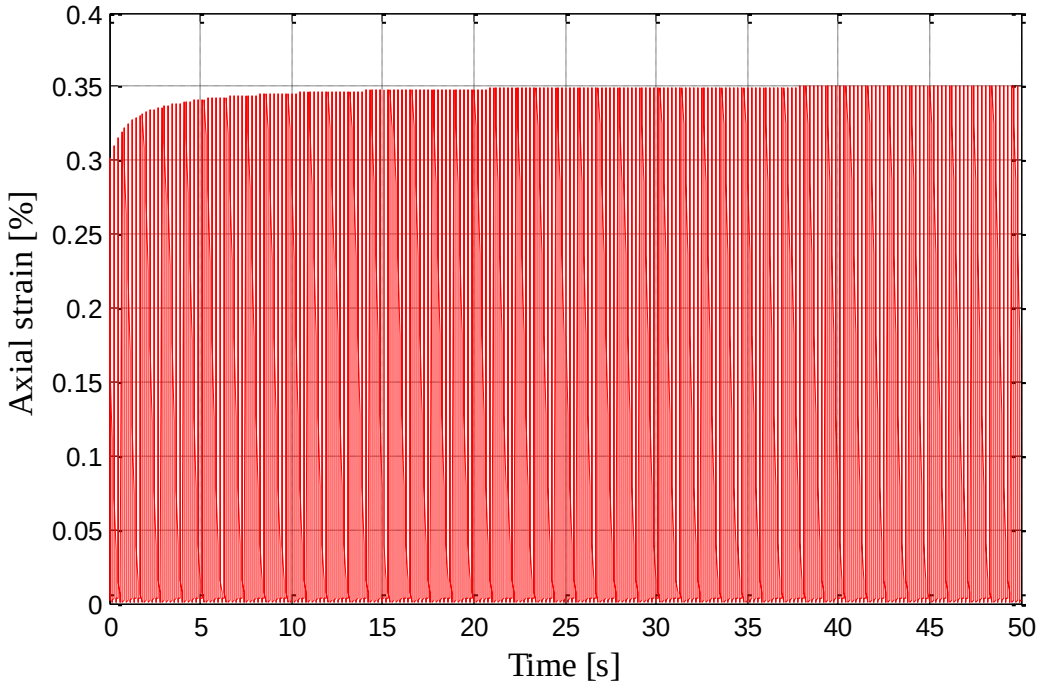

Fig .IV.13. The variation of axial strain-time under cyclic loading equal to 40% of the ultimate load of a glass/epoxy pipe.[55±] .

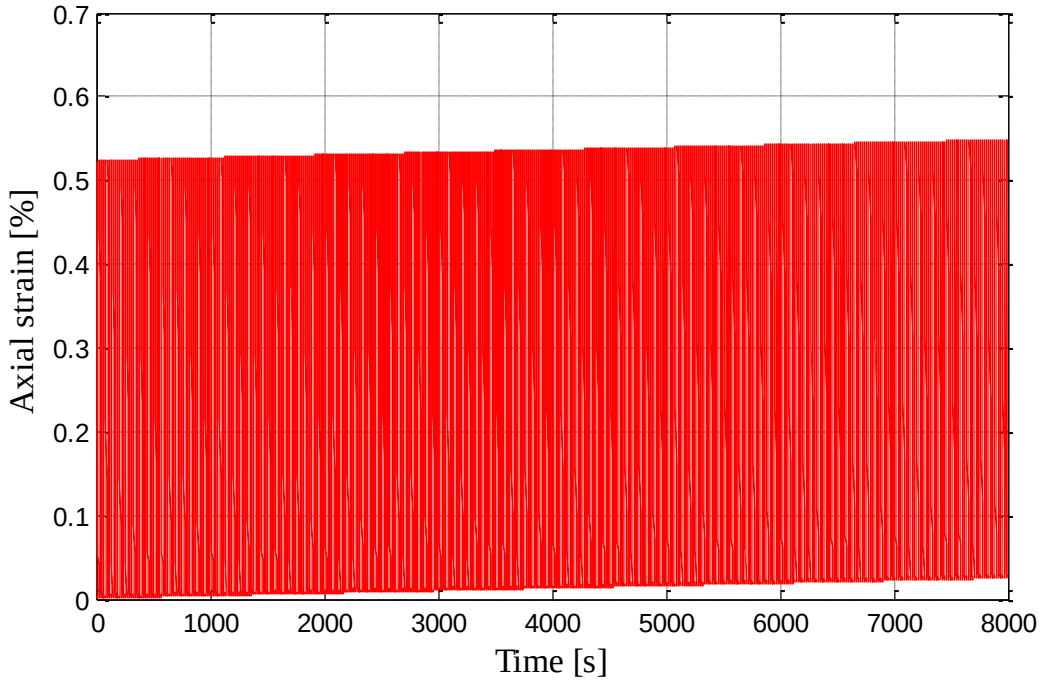

Fig .IV.14. The variation of axial strain-time under cyclic loading equal to 60% of the ultimate load of a glass/epoxy pipe.[55±]

For 40% of the stress at failure, we observe a rapid evolution of axial deformation between 0 and 100 seconds, which exhibits elastic behaviour and the onset of plasticity. After this, we observe a slow evolution characterised by plastic behaviour and damage, which ultimately leads to failure. For 60% of the stress at failure, we observe a rapid evolution of axial deformation between 0 and 30 seconds, which exhibits elastic behaviour and the onset of plasticity. After this, we observe a gradual evolution displaying plastic behaviour and damage, leading to failure. For 80% of the stress at failure is due to a rapid evolution of the axial deformation between 0 and 5 seconds, which exhibits elastic behaviour and the onset of plasticity. After this, there is a slow evolution that exhibits plastic behaviour and damage, both of which lead to failure.

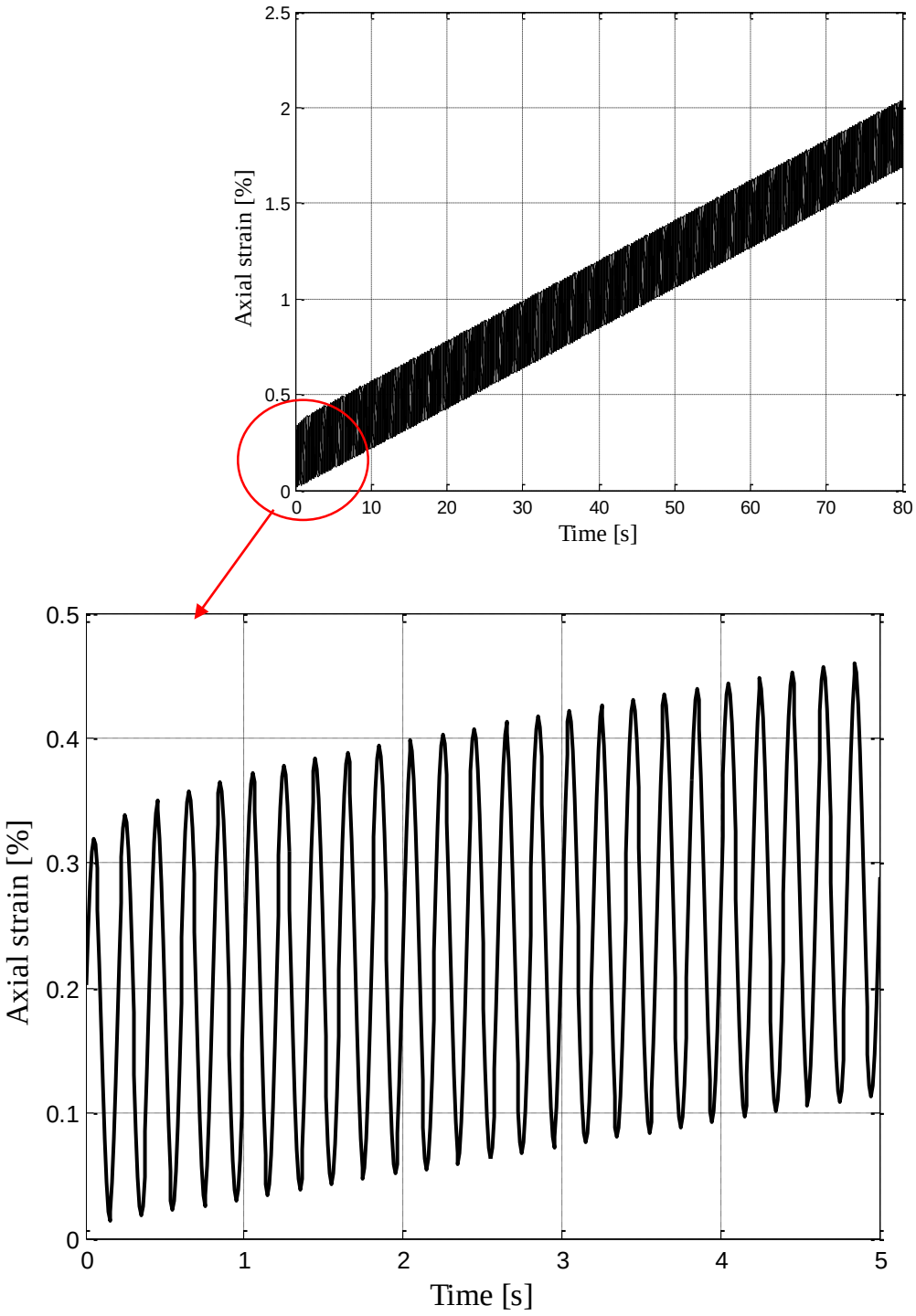

Fig .IV. 15. The variation of axial strain-time under cyclic loading equal to 80% of the ultimate load of a glass/epoxy pipe.[55±]

IV.8. Conclusion

This chapter presents a model that simulates the mechanical behaviour of a composite tube. This tool predicts the mechanical response of a cylindrical composite structure under different types of loads.

The model presented in this work describes mechanical behaviors under four types of loading:

a) Pure internal pressure (in the case of oil and gas pipelines).
b) Internal pressure with a buoyancy effect (in the case of V-type hydrogen storage).
c) Simple tension (case structural reinforcement elements).
d) Cyclic tension (case drive shafts).

The model describes all the physical phenomena that occur when the structure is subjected to mechanical loading. These phenomena include the evolution of microcracks and elastic, viscoelastic, and plastic behavior.

All of the equations included in the model are solved using a MATLAB numerical code.

For a static load, the model simulated three types of loading :

i. Simple traction : The results obtained from the analytical model were compared with the results of previous experiments, which showed good agreement. The shapes of the stress-strain curves are used to record the non-linear characteristics from the start of loading, taking into account the viscoelastic behaviour of the composite. In addition, we observe a loss of stiffness in the analytical and experimental approaches, due to the progressive damage to the composite material and also due to plasticity.

ii. Pure Internal pressure loading : The results obtained from the analytical model were compared with the results of previous experiments of literature bibliography [1], which showed good agreement.

iii. Internal pressure loading with end effects : A good agreement is obtained between our current results and the experimental [1] results for the type of loading.

Due to the results of the tensile tests, the tensile strength limit is estimated to be around 25 kN. A series of cyclic tests was performed at 40%, 60%, and 80% of this limit for the same load levels and parameters, such as frequency and load time. The analytical model's results are compared with those of the previous experiments, which show good agreement between the experiments and the analytical model in terms of axial deformation evolution.

CONCLUSION AND PRESPECTIVES

CONCLUSION AND PRESPECTIVES

Hydrogen transport and storage under high pressure, particularly using composite pipelines and tanks,is a promising but challenging solution for clean energy deployment. Despite composites' advantages (light weight, corrosion resistance, and high strength), their long-term durability and performance under complex loading conditions (tension, fatigue, combined loads) in hydrogen environments remain insufficiently understood. Existing studies often isolate loading types, leaving a gap in knowledge about their interactive effects, which are critical in real-world hydrogen infrastructure applications.

Objective

This thesis aims to investigate the influence of **static and fatigue axial loading** on **multilayered tubular composite structures**, specifically to:

- Characterize damage initiation and progression mechanisms under tension, fatigue, and combined loading.
- Quantify the effects of these loading types on structural integrity and lifespan.
- Develop a **lifespan prediction model** to support the design of reliable hydrogen transport systems.
- Contribute to optimizing composite-based infrastructure for the hydrogen economy.

Methodology

To achieve these goals, the study followed a **multi-step experimental and modeling approach**:

1. **Experimental Campaign**:
    - Tested Glass/Epoxy composite tubes ([±55°] winding) under three loading modes:
        - **Monotonic tensile loading**
        - **Cyclic fatigue loading** (with varying amplitudes)
        - **Combined loading** (fatigue followed by tensile to failure)
    - Evaluated parameters such as ultimate tensile strength, fatigue life, residual stiffness, and failure modes.
2. **Analytical Modeling**:
    - Developed a predictive **lifespan model in MATLAB**.
    - Integrated visco-elasto-plastic constitutive behavior and progressive damage mechanics.

- Supported model calibration with experimental data to estimate burst pressure and fatigue life.

This integrated approach bridges the gap between experimental observations and practical design tools, aiming to improve safety and performance standards for high-pressure hydrogen transport infrastructure.

The experimental part aimed to experimentally characterize the mechanical behavior of Glass/Epoxy cylindrical composite specimens with a $[\pm 55°]_3$ stacking sequence under various loading conditions. The objective was to assess their strength, fatigue life, and damage evolution to inform future structural design.

Main Findings:

1. **Tensile Testing** revealed an ultimate tensile strength of approximately 25 kN, along with key elastic properties, confirming the material's capacity to withstand static loads.
2. **Fatigue Testing** at stress amplitudes of 40%, 60%, and 80% of the ultimate strength showed that fatigue life decreases significantly with increasing stress, ranging from nearly 1.6 million cycles at 40% to only 634 cycles at 80%.
3. **Combined Loading (Fatigue + Tension)** demonstrated a notable reduction in residual stiffness and strength, emphasizing the impact of prior fatigue damage on structural integrity.

Additionally, the evolution of the elastic modulus and damage coefficient under cyclic loading confirmed progressive material degradation. For instance, a decrease in modulus from 10 GPa and a halving of fatigue life post-damage (from 1.8 million to 900,000 cycles) underscored the importance of fatigue considerations in design.

A phenomenological model was successfully developed to simulate the mechanical behavior of composite laminates with long fibers and an organic matrix. At the scale of a single ply, the model incorporates viscoelastic, viscoplastic, and anisotropic damage mechanisms, with matrix damage described by a single scalar variable representing the evolution of microcracks. This formulation allows for a comprehensive assessment of the material's response under cyclic loading conditions.

The model was applied to predict the fatigue life of tubular composite structures subjected to internal pressure and axial loads. For each loading increment or cycle block, the procedure involves updating the damage state, computing the viscous strains based on the mean stress, evaluating the resulting mechanical response, and verifying structural integrity through a failure criterion. All analytical formulations were implemented in MATLAB, forming the

basis for the numerical simulations and predictions discussed in the final chapter. This modeling framework contributes to enhancing the predictive capability for the durability of composite structures in hydrogen transport applications.

The analytical model of viscoelastic behavior coupled to damage of multilayer tubular structures predict the mechanical response of cylindrical composite structure under different types of loading such as pure internal pressure, tension and finally internal pressure with end effect. The obtained results are compared with respect to experiments previous results, where good agreement is reported.

The shapes of the stress - strain curves is used to record non-linear characteristic from the beginning of loading, taken into account the viscoelastic behavior of the composite. In addition, we note a loss of rigidity in the analytical and experimental gaits, due to the progressive damage of composite material. To reduce the acceptable deviation between the model results and the experimental ones, taking into account the visco-plastic behavior of the damaged multilayered cylindrical composite is important.

Thus, the tubular structures design model is validated based on the results obtained. The second part is focused on the life prediction in composite structures, which is an important tool in the conception of composite structure. In order to predict the time remaining before failure tubular structures under cyclic loading of pressure, the forthcoming paper is devoted to take into account the viscoelasticity coupled to damage behavior under fatigue pressure loading, comparing experimental results obtained on prototypes of tubular structure.

Finally this thesis **contributes** to both **academic research** and **industry (companies)**, especially in the hydrogen energy and composite structure sectors, where the key contribution are listed below:

1. For Academic Research:

- **Experimental Benchmarking**: The thesis offers a comprehensive experimental database on the tensile, fatigue, and combined loading behavior of multilayer composite tubes with [±55°] stacking sequences, which is valuable for validating numerical models and advancing failure theory in composites.
- **Fatigue and Damage Insights**: It identifies key degradation mechanisms (modulus reduction, damage accumulation, burst strength loss) under realistic loading conditions, enhancing understanding of failure in fiber-reinforced composites.

- **Hybrid Loading Characterization**: Your combined fatigue–tensile testing approach is relatively rare and adds a new dimension to existing fatigue data, offering a more accurate simulation of real service conditions, especially for hydrogen pipelines and vessels.
- **Life Prediction Modeling**: The viscoelastic–viscoplastic–viscodamage model developed can be directly used by other researchers as a foundation for further theoretical development, particularly in fatigue of composite structures.
- **Mathematical Implementation**: A fully operational MATLAB implementation of the model provides an accessible numerical tool for simulations of composite fatigue life under complex loading.

2. For Industrial Applications and Companies (e.g., in Hydrogen Infrastructure):

- **Design Optimization**: Companies developing hydrogen storage and transport solutions (e.g., pressure vessels, pipelines) can use the insights from your work to optimize winding angles, stacking sequences, and material selection to delay fatigue failure.
- **Reliability and Safety Assessment**: The damage and life prediction model supports structural health monitoring and maintenance planning by predicting remaining service life before failure—critical for hydrogen transport safety.
- **Cost Reduction**: Through better durability prediction and lightweight design via composites, manufacturers can reduce over-engineering, lower costs, and increase performance margins of hydrogen pressure systems.
- **Model Integration**: Your model could be incorporated into existing FEM software or digital twins to simulate real-time degradation in pressurized systems operating under cyclic loads.
- **Accelerated Testing Protocols**: The testing methodology developed can be adapted to establish accelerated durability tests for certification or standardization of composite hydrogen components.

Based on your experimental findings and the development of your analytical model, here are several well-grounded as research perspectives and industrial development paths which we can include in our thesis conclusion:

1. **Experimental Enhancement**

Multi-axial and Internal Pressure Testing: Extend the current study to include bi-axial and internal pressure tests on composite tubes to simulate more realistic service conditions, such as those in hydrogen storage tanks and pipelines.

High-Frequency Fatigue and Environmental Effects: Investigate the fatigue behavior under high-frequency loading and in aggressive environments (e.g., hydrogen embrittlement, temperature, humidity) to reflect operational realities.

Non-Destructive Evaluation (NDE) : Integrate NDE techniques (e.g., acoustic emission, X-ray tomography, digital image correlation) to monitor damage initiation and evolution in real time and correlate with model predictions.

2. **Model Refinement and Expansion**

Coupled Thermo-Mechanical Effects: Develop a coupled model that integrates temperature effects with viscoelastic-viscoplastic-damage behavior, particularly relevant for cryogenic or high-temperature hydrogen applications.

Micromechanical Modeling: Integrate micromechanics-based damage models (e.g., fiber-matrix debonding) to better represent the physical processes governing fatigue and failure at the micro-scale.

Probabilistic Life Prediction: Introduce stochastic modeling to account for variability in material properties and loading conditions, allowing for more robust design margins and reliability assessments.

3. **Industrial Integration and Application**

Design Certification Support: Use the validated model to support the certification and standardization of composite hydrogen pressure components by simulating long-term performance.

Scale-Up to Full Structures: Apply the approach to full-scale components (e.g., tanks, pipelines) and consider geometrical effects, joining interfaces, and structural discontinuities in industrial designs.

4. Sustainability and Circular Economy

Recyclability and Lifecycle Analysis: Investigate the end-of-life recyclability and lifecycle carbon footprint of composite hydrogen vessels compared to metallic alternatives, to align with circular economy goals.

Eco-Design Strategies: Extend your work to include sustainable material choices (e.g., bio-composites or recyclable epoxy systems) while maintaining mechanical performance.

These perspectives position our research at the intersection of fundamental science and industrial application, especially in the context of the global hydrogen transition.

Appendix

Appendix A

The function of loading is proposed by:

$$f^d = -Y - Y_C - R^d$$

If

$$f^d < 0 \quad \Rightarrow \dot{D}_I = 0$$

Elses

$$f^d = 0 \;\; \frac{\partial f^d}{dY}\dot{Y} \le 0 \quad \Rightarrow \dot{D}_I = 0$$

Elses if

$$f^d = 0 \;\; \frac{\partial f^d}{dY}\dot{Y} > 0 \Rightarrow \dot{D}_I \neq 0$$

Else if

$$f^d > 0 \quad \text{impossible}$$

When the loading caused damage, when the following condition are true:

$$f^d = 0 \quad \text{et} \quad \frac{\partial f^d}{\partial Y}\dot{Y} > 0$$

The kinetics of damage is determined by the laws of evolution:

$$\dot{D}_I = -\dot{\lambda}^d \frac{\partial f^d}{\partial Y} = \dot{\lambda}^d$$

$$\overline{D}_I = -\dot{\lambda}^d \frac{\partial f^d}{\partial Y} = \dot{\lambda}^d$$

Where $\dot{\lambda}^d$ is the Lagrange multiplier, the expression can be obtained by the consistency equation:

$$f^d = 0$$

We can write:

$$R_d = Y_c + Y$$

$$
\begin{cases}
Y = Y_I + Y_{II} \times X_{II} + Y_{III} \times X_{III} \\
Y_I = \left[-\dfrac{\partial \psi}{\partial \psi} \right]_{\sigma_4, \sigma_6} = \dfrac{s_{22}}{2 \times (1 - D_I)^2} \times \sigma_{22}^2 \\
Y_{II} = \left[-\dfrac{\partial \psi}{\partial \psi} \right]_{\sigma_2, \sigma_4} = \dfrac{s_{66}}{2 \times (1 - D_{II})^2} \times \sigma_{66}^2 \\
Y_{III} = \left[-\dfrac{\partial \psi}{\partial \psi} \right]_{\sigma_2, \sigma_6} = \dfrac{s_{44}}{2 \times (1 - D_{III})^2} \times \sigma_{44}^2 \\
X_{II} = \left[-\dfrac{\partial D_{II}}{\partial D_I} \right] \dfrac{s_{66} \sqrt{s_{11} \times s_{22}}}{\left(s_{66} + \dfrac{D_I \sqrt{s_{11} \times s_{22}}}{\sqrt{1 - D_I}} \right)^2} \dfrac{\partial}{\partial D_I} \left(\dfrac{D_I}{\sqrt{1 - D_I}} \right) = \dfrac{s_{66} \sqrt{s_{11} \times s_{22}}}{\left(s_{66} + \dfrac{D_I \sqrt{s_{11} \times s_{22}}}{\sqrt{1 - D_I}} \right)^2} \dfrac{2 - D_I}{2 \left(\sqrt{1 - D_I} \right)^3} \\
X_{II} = \dfrac{\partial D_{III}}{\partial D_I} = \dfrac{s_{66} \times s_{22}}{\left(s_{44} + \dfrac{D_I \times s_{22}}{\sqrt{1 - D_I}} \right)^2} \dfrac{2 - D_I}{2 \left(\sqrt{1 - D_I} \right)^3}
\end{cases}
$$

Appendix B

The components of A are calculated by using the boundary conditions, given below writhe $k \in [1, n]$:

Internal pressure condition

$$A_{KK} = C_{23}^{K} + \beta^{K} \times C_{33}^{K} \times \left(r^{K}\right)^{-\beta^{K}-1}$$

$$A_{Kn-1} = C_{23}^{K} + \beta^{K} \times C_{33}^{K} \times \left(r^{K}\right)^{-\beta^{K}-1}$$

If $\beta^{K} == 1$

$$A_{K2n+1} = C_{31}^{k} + \left(N_2^K \middle/ 2\right) \times C_{32}^{K} \times Logr^{K} + C_{33}^{K} \times Logr^{K+1}$$

$$A_{K2n+2} = \left(C_{36}^{K} + \alpha_2^K \times \left(C_{32}^{K} + 2C_{33}^{K}\right)\right) \times r^{K}$$

else

$$A_{K,2n-1} = \left(C_{23}^{K} + C_{33}^{k}\right)\alpha^{k} + C_{13}^{k}$$

$$A_{K2n+2} = \left(C_{36}^{K} + \alpha_2^K \times \left(C_{23}^{K} + 2C_{33}^{K}\right)\right) \times r^{K}$$

Displacements continuity condition :

$$A_{K,K-1} = \left(r^{K}\right)^{\beta^{K-1}}$$

$$A_{K,K} = \left(r^{K}\right)^{\beta^{K}}$$

$$A_{K,K+n-1} = \left(r^{K}\right)^{-\beta^{K-1}}$$

$$A_{K,K+n} = \left(r^{K}\right)^{-\beta^{k1}}$$

If $\beta^{K-1} = 1$ and $\beta^{K} = 1$

$$A_{K,2n+1} = R^{K} Logr^{K} \times \left(N_2^{K-1} - N_2^{K}\right)/2$$

$$A_{K,2n+2} = \left(\alpha_2^{K-1} - \alpha_2^{K}\right)\left(r^{K}\right)^{2}$$

If $\beta^{K-1} = 1$ and $\beta^{K} \neq 1$

$$A_{K,2n+1} = R^{K} Logr^{K} \times \left(N_2^{K-1}\right)/2 - \alpha_1^{K} r^{K}$$

$$A_{K,2n+2} = \left(\alpha_2^{K-1} - \alpha_2^{K}\right)\left(r^{K}\right)^{2}$$

If $\beta^{K-1} \neq 1$ and $\beta^{K} = 1$

$$A_{K,2n+1} = \alpha_1^{K} r^{K} - r^{K} Logr^{K} \times N^{K} \middle/ 2$$

$$A_{K,2n+2} = \alpha_2^{K} r^{K} - \alpha_2^{4}\left(r^{K}\right)^{2}$$

If $\beta^{K-1} \neq 1$ and $\beta^{K} \neq 1$

$$A_{K,2n+1}=\left(\alpha_2^{K-1}-\alpha_1^K\right)r^K$$

$$A_{K,2n+1}=\left(\alpha_2^{K-1}-\alpha_1^K\right)\left(r^K\right)^2$$

Strain continuity condition:

$$A_{n+K,K}=\left(C_{23}^K+\beta^K C_{33}^K\right)\times\left(r^{K+1}\right)^{\beta^{K-1}}$$

$$A_{n+K,K+1}=\left(C_{23}^{K+1}+\beta^{K+1}C_{33}^{K+1}\right)\times\left(r^{K+1}\right)^{\beta^{K-1}-1}$$

$$A_{n+K,n+K}=\left(C_{23}^K-\beta^K C_{33}^K\right)\times\left(r^K\right)^{-\beta^K-1}$$

$$A_{n+K,K+n+1}=-\left(C_{23}^{K+1}-\beta^{K+1}C_{33}^{K+1}\right)\times\left(r^{K+1}\right)^{-\beta^{K-1}-1}$$

If $\beta^K=1$ and $\beta^{K+1}=1$

$$A_{n+K,2n+1}=\left[C_{31}^K+\frac{N_2^K}{2}\times\left(C_{32}^K Logr^{K+1}+C_{33}^{K+1}\times\left(Logr^{K+1}+1\right)\right)\right]-\left[C_{31}^{K+1}+\frac{N_2^K}{2}\times\left(C_{32}^{K+1}Logr^{K+1}+C_{33}^{K+1}\times\left(Logr^{K+1}+1\right)\right)\right]$$

$$A_{n+K,K+n+2}=r^{K+1}\left[\left(C_{63}^K-C_{63}^{K+1}\right)+\alpha_2^K\left(C_{32}^K-C_{32}^{K+1}\right)+2\left(C_{33}^K-C_{33}^{K+1}\right)\right]$$

If $\beta^K=1$ and $\beta^{K+1}\neq 1$

$$A_{n+K,2n+1}=C_{31}^K+\frac{N_2^K}{2}\left(C_{23}^K Logr^{K+1}+C_{33}^K Log(r^{K+1}+1)\right)-\left(C_{13}^{K+1}+\alpha_1^K\left(C_{23}^{K+1}+C_{33}^{K+1}\right)\right)$$

$$A_{n+K,K+n+2}=\left[\left(C_{63}^K+\alpha_2^K\left(C_{32}^K+2C_{33}^{K+1}\right)\right)-\left(C_{63}^{K+1}+\alpha_2^{K+1}\left(C_{32}^{K+1}+2C_{33}^{K+1}\right)\right)\right]r^{K+1}$$

If $\beta^K\neq 1$ and $\beta^{K+1}=1$

$$A_{n+K,2n+1}=C_{13}^K+\alpha^K\left(C_{23}^K+C_{33}^K\right)-C_{32}^{K+1}+\frac{N_N^{K+1}}{2}C_{32}^{K+1}Logr^{K+1}+C_{33}^{K+1}Log\left(r^{K+1}+1\right)$$

$$A_{n+K,K+n+2}=\left[\left(C_{63}^K+\alpha_2^K\left(C_{32}^K+2C_{33}^K\right)\right)-\left(C_{63}^{K+1}+\alpha_2^{K+1}\left(C_{32}^{K+1}+2C_{33}^{K+1}\right)\right)\right]r^{K+1}$$

If $\beta^K\neq 1$ and $\beta^{K+1}\neq 1$

$$A_{n+K,2n+2}=C_{13}^K-C_{13}^{K+1}+\alpha_1^K\left(C_{23}^K+C_{33}^K\right)-\alpha_1^{K+1}\left(C_{23}^{K+1}+C_{33}^{K+1}\right)$$

$$A_{n+K,2n+2}=\left[\left(C_{36}^K-C_{36}^{K+1}\right)+\alpha_2^K\left(C_{23}^K-2C_{33}^K\right)-\alpha_2^{K+1}\left(C_{23}^{K+1}+2C_{33}^{K+1}\right)\right]r^{K+1}$$

External pressure condition:

$$A_{2n,K}=\left(C_{23}^n+\beta^n C_{33}^n\right)\left(r^{n+1}\right)^{\beta^n-1}$$

$$A_{2n,2n}=\left(C_{23}^n-\beta^n C_{33}^n\right)\left(r^{n+1}\right)^{\beta^n-1}$$

$$A_{2n,2n+1}=C_{13}^n+\alpha_1^n\left(C_{23}^n+C_{33}^n\right)$$

$$A_{2n,2n+2}=\left(C_{36}^n+\alpha_1^n\left(C_{23}^n+C_{33}^n\right)\right)r^{n+1}$$

The axial equilibrium condition:

If $\beta^K=1$

$$A_{2n+1,K}=\left(\left(r^{K+1}\right)^2+\left(r^K\right)^2\right)\left(C_{12}^K+C_{13}^K\right)\Big/2$$

$$A_{2n+1,K+n}=\left(Logr^{K+1}-Logr^{K+1}\right)\left(C_{12}^K-C_{13}^K\right)$$

$$A_{2n+1,K+n}=\sum_{K=1}^{K=n}C_{11}^K\frac{\left(r^{K+1}\right)^2}{2}+C_{12}^K\frac{N_2}{4}\frac{1}{2}\left(r^{K+1}\right)^2\left(\log r^{K+1}-\frac{1}{2}\right)+C_{13}^K\frac{N_2}{2}\frac{1}{2}\left(r^{K+1}\right)^2\left(\left(Logr^{k+1}\right)+\frac{1}{2}\right)-C_{11}^K\left(r^{K+1}\right)^2$$
$$+C_{12}^K\frac{N_2}{2}\left(r^K\right)^2\left(Logr^K-\frac{1}{4}\right)+C_{13}^K\frac{N_2}{2}\frac{1}{2}\left(r^K\right)^2\left(2Log\left(r^K\right)^2+\frac{1}{2}\right)$$

$$A_{2n+1,2n+K}=\sum_{k=1}^{k=n}\left(r\left(R^{K+1}\right)^3-\left(R^K\right)^3\right)\times\alpha_2^K\left(C_{12}^K+2C_{13}^K\right)+C_{16}^K$$

If $\beta^K\neq 1$

$$A_{2n+1,K}=\left(C_{12}^K+\beta^K C_{13}^K\right)\times\left(\left(r^{K+1}\right)^{\beta^K+1}-\left(r^K\right)^{\beta^K-1}\right)\Big/\left(1+\beta^K\right)$$

$$A_{2n+1,K+n}=\left(C_{12}^K-\beta^K C_{13}^K\right)\times\left(\left(r^{K+1}\right)^{-\beta^K+1}-\left(r^K\right)^{-\beta^K-1}\right)\Big/\left(1-\beta^K\right)$$

$$A_{2n+1,2n+1}=\sum_{K=1}^{K=n}\left(C_{11}^K+\alpha_1^K\left(C_{12}^K+C_{13}^K\right)\right)\times\left(\left(r^{K+1}\right)^2-\left(r^K\right)^2\right)\Big/2$$

$$A_{2n+1,K+n}=\sum_{K=1}^{k=n}\left(C_{16}^K+\alpha_2^K C_{12}^K+2C_{13}^K\right)\times\left(\left(r^{K+1}\right)^3-\left(r^K\right)^3\right)\Big/3$$

The zero torsion condition i**:**

If $\beta^K=1$

$$A_{2n+2,K}=\left(\left(r^{K+1}\right)^3-\left(r^K\right)^3\right)\times\left(C_{62}^K+C_{63}^K\right)\Big/3$$

$$A_{2n+2,K+n}=\left(r^{K+1}-r^K\right)\times\left(C_{62}^K-C_{63}^K\right)$$

$$A_{2n+2,2n+1}=\sum_{k=1}^{k=n}c_{61}^k\frac{\left(R^{K+1}\right)^3}{3}+\frac{N_2^K}{2}\frac{1}{3}\left(r^{K+1}\right)^3\left(C_{62}^K\left(Logr^{K+1}-\frac{1}{3}\right)+C_{63}^K\frac{1}{3}\left(Logr^{K+1}+\frac{2}{3}\right)\right)-$$
$$\left(C_{61}^K\left(r^K\right)^3+\frac{N_2^K}{2}\frac{1}{3}\left(r^K\right)^3\left(C_{26}^K\left(Logr^K-\frac{1}{3}\right)+C_{63}^K\left(Logr^K+\frac{2}{3}\right)\right)\right)$$

$$A_{2n+2,2n+2}=\sum_{K=1}^{K=n}C_{66}^K+\alpha_2^K\left(C_{62}^K+2C_{63}^K\right)\left(\left(R^K\right)^4-\left(r^K\right)^4\right)\Big/4$$

If $\beta^K\neq 1$

$$A_{2n+2,K+n}=\left(C_{26}^K+\beta^K C_{36}^K\right)\left(\left(r^{K+1}\right)^{\beta^K+2}+\left(r^K\right)^{\beta^K+2}\right)\Big/\left(2+\beta^K\right)$$

$$A_{2n+2,K+n}=\left(C_{26}^K-\beta^K C_{36}^K\right)\left(\left(r^{K+1}\right)^{-\beta^K+2}+\left(r^K\right)^{-\beta^K+2}\right)\Big/\left(2-\beta^K\right)$$

$$A_{2n+2,2n+1}=\sum_{K=1}^{K=n}\left(C_{16}^K+\alpha_1^K\left(C_{26}^K+C_{36}^K\right)\right)\left(\left(r^{K+1}\right)^3-\left(r^K\right)^3\right)\Big/3$$

$$A_{2n+2,2n+1}=\sum_{K=1}^{K=n}\left(C_{66}^K+\alpha_1^K\left(C_{26}^K+2C_{36}^K\right)\right)\left(\left(r^{K+1}\right)^4-\left(r^K\right)^4\right)\Big/4$$

The strains is giving by:

If $\beta^K \neq 1$

$$\varepsilon_r^k = D^k\left(\beta^k - 1\right)r^{\beta^k - 1} + E^k\left(-\beta^K - 1\right)r^{-\beta^k - 1} + \alpha_2^k\varepsilon_0 + \frac{N_4}{2}\gamma_0\left(\frac{1}{3}\left(r^k\right)^3 \ln r - \frac{1}{9}\left(r^k\right)^k\right)$$

$$\varepsilon_\theta^k = D^k r^{\beta^k - 1} + E^k r^{-\beta^k - 1} + \alpha_2^k\varepsilon_0 + \frac{N_4}{2}\gamma_0 r^k \ln r^k$$

If $\beta^K = 1$

$$\varepsilon_r^k = D^k\beta^k r^{\beta^r - 1} + E^k\left(-\beta^k\right)r^{-\beta^k - 1} + \alpha_2^k\varepsilon_0 + 2\alpha_4^k\gamma_0 r_0$$

$$\varepsilon_\theta^k = D^k r^{\beta^r - 1} + E^k r^{-\beta^k - 1} + \alpha_2^k\varepsilon_0 + \alpha_4^k\gamma_0 r_0$$

Liste of Publications and Communications

Selected International publication

GHOUAOULA A., HOCINE A., CHAPELLE D., KARA ACHIRA F., BOUBAKAR M.L. Analytical damage prediction in the composite part of a type III hydrogen storage vessel. Mechanics of Composite Materials, Vol. 48, No. 1, March, **2012**. Doi:10.1007/s11029-012-9253

HOCINE, A. **GHOUAOULA**, F. KARA ACHIRA, S.M. MEDJDOUB. Analysis of failure pressures of composite cylinders with a polymer liner of type IV CNG vessels. International Conference of composites materials – World Academy of Science, Engineering and Technology 73 2013.

A. HOCINE, F. KARA ACHIRA, **A. GHOUAOUALA.** Coupled structural/thermal analysis of cylindrical part of multilayered composite vessel. Advanced Materials Research Vol. 445 (**2012)** pp 589-594.

GHOUAOULA, A. HOCINE, D. CHAPELLE, M.L. BOUBAKAR, M. HADJ MELIANI. Analytical prediction behaviour of damaged composite tubular structures under quasi-static pressure. STRUCTURAL INTEGRITY AND LIFE, Vol.18, No.2, **2018.**

MAIZIA, A. HOCINE, **A. GHOUAOULA**, M. HADJ MELIANI. Numerical simulation of failure probability prediction: Application to cylindrical part of type III CNG storage vessel. Recueil de Mécanique Volume 3, Numéro 1, Pages 245-253. **2018.** https://www.asjp.cerist.dz/en/PresentationRevue/293.

GHOUAOULA . A. HOCINE . M. HADJ MELIANI . A. MAIZIA . R. SULEIMAN. Reliability Analysis of Type III Gas Storage Vessel Under pressure loading. Journal of Failure Analysis and Prevention. April **2019**, Volume 19, Issue 2, pp 445–452. https://doi.org/10.1007/s11668-019-00616-y.

HOCINE, A., MAIZIA, A**., GHOUAOULA, A.** et al. Reliability Prediction of Composite Tubular Structure Under Mechanical Loading by Finite Element Method

HOCINE, A., MAIZIA, A**., GHOUAOULA, A.** et al. Deterministic Analysis for Creep Behavior of Damaged Composite Tubular Structure. J Fail. Anal. and Preven. 20, 1858–1863 **(2020).** https://doi.org/10.1007/s11668-020-00994-8.

Selected International Conference paper

A. HOCINE, **A. GHOUAOUALA**, F. KARA ACHIRA. Coupled structural/thermal analysis of cylindrical part of multilayered composite vessel. 14th International conference on advances in materials and processing technologies, AMPT 2011, 13-16 July 2011 in Istanbul, Turkey.

A. HOCINE, **A. GHOUAOUALA**, F. KARA ACHIRA. Analytical analysis of a behavior damage of the composite pipe under pure internal pressure. Congrès Algérien de Mécanique; CAM2011 Guelma, 14 – 17/11/2011.

A. HOCINE, **A**. **GHOUAOUALA**, S.M. MEDJDOUB, M CHERIFI. A meso macro model prediction of laminated composite damage elastic behaviour. AMPT 2014, Novembre 2014, Dubai – UAE

A. GHOUAOUALA, A. HOCINE. Analyse du comportement viscoélastique d'une structure tubulaire multicouche endommagée sous pression quasi-statique. ICMS'2014, 21,22 et 23 Septembre 2014, Université de BLIDA, Algérie.

A. GHOUAOULA, A. HOCINE, D. CHAPELLE, M.L. BOUBAKAR. Predicting of viscoelastic damaged behavior of a multilayer composite tubular structure under a creep loading. The Third International Conference on FRACTURE MECHANICS 2016. Chlef Algeria.

A. GHOUAOULA, A. HOCINE, D. CHAPELLE, M.L. BOUBAKAR. Predicting of viscoelastic damaged behavior of a multilayer composite tubular structure under a cyclic loading ICSID 15-18/08/2017, Zagreb – Croatia.

A. HOCINE, **A. GHOUAOULA**. Damage analysis of a multilayer composite on tubular structure under different loading. ICSID 15-18/08/2017, Zagreb – Croatia.

A. GHOUAOULA, A. MAIZIA, A. HOCINE, D. CHAPPELLE. Analytical prediction of damage in a multilayer composite tubular structure under a cyclic loading. International Conference on Mechanics and Energy. December 20-22, 2018, Hammamet, TUNISIA.

SIDI MOHAMED MEDJDOUB, BELABBES BACHIR BOUIADJRA, ABDELKDER HOCINE, **ABDELHAMID GHOUAOULA** Numerical modeling of mechanical behavior of autofrettage multilayer extrusion pipe. The 13th International Workshop on Advanced Materials, 2022 Ras Al Khaimah, UAE.

A. GHOUAOULA, A. MAIZIA,G.HABBAR , A. HOCINE .Analyse du comportement mécanique dun réservoir de stockoge d'hydrogéne type III.the first national seminar on green Hydrogen for the algerien sector ,july 23,24 2022Algiers Algeria .

A. GHOUAOULA, A. MAIZIA, G.HABBAR, A. HOCINE. Evaluation of damge in glass/epoxy composite tube laminate .THE FIREST INTERNATINAL CONGRESS ON MECHANICAL ENGINEERING .15-16 Novemner 2023 CONSTANTINE, ALGERIA.

A. GHOUAOULA, A. MAIZIA, A. HOCINE.THE EFFECT OF CRACK DEPTH ON THE MECHANICAL BEHAVIOR OF MULTILAYER COMPOSITE MATERIAL. 3rd Internationel workshop on strucurel mechanics and meterials April 23-24 ,2024 Batna Algeria.

Selected National Conference paper

Ghania HABBAR, Abdelkader HOCINE, Abdelhakim MAIZIA, **Abdelhamid Ghouaoula**, João RIBEIRO Safety analysis of renewable hydrogen transmission by composite sandwich pipe under fire. The first national seminar on green hydrogen for the Algerian industrial sector. July 23rd -26th, 2022 Algiers-Algeria.